PE&RS
November 2020 Volume 86, Number 11
Photogrammetric Engineering & Remote Sensing
The official journal for imaging and geospatial information science and technology

XXIV ISPRS Congress

International Society for Photogrammetry and Remote Sensing

4 – 10 July 2021, Nice, France

www.isprs2020-nice.com

Keynote speakers

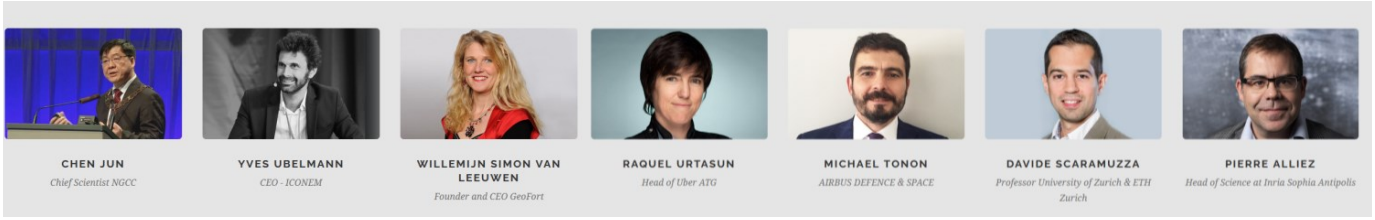

CHEN JUN
Chief Scientist NGCC

YVES UBELMANN
CEO - ICONEM

WILLEMIJN SIMON VAN LEEUWEN
Founder and CEO GeoFort

RAQUEL URTASUN
Head of Uber ATG

MICHAEL TONON
AIRBUS DEFENCE & SPACE

DAVIDE SCARAMUZZA
Professor University of Zurich & ETH Zurich

PIERRE ALLIEZ
Head of Science at Inria Sophia Antipolis

Executive committee

Nicolas Paparoditis	Laurent Polidori	Tania Landes	Clément Mallet	Florent Lafarge	Pierre Grussenmeyer	Eric Labergerie
ENSG-IGN-Univ. Gustave Eiffel	*CESBIO*	*INSA*	*IGN*	*INRIA*	*INSA*	*CNAM*
Congress Director	Congress Deputy Director	Congress Media Chair	Congress Program Chair	Congress Program co-Chair	Congress Industry Chair	Congress Financial Chair

Platinum sponsor

AIRBUS

Gold sponsors

ThalesAlenia Space

esri THE SCIENCE OF WHERE

Silver sponsors

HEXAGON

وزارة الشؤون البلدية و القروية

Bronze sponsors

PIX4D RIEGL 航天宏图 Piesat nFrames Agisoft aerometrex RACURS Trimble Bentley Advancing Infrastructure

Institutional partners, supporting graduate schools and associations

IGN cnes esa IRD UNIVERSITÉ CÔTE D'AZUR cnrs INSU Inria

INSA ENSG Géomatique le cnam esgt AFIGÉO aft EuroSDR GIM INTERNATIONAL LIDAR MAGAZINE

INDUSTRYNEWS

To have your press release published in *PE&RS*, contact Rae Kelley, rkelley@asprs.org.

ANNOUNCEMENTS

GeoCue Group Inc., a leading provider of aerial/mobile LIDAR tools and the creator of the True View® family of drone 3D imaging solutions has launched GeoCue Australia PTY. GeoCue Australia is a partnership between GeoCue Group Inc. and two Australian investors with GeoCue Group Inc. taking a majority stake in the venture. Mr. Mark Hickey, one of the investors and a company Director, will serve in the role of General Manager. This joint venture company will provide customers in Australasia with direct local sales and support of the GeoCue product line.

Plans to develop operations in Australasia stem from the success of GeoCue's Loki direct geopositioning solution within the mining and construction industries throughout Australia and New Zealand. This customer base is now anxious to move to the new True View product line.

"The Australasia market is a very important core customer base for us," said Lewis Graham, President and CTO of GeoCue Group Inc. "We have previously served this market through a very successful reseller partnership with C. R. Kennedy. With the introduction of our True View drone mapping ecosystem, we know that our customers will expect direct support from GeoCue at a local level. I have had a lot of enthusiastic conversations with Mark about the opportunities in the region and we both felt the time was right for launching this joint venture."

General Manager, Mark Hickey states "This collaboration with GeoCue Group Inc. is really exciting and is something that is the result of a heap of behind the scenes work and discussion with Lewis and the team. The GeoCue Group has had a great last few years with the success of the Loki photogrammetry system followed by the tremendous True View® solution. In APAC region the name 'GeoCue' is synonymous with a reputation for customer support and service and myself and the GeoCue Australia team certainly look forward to continuing the great work".

GeoCue Australia PTY will offer GeoCue's LIDAR and drone mapping solutions to end users and service providers throughout the Australasia region. The company will also provide local support to the large base of GeoCue product users in the region such as Geoscience Australia, a long-time user of GeoCue's LP360 LIDAR processing tools. Perhaps the most innovative offering will be the True View 410 drone LIDAR/Camera imaging system which, in addition to a purchase option, will be available via a Hardware as a Service subscription offering.

Please find more information on this endeavor at www.geocue.com.

TECHNOLOGY/EQUIPMENT

Improving and verifying accuracy is a typical objective of any survey... and this becomes more complex to achieve when undertaking a UAV LiDAR survey. Deploying **Routescene's** Ground Control Targets on known and accurately co-ordinated Ground Control Points prior to a UAV LiDAR survey provides the assurance that the survey has been properly executed and you can demonstrate the specified level of accuracy has been achieved.

UAV LiDAR surveys are typically undertaken in remote, rural and sometimes hazardous locations where there are no fixed points available, such as solid surfaces or concrete features, that could be used as Ground Control Points. Routescene's Ground Control Targets solve this problem.

The Routescene UAV LiDAR Ground Control Targets are quick and simple to deploy. Raised from the ground using a mini tripod, a built-in bubble level enables accurate levelling and removes the need for a tribrach. Robustly engineered, the targets stay in position during adverse and windy conditions, reducing the risk of repositioning during a survey.

Covered with highly retro-reflective material to provide high-intensity returns, typically each target will be hit 200-300 times by the lasers from the UAV LiDAR system. As a result the targets are easily identifiable and can be automatically extracted from the geo-referenced point cloud.

You can directly compare the known coordinate of the physical target with that visible in the point cloud. The difference between the two coordinates is the error: confirming the level of accuracy achieved in the survey.

Routescene customer Vashaun Henderson from Rekon Solutions in Canada commented, *"When working for engineering and survey clients accuracy has be paramount for us. Utilizing the special laser reflective ground control targets from Routescene we have been able to clearly identify survey monuments in the field, survey them and identify those targets in the scan. Having these targets enhances our ability to evaluate the scan's alignment and our ability to evaluate and report on horizontal and vertical accuracy. It is something that has separated us from the pack. Rekon has had great success with deploying these targets."*

To read an in-depth article on improving UAV LiDAR survey accuracy using Ground Control Points visit: https://www.routescene.com/events/uav-lidar-accuracy-with-ground-control-points/

For more information please visit: https://www.routescene.com.

ACCOMPLISHMENTS

The **URISA Exemplary Systems in Government (ESIG) awards** were first presented in 1981 to recognize outstanding achievement by government agencies in the use of geospatial information technology. This exemplary achievement is defined as the effective application of computer technologies and geospatial data that can be measured in terms of improved government service delivery and increased benefits to citizens. The award competition is international in nature and open to all public agencies at the local, regional, state/provincial and federal levels.

2020 ESIG Award winners are:

Single Process Systems

- **Winner:** City of Phoenix Street Transportation Department – Interactive Pavement Maintenance Dashboard
  Submitted by: Curtis Pulford, GIS Coordinator, City of Phoenix – Street Transportation Department, Phoenix, Arizona
- **Distinguished System:** Town of Flower Mound, Texas – Citizen Camera Program
  Submitted by: Nicole Dogan, GISP, Senior GIS Analyst, Town of Flower Mound, Texas

Enterprise Systems

- **Winner:** Palm Beach County Water Utilities Department – Enterprise GIS Portal Implementation
  Submitted by: Danny Thorpe, Systems Administrator III, Palm Beach County Water Utilities Department, West Palm Beach, Florida
- **Distinguished System:** Maryland National Capital Park & Planning Commission – PGAtlas
  Submitted by: Michael Shean, GISP, GIS Supervisor, Maryland National Capital Park & Planning Commission, Upper Marlboro, Maryland

To review the winning submissions for this year's ESIG Awards, visit http://www.urisa.org/awards/exemplary-systems-in-government/.

For details about GIS-Pro 2020, visit www.gis-pro.org

PE&RS
PHOTOGRAMMETRIC ENGINEERING & REMOTE SENSING
The official journal for imaging and geospatial information science and technology
November 2020 Volume 86 Number 11

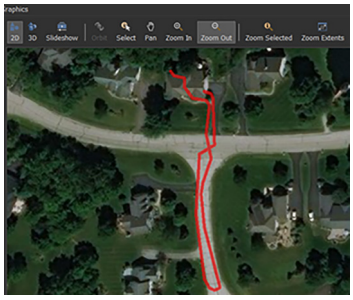

2021 ASPRS Scholarship Application Season Now Open
See page 669 for details

See the Cover Description on Page 656

COVER DESCRIPTION

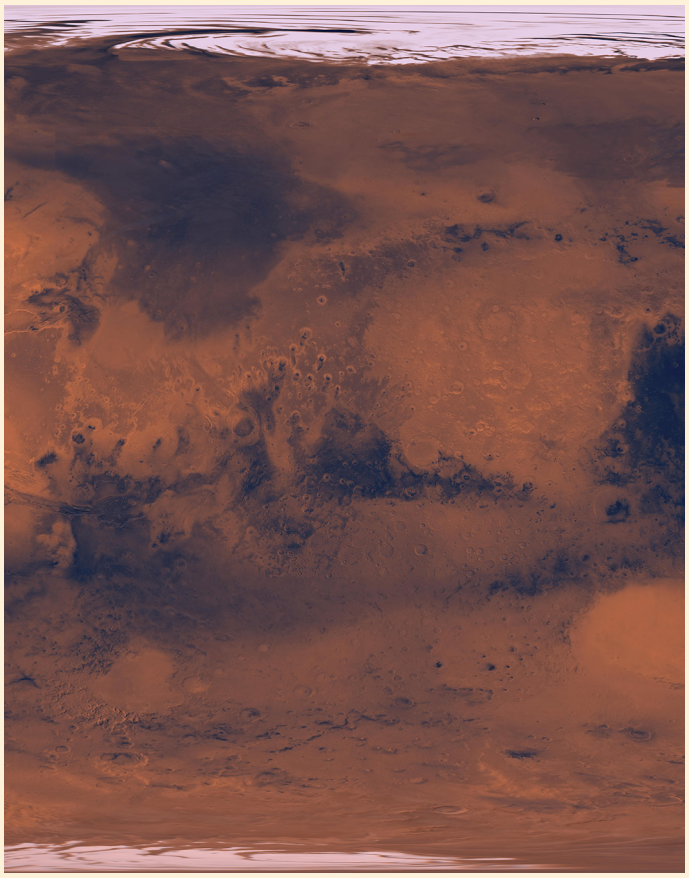

Much of Dr. Sherman Wu's work with USGS involved mapping other planets, including Mars. For this reason, this month's cover of PE&RS uses an an image mosaic of Mars from the Mars Viking Orbiter mission.

Mars Viking Global Color Mosaic 925m v1

About 1000 Viking Orbiter red- and violet-filter images have been processed to provide global color coverage of Mars at a scale of 925 meters per pixel (m). Individual image frames acquired during a single spacecraft revolution ("rev") were first processed through radiometric calibration, cosmetic cleanup, geometric control, reprojection, and mosaicking. We have produced a total of 57 "single-rev" mosaics. Phase angles range from 13 to 85 degrees. All of the mosaics are geometrically tied to the Mars Digital Image Model (MDIM), a black-and-white base map with a scale of 231 meter per pixel (m).

In producing a global mosaic from Viking images with useful color and albedo information for the surface, the largest challenge has been the photometric normalization, including removal of atmospheric effects. First, we selected a subset of single-rev mosaics that provide the best global coverage (the least atmospheric obscuration and seasonal frost). A Minnaert photometric normalization was applied to normalize the variations in illumination and viewing angles. Image data acquired at illumination or emission angles larger than 77 degrees were trimmed off, as these data are strongly affected by atmospheric scattering.

A model image of condensate haze was created from the violet images, consisting of 60% of the violet-filter reflectance greater than 0.05, smoothed over 20-km scales. The haze model was then subtracted from both the violet- and red-filter images. The residual polar caps were excluded from haze removal. This procedure is "conservative" in the sense that it errs on the side of under-correcting for the haze.

Finally, these normalized mosaics were combined into global mosaics. Global coverage is about 98% complete in the red-filter mosaic and 95% complete in the violet-filter mosaic. A green-filter image was synthesized from an average of the red- and violet-filter data to complete a three-color set.

Original image and data can be found here: https://astrogeology.usgs.gov/search/map/Mars/Viking/Color/Mars_Viking_ClrMosaic_global_925m

PHOTOGRAMMETRIC ENGINEERING & REMOTE SENSING

asprs
THE IMAGING & GEOSPATIAL INFORMATION SOCIETY

Journal Staff

Publisher ASPRS
Editor-In-Chief Alper Yilmaz
Assistant Editor Jie Shan
Assistant Director — Publications Rae Kelley
Electronic Publications Manager/Graphic Artist
Matthew Austin

Photogrammetric Engineering & Remote Sensing is the official journal of the American Society for Photogrammetry and Remote Sensing. It is devoted to the exchange of ideas and information about the applications of photogrammetry, remote sensing, and geographic information systems. The technical activities of the Society are conducted through the following Technical Divisions: Geographic Information Systems, Photogrammetric Applications, Lidar, Primary Data Acquisition, Professional Practice, and Remote Sensing Applications. Additional information on the functioning of the Technical Divisions and the Society can be found in the Yearbook issue of *PE&RS*.

Correspondence relating to all business and editorial matters pertaining to this and other Society publications should be directed to the American Society for Photogrammetry and Remote Sensing, 425 Barlow Place, Suite 210, Bethesda, Maryland 20814-2144, including inquiries, memberships, subscriptions, changes in address, manuscripts for publication, advertising, back issues, and publications. The telephone number of the Society Headquarters is 301-493-0290; the fax number is 225-408-4422; web address is www.asprs.org.

PE&RS. *PE&RS* (ISSN0099-1112) is published monthly by the American Society for Photogrammetry and Remote Sensing, 425 Barlow Place, Suite 210, Bethesda, Maryland 20814-2144. Periodicals postage paid at Bethesda, Maryland and at additional mailing offices.

SUBSCRIPTION. For the 2020 subscription year, ASPRS is offering two options to our *PE&RS* subscribers — an e-Subscription and the print edition. E-subscribers can plus-up their subscriptions with printed copies for a small additional charge. Print and Electronic subscriptions are on a calendar-year basis that runs from January through December. We recommend that customers who choose both e-Subscription and print (e-Subscription + Print) renew on a calendar-year basis.

The rate of the e-Subscription (digital) Site License Only for USA and Non-USA is $1000.00 USD. e-Subscription (digital) Site License Only for Canada* is $1049.00 USD. e-Subscription (digital) Plus Print for USA is $1365.00 USD. e-Subscription (digital) Plus Print for Canada* is $1424.00 USD. e-Subscription (digital) Plus Print for Non-USA is $1395.00 USD. Printed-Subscription Only for USA is $1065.00 USD. Printed-Subscription Only for Canada* is $1124.00 USD. Printed-Subscription Only for Non-USA is $1195.00 USD. *Note: e-Subscription/Printed-Subscription Only/e-Subscription Plus Print for Canada include 5% of the total amount for Canada's Goods and Services Tax (GST #135123065). **PLEASE NOTE: All Subscription Agencies receive a 20.00 USD discount.**

POSTMASTER. Send address changes to *PE&RS*, ASPRS Headquarters, 425 Barlow Place, Suite 210, Bethesda, Maryland 20814-2144. CDN CPM #(40020812)

MEMBERSHIP. Membership is open to any person actively engaged in the practice of photogrammetry, photointerpretation, remote sensing and geographic information systems; or who by means of education or profession is interested in the application or development of these arts and sciences. Membership is for one year, with renewal based on the anniversary date of the month joined. Membership Dues include a 12-month electronic subscription to *PE&RS*. Or you can receive the print copy of *PE&RS* Journal which is available to all member types for an additional fee of $60.00 USD for shipping USA, $65.00 USD for Canada, or $75.00 USD for international shipping. Dues for ASPRS Members outside of the U.S. will now be the same as for members residing in the U.S. Annual dues for Regular members (Active Member) is $150.00 USD; for Student members $50.00 USD for USA and Canada $58.00 USD; $60.00 USD for Other Foreign members. A tax of 5% for Canada's Goods and Service Tax (GST #135123065) is applied to all members residing in Canada.

GIS Tips & Tricks

James Parker and
Al Karlin, Ph.D. CMS-L, GISP

FME Tool Tips

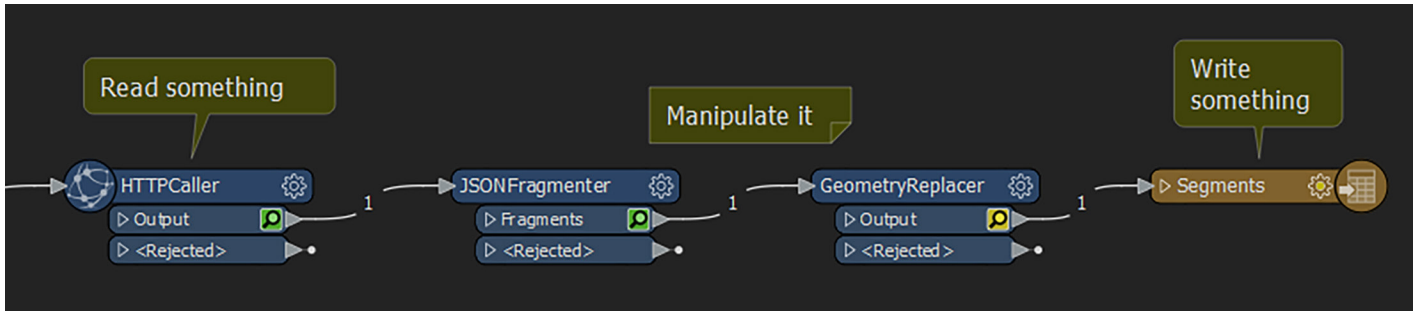

For this month's Tips & Tricks, I am turning the column over to a guest writer, Mr. James Parker, with Dewberry Geospatial and Technology Services group. James joined Dewberry several months ago and was anxious to share some software tips he had developed with a previous firm. As I am always looking for alternative ways to perform GIS tasks, this seems like a perfect opportunity. (I also encourage others to contribute to this column with your personal favorites.)

FME (standing for Feature Manipulation Engine) is my favorite spatial data ETL (Extract, Transform & Load) and automation tool. It's developed by Safe Software – no they're not an antivirus company – who'll tell you it does far more than convert GIS data from one format to another. And if you're a seasoned user you'll know that to be true.

I only started using FME about three years ago whilst working for a very large energy firm. Before I took the job, I exaggerated my experience with FME, which was pretty much limited to using Esri's Interoperability extension and making a 'Hello World' workbench. But I soon learned my new employer used FME to automate pretty much everything, and I was going to be spending a lot of time with my head in a workbench. Did I get away with it? I think so. Luckily workbench is very intuitive. It's essentially a drag and drop model builder. The basic workflow follows the format: (1) You usually read some data, (2) manipulate that data, and then (3) write it somewhere else. When you've debugged and tested it, you can set it up to run on a schedule and reach for the hammock. This image below is me reading data about a jog I did from Strava.com, turning JSON into a polyline, and writing to a feature service on ArcGIS Online. Easy!

So… here are my Top 5 tips for using FME (not necessarily in order):

1. **Keep your workbench clean!** Write every workbench as if you'll hand it over to someone who knows nothing about the data or problem set. Use Annotation liberally. Use bookmarks to group transformers. Collapse those groups if it makes the workbench easier to view. Instead of having crazy long connector lines, tunnel them straight to where they're headed (right click > Create Tunnel). Or at least add some vertices so lines don't cut across everything else. Use junctions to bring connection lines back together before they go into transformers. You'll be glad you did all this when you open a workbench you haven't seen in a while.
2. **Apply your style.** Change the theme, label colors, connector line shapes and more. Go into Tools > FME Options > Appearance and setup things how you like them. You'll see from my screenshots I like the dark theme.
3. **Setup some background maps to the Graphics view.** You can preview your data on a map at any stage of your model. But by default, there is no base map. Spend a moment setting up your favorites from some of the most common in-built sources. Right click Graphics View > Background Map. The squiggly feature on the left could be anything, anywhere. By adding a basemap I can see it's a short neighborhood walk, projected correctly.

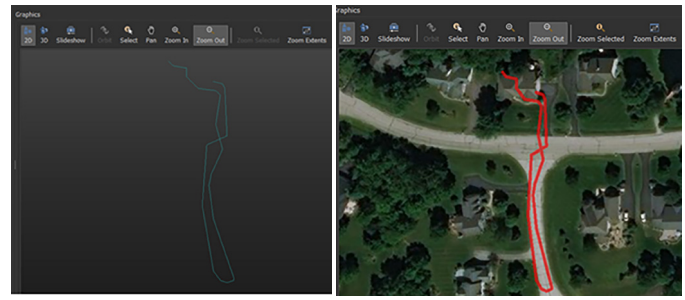

Photogrammetric Engineering & Remote Sensing
Vol. 86, No. 11, November 2020, pp. 657–658.
0099-1112/20/657–658

doi: 10.14358/PERS.86.11.657

5. **Mind that table handling.** When writing records to database tables FME gives you a few options - choose wisely. You can drop and recreate tables, append to tables or truncate records in existing tables. I often use database tables as the source for web services. A common problem is accidentally breaking your web service by dropping a table with FME, instead of appending or truncating.

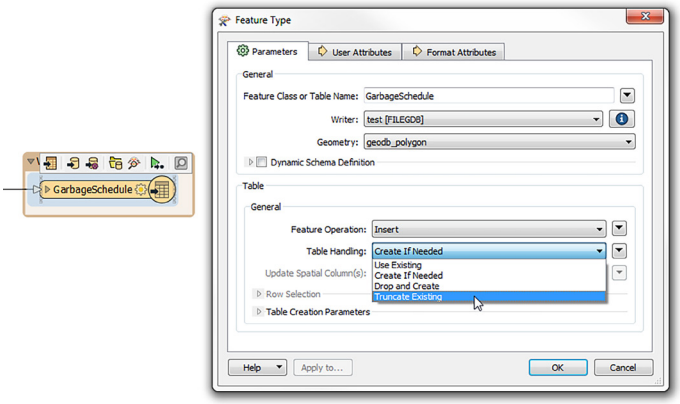

6. **Ctrl + E.** Highlight and disable whole strands of your models with this keyboard shortcut. You'll do this all day long.

BONUS TIP: I picked up lots of tips and tricks along my short journey with FME. I learned through trial and error, by asking colleagues, and by using the Safe FME community. The latter is loaded with forum postings, FAQs, sample workbenches and lots more. **Check it out https://knowledge.safe.com/.**

James Parker, GISP and Al Karlin, Ph.D., CMS-L, GISP are with Dewberry's Geospatial and Technology Services group. James is a senior project manager with the Dewberry-Fairfax Office with a passion for location analytics and spatial information management. As a senior geospatial scientist, Al works with all aspects of Lidar, remote sensing, photogrammetry, and GIS-related projects.

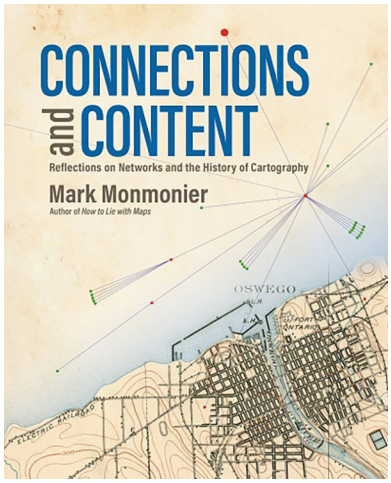

Connections and Content: Reflections on Networks and the History of Cartography

Mark Monmonier

Esri Press, Redlands, California. 2019. xiv and 275 pp, 90 black and white illustrations, index. Softcover. ISBN 978-1-58948-559-4. $39.99. eBook also available.

Reviewed by Stewart Walker, sole proprietor, photogrammetry4u llc, San Diego, California.

Mark Monmonier, distinguished professor of geography at Syracuse University and prolific book writer, is perhaps the world's best-known living cartographer. Readers have been entertained and educated by his *How to Lie with Maps*, though professional cartographers perhaps know him better for his editorship of the massive, encyclopedic *Cartography in the Twentieth Century*. Here he has written another intriguing volume, not a textbook, rather a "personal reflection on networks historically important in the development of cartography" (p xii), brimming with ideas for students and practitioners alike. Motivated by his fascination with networks, or interconnected systems, he picked topics that interested him, for example, the histories of surveying and mapping, and of the northeastern United States, and molded them into something gripping.

The structure of the book began thirty years ago, but it was not written until recently. Monmonier's family had no car: public transportation was a part of daily life, memories that nurture some portions of the book. There are seven chapters. Chapter 1, "Baselines," examines how the scale of maps depends on triangulation from measured baselines, while chapter 2, "Geometry," samples geodetic concepts - its focus on latitude and longitude dwells on the use of telegraphic networks to measure the latter. Though those grounded in land surveying would doubtless wish for more, it is amazing how much detail and instruction the author has packed into a few pages. Chapter 3, "Symbols," is more directly cartographic, quite fresh for those of us who left cartography for other geospatial pastures. Monmonier's examples from the upper New York region that he knows are successful. Chapter 4, "Infrastructure," is equally captivating, transiting from extensive material on canals to consideration of railroad and power networks. Chapter 5, "Telecommunications," is also eclectic and the better for it, charming the reader with the practicalities of collecting weather data across the US from the nineteenth century to the present day. Chapter 6, "Topology," introduces concepts from digital cartography, simply and persuasively, all the way to Google Maps, Waze, crowdsourcing, and positive train control. Chapter 7, "Control," is a *potpourri*, from the navigation of vehicles with and without human drivers (cars, trains, drones), to ARPANET, the internet and psephological musings on the electoral college and the definition of congressional districts. Maps, therefore, "… depend on networks of measurements, observations and other data to provide the content portrayed by cartographic symbols" and the reverse reliance is true too, since, "many networks … depend on maps for their design, planning, construction, maintenance and continued operation" (p 206).

There are two pages of acronyms and forty-one of notes, including not just references but useful, insightful comments. Readers can find, for example, information on the author's political convictions, interesting given his less than fulsome assessment of gerrymandering earlier in the book! Your reviewer's progress through the book was spurred, serendipitously, by a reference in the popular press[1] to Carl Abbott's *Imagined Frontiers: Contemporary America and Beyond*, where the role of boundary lines on maps is also pondered.

Your reviewer noticed but two typos in an attractive, copiously illustrated, well-produced book. In a discussion of scale errors (p 9), where readers are struggling to visualize the effect of incorrect measurement of the angles of an isosceles triangle (in the absence of the formula for the propagation of errors), 499.9 is printed as "4,999". A complaint on the incorrect placement of names on an 1850s government basemap (p 133) seems to confuse Oswego, NY with Owego, NY! Intriguingly, Esri Press deocates the outer margin of every page with a colored map excerpt that fades into the text, but the author's maps are monochrome because the book was originally planned to be printed in black and white. Monmonier

[1]Anon, 2020. Lexington: trouble in Trumplandia, *The Economist*, 436(9204): 21, 25 July.

Photogrammetric Engineering & Remote Sensing
Vol. 86, No. 11, November 2020, pp. 659–660.
0099-1112/20/659–660

doi: 10.14358/PERS.86.11.659

takes the opportunity to discuss how they were created – short descriptions that inform modern cartographers how to use greyscale to tell the story best.

Cartographic students and professionals may experience a stab of disappointment on opening this book. Maybe "Networks" in the title kindled an expectation of geometric rigor or conjured an image of a textbook with a new angle. Despite the author's assertion that "Maps as networks is an ideal theme for teaching and understanding the historical development of modern cartography" (p x), *Connections and Content: Reflections on Networks and the History of Cartography* does not meet these dreams. They should read it regardless and so should a broader public. As geospatial technologies diffuse through society, accessible works should be available to interested citizens. This is one: it links familiar aspects of the world with their depiction on maps in a compelling way and provides insights into the mapmaker's art. It is remarkably wide-ranging, yet the material is well woven into a cartographic cloth that we recognize. Let us enjoy the output of a doyen articulating his introspections, and learn about cartography as we do.

CALENDAR

- 30 November - 4 December 2020, **Climate Change and Disaster Management — Technology and Resilience in a Troubled World**, Sydney, Australia. For more information, visit https://conference.unsw.edu.au/en/ccdm2020.
- 28 January - 4 February 2021, **43rd COSPAR Scientific Assembly**, Sydney, Australia. For more information, visit https://www.cospar2020.org/.
- 7-11 June 2021, **URISA GIS Leadership Academy**, Minneapolis, Minnesota. For more information, visit www.urisa.org/education-events/urisa-gis-leadership-academy/.
- 16-20 August 2021, **URISA GIS Leadership Academy**, Portland, Oregon. For more information, visit https://www.urisa.org/education-events/urisa-gis-leadership-academy/.
- 8-12 November 2021, **URISA GIS Leadership Academy**, St. Petersburg, Florida. For more information, visit www.urisa.org/education-events/urisa-gis-leadership-academy/.
- 23-25 April 2021, **GISTAM 2021**, Prague, Czech Republic. For more information, visit www.gistam.org/.

Grids & Datums

The Lebanese Republic

BY Clifford J. Mugnier, CP, CMS, FASPRS

The Grids & Datums column has completed an exploration of every country on the Earth. For those who did not get to enjoy this world tour the first time, *PE&RS* is reprinting prior articles from the column. This month's article on the Lebanese Republic was originally printed in 2002 but contains updates to their coordinate system since then.

There is evidence of human habitation in Lebanon for several thousand years from the mid-3rd millennium B.C. that had been under the control variously of Sumerians, Akkadians, Amorites, Egyptians, Assyrians, and Babylonians. Once part of the Persian Empire, Alexander the Great conquered the region in the 4th century B.C., and it later flourished under the Roman Empire. Lebanon was overrun by Muslim Arabs in A.D. 635–636, and remained under the Turks during the Crusades until the British and French invaded during WWI because Turkey was an ally of Germany.

Lebanon is almost three-fourths the size of Connecticut, and is comprised of a narrow coastal plain; the Bekaa Valley separates Lebanon and the Anti-Lebanon Mountains. Bordered by Israel (79 km) to the south and by Syria (375 km) to the east and north; the western side of the republic is the Mediterranean Sea (225 km). Lebanon has a territorial sea claim of 12 nautical miles, and the highest point in the country is Qurnat as Sawda' at 3,088 m. The League of Nations declared the republic independent of the French Mandate on 22 November 1943.

In 1799, Napoleon Bonaparte commenced his military campaign for the conquest of Egypt and "Upper Egypt" (the Palestine and Greater Syria). *La Carte d'Egypte et de Syrie* was published by the *Dépôt de la Guerre* beginning in 1808. The ersatz Datum was based on astronomical observations in Cairo and Jerusalem, and was referenced to the Plessis ellipsoid where the semi-major axis a = 6,375,738.7 m and the reciprocal of flattening $1/f$ = 334.29. Much of the coast was actually based on published British Admiralty charts of the time (see The State of Israel, *PE&RS*, August 2000). The projection was the ellipsoidal Bonne, the "standard" for France and most of Europe at the time. "*Le centre de la projection correspond à l'axe de la grande pyramide du Nord, à Memphis.*" (The center of the projection corresponds to the axis of the great pyramid of the North at Memphis.)

The French *Expédition du Liban* (1860–1861) was made

after the massacre of Christians in Syria (and Lebanon) occurred during the months of May and June of 1860. After enforcing the peace, one topographic brigade remained to perform some exploratory mapping. Some minor triangulation was performed from Tyre to Tripoli along the coast. This resulted in one reconnaissance sheet at 1:100,000 scale, and one 1:200,000-scale sheet being published in 1862.

The early maps of Turkey, including the Levant area, were on the Bonne projection also, but the projection origin was the finial of the dome of the Aya Sofia Mosque. The Ottoman Turkish ellipsoidal Bonne of Syria, used from 1909 to 1923 (and the territory of what is now Lebanon), had a projection Latitude of Origin (φ_o) = 28° 58′ 50.8188″ N and the Central Meridian (λ_o) = 39° 36′ East of Greenwich. The geodetic network was calculated on the Clarke 1880 (IGN) ellipsoid where a = 6,378,249.2 m and $1/f$ = 293.4660208, and according to the *Service Géographique de l'Armée* (SGA), the Datum Origin was at the South End of the Base of Makri Keuî, near Constantinople (Istanbul). The 1:200,000- scale general map of Asia Minor was published in 1911 under the direction of General Mehmed Sevki Pacha,

Photogrammetric Engineering & Remote Sensing
Vol. 86, No. 11, November 2020, pp. 661–664.
0099-1112/20/661–664

doi: 10.14358/PERS.86.11.661

director of the Turkish Map Service. (In my column on Israel, I mistakenly referred to General Sevki as a Syrian officer.)

The French established the *Bureau Topographique du Levant* in 1918, and after 1920, the chain of triangulation was extended eastward along the northern border of Syria with Turkey to Iraq. The French geodetic triangulation parties were quite impressed with the Bekaa Valley and the vast bounty of orange and banana harvests. Planimetric compilation was aided by aerial photography flown by a French military aviation squadron of the 39th Regiment. The Topographic Brigade was commanded by Lieutenant Colonel G. Perrier, and he organized the observations for the establishment of an astronomical origin for a datum in the Bekaa Valley of Lebanon that would serve Syria as well. The baseline was measured, and the South End of the Base at Bekaa was the fundamental origin for the astronomical observations. The Latitude of the pillar was observed by Captain Volontat in 1920 with a prismatic astrolabe where Φ_o = 33° 45′ 34.1548″ N. An azimuth was obtained at the same pillar with a microscopic theodolite by Captain Volontat, by observing Polaris at elongation. The direction was defined to a pillar constructed at the Ksara Observatory where α_o = 28° 58′50.8188″. Longitude was also observed by Volontat at the same observatory where Λ_o = 35° 53′ 25.26″ East of Greenwich. (The longitude was then geodetically transferred to the South End of the Bekaa Base).

In November of 1997, Colonel George Massaad, then the director of Geographic Affairs of the Lebanese Army, sent a photograph to me of the fundamental point at Bekaa South Base. The point is monumented by a stone pyramid that is over 2 m high, is approximately 2 m square, has an (apparently) bronze tablet describing the significance of the monument, is straddled by a great iron skeleton target obviously over 4 meters high, and the entire structure is enclosed by a formal iron fence! The monument recalls the aviation accident that took the lives of Captains Govin and Renaud of the Geodetic Section of the SGA on 15 July 1924 at Muslimié, near Aleppo. Shortly after WWII, the U.S. Army Map Service computed the coordinates of the origin of the Bekaa geodetic system on the New Egyptian Geodetic Datum as φ = 35° 45′ 34.2205″ N and λ = 35° 54′ 36.4962″ E. The geodetic coordinates of station Ksara are φ = 33° 49′ 25.58″ N and λ = 35° 53′ 25.26″ E. The Bekaa Valley Datum of 1920 is referenced to the Clarke 1880 (IGN) ellipsoid as previously defined. A check baseline was measured at Bab in Syria, and another astronomical position was observed (Laplace Station) where Φ_o = 36° 13′ 48.77″ N, Λ_o = 37° 30′ 30.195″ East of Greenwich, and the reference azimuth from Bab to Cheikh Akil signal is α_o = 179° 58′ 33.152″. The triangulation was computed on the Clarke 1880 ellipsoid, Levant Zone Grid, Lambert Conical Orthomorphic projection.

The Levant Lambert Zone (1920) is based on the French Army Truncated Cubic formulae where the developed meridional arc is expressed in series form and is truncated at terms higher than the cubic. Furthermore, another idiosyncrasy of the French Army formulae is that the Lambert (fully) Conformal Conic utilizes one of the principal radii of the ellipsoid called the Radius of Curvature in the Plane of the Meridian (ρ). The French Army instead substitutes the Length of the Ellipsoid Normal Terminated by the Semi-Minor Axis (υ). Although not strictly conformal, this is the system which was commonly used by the French in all their colonies (before WWII) that utilized the Lambert Conic projection. The Levant Lambert Zone, also known as the Syrian North Lambert Zone, has a Latitude of Origin (φ_o) = 34° 39′ N and the Central Meridian (λ_o) = 37° 21′ East of Greenwich. The Scale Factor at Origin (m_o) = 0.9996256 (secant conic) and the False Easting and False Northing = 300 km. The scale of the triangulation was governed by the two bases (Bekaa and Bab) which had an internal precision of one part in two million. In the case of the initial azimuth of the Bekaa Base, a large number of observations were made in order to determine the mean azimuth. The maximum range of the observations was 48″ which does not represent good geodetic accuracy. Then a check azimuth, Latitude, and Longitude were measured at the Bab Base at Aleppo in Syria, and the differences from the geodetic values mathematically carried through the chain from Bekaa are as follows (Astronomic ″ Geodetic): $\Delta\varphi$ = –6.318″, $\Delta\lambda$ = +10.789″, and $\Delta\alpha$ = +21.125″. Thus the SGA decided not to apply a Laplace correction to the azimuths, assuming the 21″ was due to an error at the origin and not over the network. That 21″ error was later verified by the U.S. Army Map Service (AMS), in the 1950s. AMS computed an azimuth between two stations in the area utilizing the geodetic coordinates of the station in terms of the European Datum Mediterranean Loop and the Bekaa Valley Datum values.

The Tripoli Lambert Grid of 1920 origin is based on the North End of the Tripoli Base where the Latitude of Origin (φ_o) = 34° 27′ 04.7″ N and the Central Meridian (λ_o) = 35° 49′ 01.6″ East of Greenwich. The Scale Factor at Origin (m_o) = 1.0 (tangent conic), and the False Easting and False Northing = zero. This quite obscure grid was probably used only for a hydrographic survey in the vicinity of Tripoli, and the South End of the Tripoli Base cartesian coordinates were published by the French as X = +1,257.02 m and Y = –1,197.29 m. Considering the tiny geographic extent of the survey, the Hatt Azimuthal Equidistant or the Roussilhe Oblique Stereographic equations would yield the same transformation results to cartesian coordinates.

In 1922, the *Travaux du Cadastre et d'Amelioration Agricole des Etats, de Syrie, des Alaouites et du Liban sous Mandat Francais* established the SCHEMA DE LA PROJECTION STÉRÉOGRAPHIQUE which was based on the Roussilhe Oblique Stereographic projection. The Latitude of Origin (φ_o) = 34° 12′ N, the Central Meridian (λ_o) = 39° 09′ East of Greenwich, the Scale Factor at Origin (m_o) = 0.9995341 (secant plane), and the False Easting and False Northing = zero. This grid has caused some consternation in the literature because attempts to substitute the fully conformal formulae of Paul D. Thomas' "Conformal

continued on page 664

GREETINGS FROM THE ASPRS STUDENT ADVISORY COUNCIL (SAC)!

At SAC we are encouraging the broader ASPRS Chapter community to become more involved in the SAC community network. As part of this effort, we are highlighting the Portland Community College (PCC) ASPRS/GIS Club for their innovative community mapping projects and to introduce their elected officers - *https://pccgisclub2020.wixsite.com/mysite-2*

The Portland Community College (PCC) GIS Club is a professionally-focused academic club that is open to all PCC students who are interested in GIS. The students come from a variety of academic backgrounds, including the geosciences, education, and real estate. Student experiences range from mid-career professionals to students just now beginning GIS.

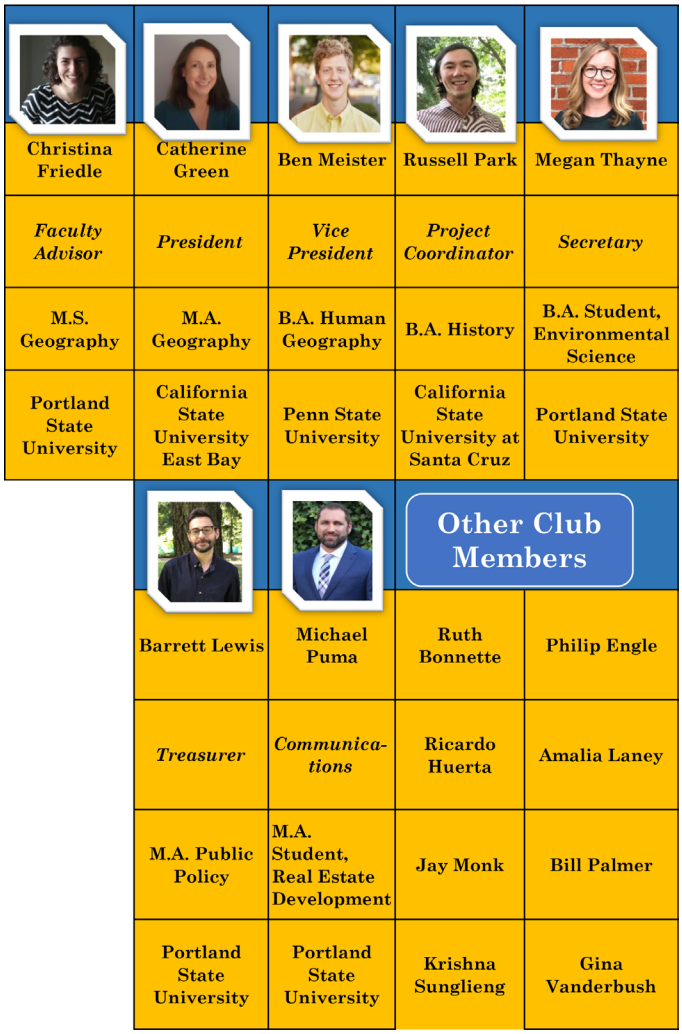

A Few Club Opportunities

- technical skill workshops
- community mapping projects
- leadership development
- project management
- Portland area networking

Last year, the PCC GIS Club organized a UAS workshop, a GIS Programming workshop, and a Red Cross Missing Maps Mapathon.

Educational Outreach Highlights: Art Murals & Black Lives Matter

Art Murals

Each year the GIS Club works on a group project, and this year we chose to create an interactive map of art murals in the Portland Metro Area. Mural art is significant part of Portland's urban landscape, that brings art installations into the streetscape. It's a democratic cultural expression that makes art available to all, not just those who visit art galleries. Many of the murals tell the story of Portland's history or ecology. In January 2020, we envisioned the project as an engaging way the students could learn more about their city, and work together in the GIS lab to share

skills and learn new methods. Unfortunately, with the arrival of COVID-19 in our community in March, we were forced to adjust our vision of working together in person and participating in field trips to view murals and meet artists to adapt to social distancing. Despite these obstacles, we were motivated to continue and create this resource. We held planning meetings and skills trainings remotely, every other week at first, and then every week. The more experienced students trained others on how to collect data using Esri's ArcGIS Collector mobile app. We also discussed research methods to compile information about each mural and artist to form a full informational picture of each mural that was incorporated into the web map. We also conducted remote training of how to use the mapping software; and formed a work group specifically to design and create an interactive map using Esri's ArcGIS Online.

Black Lives Matter

Our original idea was to create a single feature layer of art murals. But some students noticed a number of murals were painted directly on street intersections from community organizing. We decided to create a separate feature layer for these intersections because they were significantly different from other art murals and a challenge to photograph. We used a UAS to capture photos from above. PCC offers classes preparing students to become UAS pilots, so we used our classroom knowledge to plan the flights, scout the locations, and photographed the murals with an UAS, once the dense smoke from the severe fires along the West Coast dissipated. Additionally, as we worked on the project, Black Lives Matter protests occurred nightly in Portland, Artists and community members collaborated in creating Black Lives Matter-themed street art on boarded-up buildings. While these impermanent art works did not fit our initial criteria, we thought they were significant and that it was important to document these political and cultural expressions. We created another separate feature layer to collect these important mural points. Between the movement for Black Lives Matter, the disruption due to extreme wildfires, and COVID-19 impacts, our GIS project essentially became a time capsule reflecting the events of 2020.

Media Links

Email photogrammetry@oregonstate.edu
Instagram https://www.instagram.com/asprs1868/
OSU Club Website https://clubs.oregonstate.edu/asprs
Twitter https://twitter.com/asprs1868

Grids & Datums *continued from page 662*

Projections" fail to yield correct transformation results. In fact, the Roussilhe (Russell) formulae were developed by the Hydrographer of the French Navy in the late 19th century, and this is a common grid used on many hydrographic surveys by the French well into the 20th century.

The latest available transformation parameters from the Bekaa Valley Datum of 1920 to the WGS84 Datum are $\Delta X = -182.966$ m, $\Delta Y = -14.745$ m, and $\Delta Z = -272.936$ m. The mean planimetric error for these parameters is 5 meters. Example test point: Bekaa Datum Origin: $\varphi = 33°\ 45'\ 34.1548''$ N, $\lambda = 35°\ 54'\ 37.1188''$ E, and H = 870.513 m. WGS84 Datum coordinates of the same point are $\varphi = 33°\ 45'\ 33.8602''$ N, $\lambda = 35°\ 54'\ 40.6802''$ E, and h = 868.64 m. According to NIMA TR 8350.2, transformation parameters from the European Datum 1950 to WGS84 Datum are $\Delta X = -103$ m, $\Delta Y = -106$ m, and $\Delta Z = -141$ m for Lebanon.

LEBANON UPDATE

According to the World Bank,
"The leading geospatial agency in Lebanon is the Directorate of Geographic Affairs of the Lebanese Army (GAD), which produces topographical mapping and geospatial data for both military and civil purposes. The Directorate's products can be purchased subject to case by case approval. In an attempt to open broader access through a National Spatial Data Infrastructure (NSDI) approach, the Ministry of Administrative Reforms (OMSAR) implemented a GIS portal few years ago, and created a NSDI regulatory framework and coordination mechanism for access to geospatial data, but the implementation failed due to lack of funding or sustainable arrangements for coordination, access, sharing and dissemination of data. However, there was progress in standardization and for example the Lebanon-Syria coordinate reference system is used for all mapping in Lebanon and thus, the most important key standard for NSDI is being applied."

The World Bank Land Administration System Modernization Project (P159692)

This column was previously published in *PE&RS*.

Sherman Wu

1928-2020

Dr. Sherman Shou-Chou Wu passed away on August 22, 2020 at the age of 92 with family members by his side. With his passing, our profession lost a very unique person who was a renowned leader in the field of planetary photogrammetry and topographic mapping. He was an avid supporter of ASPRS and ISPRS and his contributions to the field have had a significant global impact. Dr. Wu's colleagues and friends will miss him greatly.

As background to Dr. Wu's significant scientific achievements, it is of interest to note his humble beginnings in his hometown, a remote village in China accessible only by foot. When he visited, the villagers would welcome their celebrity home with banners and firecrackers in the Chinese tradition. They also prepared a feast to show their respect and to thank him for the roads and schools he built for them. They are currently working to erect a monument in his honor as a beacon of hope to future generations.

From those humble beginnings, Sherman was only able to attend college through a scholarship from a military school, although anyone who knew Sherman knows he didn't fit the model of a military man.

Sherman later attended The Ohio State University for his Ph.D. while Dr. Fred Doyle was Chairman of the Department of Geodetic Sciences. However, he did not complete his dissertation while at Ohio before getting a job with USGS. He completed his dissertation while working and received his Ph.D. from the University of Arizona.

Dr. Wu began his professional career in 1965 with the U.S. Geological Survey (USGS) in the Branch of Astrogeology as a photogrammetrist. For over 30 years he made significant contributions to planetary mapping by engineering a mapping program for NASA which was essential to the planetary exploration program for the Moon, Mars, Venus, Jupiter and their satellites. The topographic maps and products of this program were critical to planning and executing many of NASA's space flight missions including Ranger, Lunar Orbiter, Apollo, Mariner 9, Viking, Voyager, SIR-B and the Magellan radar mission to Venus.

The results of Dr. Wu's research contributions are represented in over 150 published papers in journals and book chapters including the *Encyclopedia of Planetary Science*, the ASPRS *Manual of Photogrammetry*, *Nature*, *International Journal of Solar System Studies*, and chapters of planetary science by Cambridge University, University of Arizona, ASPRS and ISPRS journals, and NASA's Lunar and Planetary Science conference proceedings and special publications. He shared his knowledge and research findings to the planetary community by organizing numerous national and international scientific and technology conferences which also bought others together to share their research work.

He advanced in his career at the USGS to become the supervisory physical scientist in charge of the Branch of Astrogeology photogrammetry group. He is recognized as one of the world's rare authorities and leader in planetary topographic mapping for which he received the Department of the Interior's Meritorious Service Medal.

Dr. Wu's supervisor and co-workers also contributed their memories of Sherman while at USGS. Dr. Jerry Schaber was the Chief of the Branch of Astrogeology and described Sherman as a good supervisor and one of the best section managers in the Branch. He relied on Sherman to just get the job done with limited funding through his resourcefulness and professional contacts. Sherman is often fondly called a "wheeler-dealer" or an "operator", meaning that whatever task he undertakes, no matter how difficult or complex, he will find the necessary resources, support, and personnel to achieve it well.

Annie Howington and Jenny Blue who have fond memories of working for Sherman as students recall that he only hired students that made straight A's but also said that he was always looking out for their careers even though they didn't realize it at the time.

The Asteroid (2075) discovered on October 9, 1980 was named after Dr. Wu's (WU) in honor of his unique achievements and contributions in the field of planetary topographic mapping.

Everyone also knew that Sherman would know that he would not let retirement from the USGS be the end for passion for working and learning new technologies. It was no surprise that he soon started working for Bechtel Nevada's Remote Sensing Laboratory where he worked on application of new technologies including Radar, Lidar, and Interferometric Radar (IFSAR) to construction projects. Of course, as always, Sherman was dedicated to his work and he received Bechtel Nevada's Science and Engineering Award in 2002. Laure Ogiela along with other co-workers in Image Science Section of the Remote Sensing Laboratory summarizes Dr. Wu's characteristics as: brilliant, intellectual, resourceful, creative, aggressive, persistent, patient, enthusiastic, passionate, inspirational, likeable, lovable, and a hard worker with a great sense of humor and highly skilled at interpersonal relationships. Others who have come to know Sherman would probably agree. Heather Gledhill, another co-worker, in the Remote Sensing Laboratory describes Sherman as "My Best Teacher and Best Mentor." Dr. Wu can be proud of what he has done for the profession and what he has done for others.

Dr. Wu's career awards and honors also include the ASPRS Fairchild (Photogrammetric) Award in 1992, the ISPRS

Gino Cassinis Award in 2004, and the Outstanding Alumnus Award from the National Defense University's Chung-Cheng Institute of Technology. Dr. Wu believed in the significant value of giving back to his profession and was a career-long member and contributor to both ASPRS and ISPRS.

An ISPRS special conference was held in Urcumchi, China in 2008 to celebrate Dr. Wu's 80th birthday. His colleagues, co-workers, friends and family members were invited to share their thoughts, memories and pictures for this event. The proceedings of this celebration provide a complete picture of Dr. Wu's academic background, his professional career and his contributions and achievements. Moreover, they provide a glimpse of his values and his philosophy on life. Among those who contributed to this event included Dr. Frederick Doyle, Dr. Gottfried Konecny, Dr. John Trinder, Dr. Charles Toth and Larry Fritz. Each of these luminaries in ISPRS acknowledged the significance of Dr. Wu's research and contributions to the field of planetary mapping and considered him as an esteemed scientific colleague. Moreover each of these leaders in ISPRS considered Sherman as a personal friend and described his generosity and give back attitude. He is well known as the ultimate host by his ISPRS colleagues, co-workers and friends. Although Sherman was always very busy with his work, Sherman always made time to contribute significantly to the activities of the ASPRS and ISPRS. When Dr. Wu received the prestigious ISPRS Gino Cassinis Award in 2004 which includes a significant honorarium, he promptly doubled it and donated it to the ISPRS Foundation's Scholarship Fund.

Even while contributing significantly to the photogrammetry and remote sensing profession, Sherman was actively involved in his x children's lives and, just as he pushed himself and his employees towards excellence, he also pushed his children to perform well in school. Even games they played as children had mathematical lessons it in. While his children probably thought it as "Forced learning" because there were no summer vacations for them since Sherman had summer assignments for them. It must have "taken" given all of them have achieved significant academic and professional success. As accomplished adults they now understand the love of their father and the struggles he endured to get his own education. Sherman appreciated the richness (value?) that an education brought to him and he wanted no less for his children. One of his daughter describes "The Seven Axioms of Sherman Wu which was Sherman's philosophical "rulebook" which he believed everyone should live their lives. One phrase he liked very much was, "Imagination is more important than knowledge." Sherman used his imagination to get things done.

And, last but not least, while Sherman enjoyed working and learning new things, he also enjoyed hosting dinners for his friends and family as well as playing blackjack. He is known for his card-counting in Las Vegas casinos but John Rush, Supervisor and Manager, at the Bellagio Casino considered Sherman a friend and welcomed his visits, saying that "Sherman wins a prodigious amount of the time, but is a gentleman win and lose."

So, for all who knew Dr. Sherman Wu, we would agree that he worked hard, played hard, and was respected by all.

PE&RS SEEKS HIGHLIGHT ARTICLES

Are you looking for publishing opportunities? Consider publishing a Highlight Article in *PE&RS*.

PE&RS Highlight Articles are semi-technical or non-technical articles that appeal to a broad range of industry professionals. A variety of topics in geospatial science and technology, photogrammetry, and remote sensing can be addressed.

- geomatics education and programs
- new technologies
- non-traditional applications
- historical events and development
- collaborative initiatives
- new or unusual approaches to common problems
- recent or historical developments in technology or the industry

PE&RS Highlight Articles are always open access, published in color, and assigned a DOI number. For more information on this publishing opportunity or to discuss other opportunities, contact Rae Kelley, rkelley@asprs.org.

NEW ASPRS MEMBERS

ASPRS would like to welcome the following new members!

At Large
Dr. Abdulla Al-Rawabdeh
Leo Stalin
Christina Aragon
Varun Aditya Mittagunta
Renga Samy
Tarini Shukla
John M. Skelton, III

Cascadia
McKenzie Scott Kramer

Central New York
Scot Harrigan

Columbia River
Nicholas Garnder

Eastern Great Lakes
Peter Timashenka
Brendan Welsh

Florida
Eric John Archer
Dr. Eve Bohnett

Heartland
Wesley Street
Dr. Samson Tesfaye

Intermountain
Brandi Flanagan

Mid South
Randall Grip
Christopher Morris
George Jamal Pualwan

North Atlantic
Christopher M. Sanfino, CP

- Pacific Southwest

Gencaga Aliyazicioglu, CP
James Alan Riechel

Potomac
Dana Curtis
James Lance

Rocky Mountain
Matthew Emmett
Sara Marie Hedrick

Western Great Lakes
Cadan Cummings

FOR MORE INFORMATION ON ASPRS MEMBERSHIP, VISIT
HTTP://WWW.ASPRS.ORG/JOIN-NOW

Your Path To Success In The Geospatial Community

WHO'S WHO IN ASPRS

BOARD OF DIRECTORS

BOARD OFFICERS

President
Jeff Lovin
Woolpert

President-Elect
Jason M. Stoker, Ph.D
U.S. Geological Survey

Vice President
Christopher Parrish, Ph.D
Oregon State University

Past President
Thomas Jordan, Ph.D.
University of Georgia

Treasurer
Stewart Walker, Ph.D.

Secretary
Lorraine B. Amenda, PLS, CP

BOARD MEMBERS

Sustaining Members Council – 2021
Chair: Joe Cantz
www.asprs.org/About-Us/Sustaining-Members-Council.html

Committee Chairs Council – 2022
Chair: Mike Zoltek
Vice-Chair: TBA

Early-Career Professionals Council – 2021
Chair: Bobby Arlen
Vice Chair: Melissa Martin

Region Officers Council – 2021
Chair: Lorraine B. Amenda, PLS, CP
Vice Chair: Demetrio Zourarakas

Student Advisory Council – 2021
Chair: Youssef Kaddoura
http://www.asprs.org/Students/Student-Advisory-Council.html

Technical Division Directors Council – 2021
Chair: Bandana Kar, Ph.D
Vice Chair: Denise G. Theunissen

TECHNICAL DIVISION OFFICERS

Geographic Information Systems Division – 2021
Director: Xan Fredericks
Assistant Director: Denise G. Theunissen
www.asprs.org/Divisions/GIS-Division.html

Lidar Division – 2022
Director: Joshua Nimetz, CMS
Assistant Director: Ajit Sampath
www.asprs.org/Divisions/Lidar-Division.html

Photogrammetric Applications Division – 2022
Director: Kurt Rogers
Assistant Director: Benjamin Wilkinson
www.asprs.org/Divisions/Photogrammetric-Applications-Division.html

Primary Data Acquisition Division – 2021
Director: Jon Christopherson
Assistant Director: J. Chris Ogier
www.asprs.org/Divisions/Primary-Data-Aquisition-Division.html

Professional Practice Division – 2022
Director: Harold W. Rempel, III, CP
Assistant Director: Bill Swope
www.asprs.org/Divisions/Professional-Practice-Division.html

Remote Sensing Applications Division – 2022
Director: Raechel A. Portelli, Ph.D.
Assistant Director: Amr Abd-Elrahman
www.asprs.org/Divisions/Remote-Sensing-Applications-Division.html

Unmanned Autonomous Systems (UAS) – 2022
Director: Megan Ritelli, Ph.D.
Assistant Director: Dan Hubert

REGION PRESIDENTS

Alaska Region
David Parret
http://www.asprsalaska.org/

Cascadia Region
Robert Hairston-Porter

Eastern Great Lakes Region
Shawana P. Johnson, Ph.D, GISP
http://egl.asprs.org/

Florida Region
Xan Fredericks
http://florida.asprs.org/

Heartland Region
Whit Lynn
http://heartland.asprs.org/

Mid-South Region
https://www.asprs.org/all-regions/mid-south.html

Northeast Region
(representing the merger of The New England and Central New York Regions)
Trevis Gigliotti, Interim President

North Atlantic Region
Richard W. Carlson, Jr., P.L.S., C.P.
http://natlantic.asprs.org/

Pacific Southwest Region
Omar G. Mora
https://pswasprs.org/

Potomac Region
Dave Lasko
http://www.asprspotomac.org/

Rocky Mountain Region
http://www.asprs-rmr.org/

Western Great Lakes Region
Brandon Krumwiede
http://wgl.asprs.org/

ASPRS ANNOUNCES THE OPENING OF THE 2021 SCHOLARSHIP APPLICATION SEASON!

ASPRS is pleased to offer nine scholarship awards totaling more than $30,000 in value! Available to both undergraduate and graduate student members of ASPRS, these resources have been generated with the intention of advancing academic and professional goals in the geospatial sciences. ASPRS recognizes that students are the future of these rapidly evolving fields and encourages all who are qualified to take advantage of these unique opportunities.

IMPORTANT DATES

- Scholarship Application Window: September 30 – November 15
- Letters of recommendation deadline: November 22
- Anticipated Award Announcements Mid-Late January
- Award winners will be honored at the ASPRS 2021 Annual Meeting

All complete applications must be received at ASPRS no later than midnight, Eastern time on November 15, 2020. The deadline for recommendation letters is November 22, 2020.

Visit www.asprs.org/education/asprs-awards-and-scholarships for more information!

Summary of ASPRS Awards & Scholarships

Award/ Short name	Eligibility	Type of Grant	Grant Amount	Expectations
Altenhofen	Undergraduate or Graduate Students	One Year Award	$2,000	Report of scholastic accomplishments to ASPRS
Anson*	Undergraduate Students; USA Only	One Year Award	$2,000	Final Report to ASPRS
Behrens*	Undergraduate Students; USA Only	One Year Award	$2,000	Final Report to ASPRS
Colwell*	Doctoral Students USA or Canada	One Year Award	$7,000	Final Report to ASPRS
Fischer	Current or Prospective Graduate Students	One Year Award	$2,000	Final Report to ASPRS
Moffitt*	Graduate or Undergraduate Students	One Year Award	$7,000	Final Report to ASPRS
Osborn*	Undergraduate Students; USA Only	One Year Award	$2,000	Final Report to ASPRS
Ta Liang	Graduate Students	Travel Grant	$2,000	Report of accomplishments to ASPRS and to Ta Liang's family
Wolf	Prospective Teachers/Graduate Students; USA only	One Year Award	$4,000	Final Report to ASPRS

*Recipient also receives a complementary membership renewal in ASPRS.

Francis H. Moffitt Scholarship

The purpose of the award is to encourage upper-division undergraduate and graduate-level college students to pursue a course of study in surveying and photogrammetry leading to a career in the geospatial mapping profession.

Eligibility

Students currently enrolled or intending to enroll in a college or university in the United States or Canada, who are pursing a program of study in surveying or photogrammetry leading to a career in the geospatial mapping profession.

Award

- The award consists of a certificate and a check in the amount of $7,000 and a one-year student membership (renewal) in ASPRS.
- This award is presented by ASPRS through the ASPRS Foundation from funds donated by students, associates, colleagues, and friends of Frank Moffitt as a memorial to his lifetime contributions to the photogrammetric surveying profession.

William A. Fischer Scholarship

To facilitate graduate-level studies and career goals directed towards new and innovative uses of remote sensing data/techniques that relate to the natural, cultural, or agricultural resources of the Earth.

Eligibility

Current or prospective graduate student members of ASPRS.

Award

- One year scholarship of $2,000 and a certificate.
- This award is presented by ASPRS with funding provided by a grant from the ASPRS Foundation, on behalf of individual and corporate contributions to the Foundation in memory of William A. Fischer, a pioneer in the use of remote sensing from space for the study of the planet Earth.

Robert N. Colwell Fellowship

The purpose of the Award is to encourage and commend college/university graduate students at the PhD level who display exceptional interest, desire, ability, and aptitude in the field of remote sensing or other related geospatial information technologies, and who have a special interest in developing practical uses of these technologies.

Eligibility

The Award is made to a graduate student (PhD level) currently enrolled or intending to enroll in a college or university in the United States or Canada who is pursuing a program of study aimed at starting a professional career where expertise is required in remote sensing or other related geospatial information technologies.

Award

- The award consists of a certificate and a check in the amount of $7,000 and a one-year student membership (renewal) in ASPRS.
- The award is presented by the ASPRS Foundation from funds donated by students, associates, colleagues, and friends of Robert Colwell, one of the world's most respected leaders in remote sensing, a field that he stewarded from the interpretation of World War II aerial photographs to the advanced acquisition and analysis of many types of geospatial data from military and civilian satellite programs.

John O. Behrens Institute for Land Information (ILI) Memorial Scholarship

The purpose of the Award is to encourage students/persons who have an exceptional interest in pursuing scientific research or education in geospatial science or technology or land information systems/records to enter a professional field where they can use the knowledge of this discipline to excel in their profession.

Eligibility

The Scholarship is made to an under-graduate student currently enrolled or intending to enroll in a university in the United States for the purpose of pursuing a program of study that prepares them to enter a profession in which education in geospatial science or land information disciplines will advance the value of those disciplines within that profession.

Award

- The award consists of a certificate and a check in the amount of $2,000 and a one year student membership (renewal) in the Society.
- Funds from the ILI have been donated to the ASPRS Foundation to support the John O. Behrens ILI memorial Scholarship in recognition of Mr. Behrens' outstanding contributions over the many years of his distinguished career

Ta Liang Award

The purpose of the award is to facilitate research-related travel by outstanding graduate students in remote sensing. Such travel includes field investigations, agency visits, participation in conferences, or any travel that enhances or facilitates a graduate research program.

Eligibility

Graduate Student members of ASPRS.

Award

- A grant of $2,000 and a hand-engrossed certificate.
- This award is presented by ASPRS, with funding provided by a grant from the ASPRS Foundation on behalf of individual and corporate contributions to the Foundation in memory of Ta Liang, a skilled civil engineer, an excellent teacher, and one of the world's foremost air-photo interpreters.

Abraham Anson Scholarship

The purpose of the Award is to encourage students/persons who have an exceptional interest in pursuing scientific research or education in geospatial science or technology related to photogrammetry, remote sensing, surveying and mapping to enter a professional field where they can use the knowledge of this discipline to excel in their profession.

Eligibility

The Award is made to an under-graduate student currently enrolled or intending to enroll in a college or university in the United States for the purpose of pursuing a program of study to enter a profession in which education in photogrammetry, remote sensing, surveying and mapping and geospatial science or technology disciplines will advance the value of those disciplines within that profession.

Award

- The award consists of a certificate, a check in the amount of $2,000 and a one-year student membership (renewal) in the society.

- This award is presented by the ASPRS Foundation from funds donated by the Anson bequest and contributions from the Society and the Potomac Region as a tribute to Abe Anson's many contributions to the field of photogrammetry, remote sensing, and long, dedicated service to the Society.

Robert E. Altenhofen Scholarship

The purpose of the Award is to encourage and commend college students who display exceptional interest and ability in the theoretical aspects of photogrammetry

Eligibility

The Award is made to an undergraduate or graduate student currently enrolled in a college or university in the United States or elsewhere, who is either a student or active member of ASPRS.

Award

- Cash prize of $2,000 and a certificate.
- The award is administered by the ASPRS Foundation from funds provided by the estate of Mrs. Helen Altenhofen as a memorial to her husband, Robert E. Altenhofen. A past president of ASPRS, Mr. Robert Altenhofen was an outstanding practitioner of photogrammetry and made notable contributions to the mathematical aspects of the science.

Paul R. Wolf Scholarship

The purpose of the Award is to encourage and commend college students who display exceptional interest, desire, ability, and aptitude to enter the profession of teaching Surveying, Mapping, or Photogrammetry.

Eligibility

The Award is made to a graduate student member of ASPRS currently enrolled or intending to enroll in a college or university in the United States, who is pursuing a program of study in preparation for entering the teaching profession in the general area of Surveying, Mapping, or Photogrammetry.

Award

- The award consists of a certificate and a check in the amount of $4,000.
- This Award is administered by the ASPRS Foundation from funds donated by the friends and colleagues of Paul R. Wolf as a memorial to him. Recognized nationally and internationally, Paul was an outstanding educator and practitioner of Surveying, Mapping, and Photogrammetry and a great friend of the Society. As author, teacher, and mentor, Paul made significant educational and academic contributions to these fields.

Kenneth J. Osborn Scholarship

The purpose of the Scholarship is to encourage and commend college students who display exceptional interest, desire, ability, and aptitude to enter the profession of surveying, mapping, photogrammetry, or geospatial information and technology. In addition, the Scholarship recognizes students who excel at an aspect of the profession that Ken Osborn demonstrated so very well, that of communications and collaboration.

Eligibility

The Scholarship is made to an undergraduate student currently enrolled or intending to enroll in a college or university in the United States, who is pursuing a program of study in preparation for entering the profession in the general area of surveying, mapping, photogrammetry, or geospatial information and technology.

Award

- This annual Scholarship consists of a certificate and a check in the amount of $2,000 and a one year student membership (renewal) in the Society.
- This award is presented by the ASPRS Foundation, with funding provided by donations from friends and colleagues of Kenneth Osborn as a tribute to him.

SUSTAININGMEMBERS

Aerial Services, Inc.
Cedar Falls, Iowa
www.AerialServicesInc.com
Member Since: 5/2001

Airbus Defense and Space
Chantilly, Virginia
www.intelligence-airbusds.com
Member Since: 11/2018

Ayres Associates
Madison, Wisconsin
www.AyresAssociates.com
Member Since: 1/1953

Cardinal Systems, LLC
Flagler Beach, Florida
www.cardinalsystems.net
Member Since: 1/2001

Dewberry
Fairfax, Virginia
www.dewberry.com
Member Since: 1/1985

Esri
Redlands, California
www.esri.com
Member Since: 1/1987

F.R. Aleman & Associates, Inc.
Miami, Florida
https://fr-aleman.com/
Member Since: 7/2020

GeoWing Mapping, Inc.
Richmond, California
www.geowingmapping.com
Member Since: 12/2016

GPI Geospatial Inc.
formerly Aerial Cartographics of America, Inc. (ACA)
Orlando, Florida
www.aca-net.com
Member Since: 10/1994

Green Grid Inc.
San Ramon, California
www.greengridinc.com
Member Since: 1/2020

Kucera International
Willoughby, Ohio
www.kucerainternational.com
Member Since: 1/1992

L3Harris Corporation
Broomfield, Colorado
www.harris.com
Member Since: 6/2008

Pickett and Associates, Inc.
Bartow, Florida
www.pickettusa.com
Member Since: 4/2007

Quantum Spatial, Inc.
Sheboygan Falls, Wisconsin
www.quantumspatial.com
Member Since: 1/1974

Sanborn Map Company
Colorado Springs, Colorado
www.sanborn.com
Member Since: 10/1984

Surveying And Mapping, LLC (SAM)
Austin, Texas
www.sam.biz
Member Since: 12/2005

T3 Global Strategies, Inc.
Bridgeville, Pennsylvania
https://t3gs.com/
Member Since: 6/2020

Towill, Inc.
San Francisco, California
www.towill.com
Member Since: 1/1952

Trimble
Munich, Germany
www.trimble.com/geospatial
Member Since: 4/1942

Wingtra
Zurich, Switzerland
https://wingtra.com/
Member Since: 6/2020

Woolpert LLP
Dayton, Ohio
www.woolpert.com
Member Since: 1/1985

SUSTAININGMEMBER**BENEFITS**

Membership

- ✓ Provides a means for dissemination of new information
- ✓ Encourages an exchange of ideas and communication
- ✓ Offers prime exposure for companies

Benefits of an ASPRS Membership

- Complimentary and discounted Employee Membership*
- E-mail blast to full ASPRS membership per year*
- Professional Certification Application fee discount for any employee
- Discounts on *PE&RS* Classified Ad
- Member price for ASPRS publications
- Discount on group registration to ASPRS virtual conferences
- Sustaining Member company listing in ASPRS directory/website
- Hot link to company website from Sustaining Member company listing page on ASPRS website
- Press Release Priority Listing in *PE&RS* Industry News
- Priority publishing of Highlight Articles in *PE&RS* plus, 20% discount off cover fee, one per year
- Discount on *PE&RS* full-page advertisement
- Exhibit discounts at ASPRS sponsored conferences (exception ASPRS/ILMF)
- Free training webinar registrations per year*
- Discount on additional training webinar registrations for employees
- Discount for each new SMC member brought on board (Discount for first year only)

*quantity depends on membership level

MAPPINGMATTERS

The layman's perspective on technical theory and practical applications of mapping and GIS

YOUR QUESTIONS ANSWERED

- **Have you ever wondered about what can and can't be achieved with geospatial technologies and processes?**
- **Have you been intimidated by formulas or equations in scientific journal articles and published reports without giving you a straight answer?**
- **Would you like to understand the geospatial industry in layman's terms?**
- **Do you have a challenging technical question that no one you know can answer?**

If you answered "*YES*" to any of these questions, then you need to read Dr. Qassim Abdullah's column, Mapping Matters. In it, he answers all geospatial questions —no matter how challenging—and offers accessible solutions.

"I've read through your comments and calculations … twice. It is very clear and now I understand it. I never would have known this information otherwise. I am honored that there are experienced professionals like you, willing to help fellow members of the geospatial community and promote knowledge in the geospatial sciences."

MAPPING MATTERS — YOUR COMPANION TO SUCCESS!

Send your questions to Mapping_Matters@asprs.org

To browse previous articles of Mapping Matters, visit http://www.asprs.org/Mapping-Matters.html

asprs
THE IMAGING & GEOSPATIAL INFORMATION SOCIETY

NOW AVAILABLE!

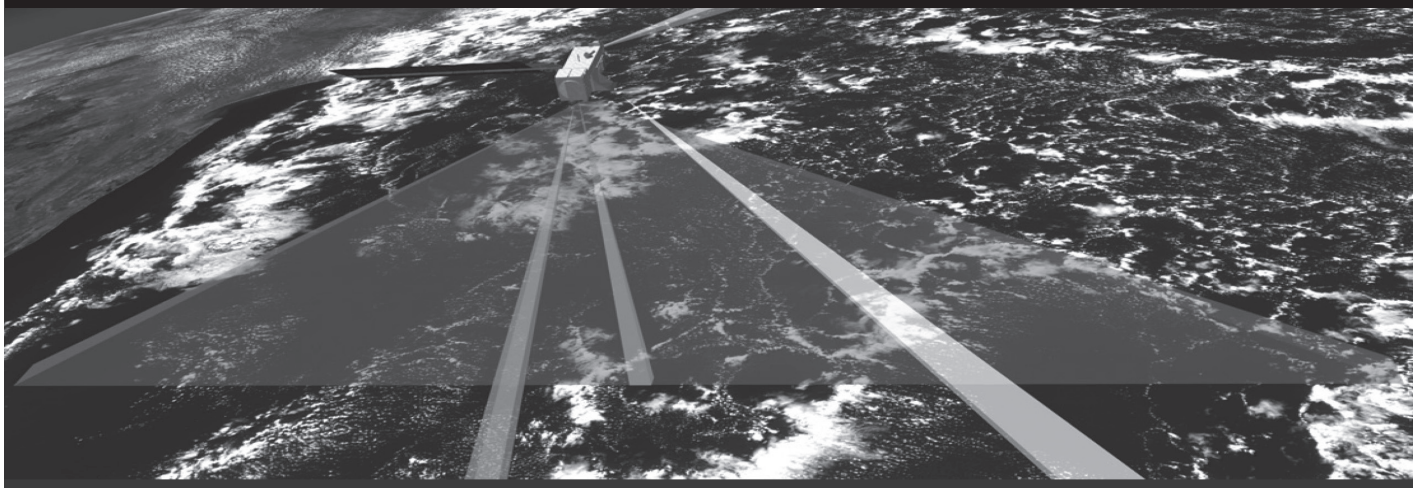

MANUAL OF REMOTE SENSING

Fourth Edition

ASPRS Announces the 4th Edition of the *Manual of Remote Sensing!*

The *Manual of Remote Sensing, 4th Ed.* (MRS-4) is an "enhanced" electronic publication available online from ASPRS. This edition expands its scope from previous editions, focusing on new and updated material since the turn of the 21st Century. Stanley Morain (Editor-in-Chief), and co-editors Michael Renslow and Amelia Budge have compiled material provided by numerous contributors who are experts in various aspects of remote sensing technologies, data preservation practices, data access mechanisms, data processing and modeling techniques, societal benefits, and legal aspects such as space policies and space law. These topics are organized into nine chapters. MRS4 is unique from previous editions in that it is a "living" document that can be updated easily in years to come as new technologies and practices evolve. It also is designed to include animated illustrations and videos to further enhance the reader's experience.

MRS-4 is available to ASPRS Members as a member benefit or can be purchased by non-members. To access MRS-4, visit https://my.asprs.org/mrs4.

edited by: Stanley A. Morain,
Michael S. Renslow and Amelia M. Budge

MANUAL OF REMOTE SENSING 4

The goal of the Manual of Remote Sensing-4 was to create a more effective, affordable, and durable Manual, and to broaden its scope to include economic and societal benefits. Effective in the sense that MRS-4's content could be found online as an enhanced e-book; affordable in the sense that content could be retrieved by everyone on an annual subscription basis; and durable in the sense that it could be easily updated as a "living" manual through fresh, contributor-driven and vetted material as technologies advance. It does not reprise the extensive mathematical basis for remote sensing given in MRS-2, but instead focuses on system designs; data processing, storage, and retrieval; and on societal applications. A key feature of this concept is to facilitate timely updates of cutting edge or new developments from a wide spectrum of sophisticated contributors facile collectively with the technological, mathematical, and utilitarian aspects of Earth and space sciences.

Table of Contents

MRS-4 is available to ASPRS Members as a member benefit or can be purchased by non-members. To access MRS-4, visit https://my.asprs.org/mrs4.

ASPRS BOOKSTORE

visit **asprs.org**

Digital Elevation Model Technologies & Applications, 3rd Ed
Co-Editors: David F. Maune, PhD, CP, CFM, PSM, PS, GS, SP and Amar Nayegandhi, CP, CMS-Remote Sensing
List Price: $100 | **ASPRS Members:** $80
ASPRS Student Members: $50†
Also available for Amazon Kindle
Amazon Kindle Price:** $85

Landsat's Enduring Legacy: Pioneering Global Land Observations From Space
Landsat Legacy Project Team
ISBN: ISBN 1-57083-101-7 · Hardcover · 586 pages · 2017 · Stock #4958
List Price: $95 | **ASPRS Members:** $65
Student Members: $60
Amazon Price*: $100

Manual of Airborne Topographic Lidar
Editor: Michael S. Renslow
ISBN: 1-57083-097-5 · Hardcover · 528 pages · 2012 · Stock #4587
List Price: $150 | **ASPRS Members:** $95
Student Members: $75
Amazon Price (hardcover)*: $135
Also available for Amazon Kindle
AmazonKindle Price:** $110

Manual of Photogrammetry, Sixth Edition
Editor: J. Chris McGlone
ISBN: 1-57083-099-1 · Hardcover · 1372 pages · 2013 · Stock #4737
List Price: $175 | **ASPRS Members:** $125
Student Members: $98
Amazon Price*: $175

Glossary of the Mapping Sciences
Co-published by ASPRS, ACSM and ASCE
ISBN: 1-57083-011-8
563 pp · Paperback · 1994 · Stock #5021
List Price: $50 | **ASPRS Members:** $35
Student Members: $25 | **Amazon Price*:** $50

Hyperspectral Remote Sensing for Forestry
Paul Treitz, Valerie Thomas, Pablo J. Zarco-Tejada, Peng Gong, and Paul J. Curran
ISBN: 1-57083-093-2
107 pp · Softcover · 2010 · Stock #4584
List Price: $26 | **ASPRS Members:** $21
Student Member: $21 | **Amazon Price*:** $26

available at amazon

Manual of Geographic Information Systems
Editor: Marguerite Madden, PhD
Foreword: Jack Dangermond, Esri
ISBN: 1-57083-086-X · Hardcover · 1352 pages + DVD · July 2009 · Stock #4650
List Price: $53 | **ASPRS Members:** $40
Student Members: $40
Amazon Price*: $55

Meeting Environmental Challenges with Remote Sensing Imagery
Editors: Rebecca Dodge & Russ Congalton
Published by American Geosciences Institute; Publishing Partners: AmericaView, USGS Land Remote Sensing Program, ASPRS
ISBN: 978-0-922152-94-0 · 82 pp · Softcover · 2013 · Stock #4589
List Price: $7.50 | **ASPRS Members:** $6
Bulk Orders (3 or more copies): $4.50 each
Amazon Price*: $9.95

MANUAL OF REMOTE SENSING, 3RD EDITION (A SERIES)

Earth Observing Platforms & Sensors
Volume 1.1
Volume Editor: Mark Jackson
ISBN: 1-57083-089-4
550 pp · Hardcover · 2009 · Stock #4582
List Price: $95 | **ASPRS Members:** $75
Student Members: $55 | **Amazon Price*:** $95

Remote Sensing of Human Settlements
Volume 5
Editor-in-Chief: Andrew B. Rencz
Volume Editors: Merrill K. Ridd & James D. Hipple
ISBN: 1-57083-077-0
747+ pp · Hardcover · 2005 · Stock # 4576
List Price: $99 | **ASPRS Members:** $80
Student Members: $60
Amazon Price*: $69.99

Remote Sensing of the Marine Environment
Volume 6
Editor-in-Chief: Andrew B. Rencz
Volume Editor: James F.R. Gower
ISBN: 1-57083-080-0 · 360 pp · Hardcover · 2006 · Stock # 4578
List Price: $95 | **ASPRS Members:** $75
Student Members: $50 | **Amazon Price*:** $95

*Member discounts are not available when ordering directly from Amazon.

**Member discounts are not available on Amazon Kindle e-books,

†Students must order via the ASPRS Bookstore & a copy of your valid student ID must be submitted to be eligible for student pricing.

Building Facade Reconstruction Using Crowd-Sourced Photos and Two-Dimensional Maps

Jie Wu, Junya Mao, Song Chen, Gesang Zhuoma, Liang Cheng, and Rongchun Zhang

Abstract

To address the high-cost problem of the current three-dimensional (3D) reconstruction for urban buildings, a new technical framework is proposed to generate 3D building facade information using crowd-sourced photos and two-dimensional (2D) building vector data in this paper. The crowd-sourced photos mainly consisted of Tencent street view images and other-source photos, which were collected from three platforms, including search engines, social media, and mobile phones. The photos were selected and grouped first, and then a structure from motion algorithm was used for 3D reconstruction. Finally, the reconstructed point clouds were registered with 2D building vector data. The test implementation was conducted in the Jianye District of Nanjing, China, and the generated point clouds showed a good fit with the true values. The proposed 3D reconstruction method represents a multi-sourced data integration process. The advantage of the proposed approach lies in the open source and low-cost data used in this study.

Introduction

The three-dimensional (3D) reconstruction of buildings is a research hotspot in the fields of geographic information science and remote sensing (RS). With the ongoing development of digital cities, there is a growing need for effective 3D urban modeling methods. The emergence of computer vision, high-resolution, and high-precision photogrammetry, and unmanned aerial vehicles has provided new techniques for developing high-quality 3D models of buildings (Malihi *et al.* 2018; Ye and Wu 2018). Indeed, 3D reconstruction technology has been widely employed in urban planning, real-life navigation, urban virtual tourism, and other fields (Zhu *et al.* 2015; Nina *et al.* 2018). One of the practical applications of large-scale reconstruction for urban buildings is in multi-directional geographic information analysis such as estimating urban solar energy potential (Chen *et al.* 2017).

Aerial oblique photogrammetry enables the acquisition of building facade information through multiple sensors carried on the same flight platform, which are used to collect multi-angle data. However, the utilized hardware and software are too expensive (Aicardi *et al.* 2016). In addition, problems may be encountered while dealing with densely distributed high-rise buildings, such as occlusion and large camera tilt angles. These problems will cause inaccuracy on the generated 3D models. The vehicle light detection and ranging (lidar) system can be used to acquire 3D information of streets and ground objects. However, the scene targets are often complex and diverse. There will be a lot of challenges while extracting features from a massive lidar point cloud (Zhu *et al.* 2011; Varney and Asari2015). In addition, the lidar equipment is very expensive. There is thus a pressing need for the development of a low-cost method for the rapid 3D reconstruction of large-scale buildings.

Recent years have witnessed the generation of massive amounts of crowd-sourced photos on different platforms. Among them, street view images provide street-level data including buildings, trees, and transportation facilities on both sides of roads and pavements. In addition, a large number of urban building photos have been taken by mobile phones and uploaded to the Baidu Photo Gallery or other social media such as Flickr and Weibo. Such photos are hereafter called "other-source photos". The use of crowd-sourced photos has the advantages of convenience, low cost, and mass availability. In this study, we proposed a method of developing a building facade point cloud using street view images and other-source photos. Tencent street view images were used as the main data, with other-source photos as supplement. We then integrated the point cloud with two-dimensional (2D) building vector data. Point cloud registration was used to transform the reconstruction points into the real world coordinate system. The main innovation of this study is a new technical framework to extract 3D building facade information. The data used in this study (i.e., street view images and 2D vector contour data) are all open source and low-cost.

The rest of this paper is organized as follows. In the section "Review of Relevant Studies", we review some relevant works. In the section "Proposed Method", we present the detailed steps of the proposed 3D reconstruction method. The section "Experiment" shows an experimental application of the method in the Jianye District in Nanjing, China. The reconstruction results are presented, evaluated, and discussed in the section "Results and Discussion". Finally, the conclusions are drawn from the study are presented in the last section.

Review of Relevant Studies

Existing methods for 3D building reconstruction can be roughly divided into three categories. The first one includes the methods that utilize laser point cloud data such as terrestrial lidar data, airborne lidar data, and integrated multi-platform lidar data. For example, Shi and George (2009) proposed a method for developing building facade models using terrestrial lidar data. The

Liang Cheng is with Jiangsu Provincial Key Laboratory of Geographic Information Science and Technology, Nanjing University, Nanjing, China (lcheng@nju.edu.cn).

Liang Cheng is also with the Collaborative Innovation Center for the South Sea Studies, Nanjing University, Nanjing, China.

Liang Cheng is also with the Collaborative Innovation Center of Novel Software Technology and Industrialization, Nanjing University, Nanjing, China.

Jie Wu, Junya Mao, Song Chen, Gesang Zhuoma, and Liang Cheng are with the School of Geography and Ocean Science, Nanjing University, Nanjing, China.

Rongchun Zhang is with the School of Geographic and Biologic Information, Nanjing University of Posts and Telecommunications, Nanjing, China.

Photogrammetric Engineering & Remote Sensing
Vol. 86, No. 11, November 2020, pp. 677–694.
0099-1112/20/677–694

doi: 10.14358/PERS.86.11.677

method involves segmentation of the original high-density point cloud, extraction of the facade features, and categorizing them into various semantics (walls, doors, windows, etc.) to form a polyhedron building model. However, this method can only build an untextured wireframe model, and required complex data acquisition and processing. Elberink and George (2011) proposed a theoretical empirical method for the quality analysis of the advantages and disadvantages of 3D building models developed using airborne lidar data. They noted that it was difficult to obtain facade information based on airborne lidar data, which made it impossible to achieve fine reconstruction of building facades from different directions and perspectives. Chen *et al.* (2015) proposed an integrated approach that utilized vehicle lidar data and airborne lidar data for multi-view reconstruction of building roofs and facade models. However, the proposed method is complex and the airborne lidar data is high-cost.

The second category of 3D building reconstruction methods includes those that utilize RS satellite image data and shadow measurements (Hartl and Cheng 1995; Zhang *et al.* 2011; Liasis and Stavrou 2016). These methods mainly use interferometric synthetic aperture radar (InSAR) data and optical image data. Stilla *et al.* (2003) analyzed the potentials and limitations of using InSAR data for building reconstruction in built-up areas. Soergel *et al.* (2009) matched the high-resolution InSAR images and estimated the heights of buildings by 3D clustering. However, InSAR data consist of noise, and in dense building areas the mutual interference between building signals may affect the reconstruction results. Huang and Kwoh (2007) proposed a semiautomatic method to extract buildings and measure their height using the top, base, and shadow information obtained from a single IKONOS image. Although the method is suitable for extracting height information, it cannot be used to restore facade details.

The third category includes those that utilize photo data, such as aerial and terrestrial images, image sequence, or the integration of photo and vector data. Aerial and panoramic terrestrial images are currently the most employed data sources in 3D building reconstruction (Christian and Avideh 2004; Hu *et al.* 2006; Wang *et al.* 2007; Toschi *et al.* 2017). Given the complementarity between aerial and terrestrial data sets, many studies have utilized the combination of them. Wu *et al.* (2018) achieved 3D modeling and optimization for urban areas by combining oblique aerial images and terrestrial images using automatic feature matching and bundle adjustment. However, the data acquisition is difficult, and the reconstruction process is complex. In addition, the 3D reconstruction of landmarks such as buildings using image sequences and video data has attracted significant interest (Mayer and Reznik 2007; Cornelis *et al.* 2008; Pollefeys *et al.* 2008; Snavely *et al.* 2008). Tian *et al.* (2010) integrated building structure information in a video sequence for the 3D reconstruction. However, in most of these studies, polyhedral models were used to represent the structures of buildings, which made it difficult to achieve fine reconstruction of the facades. Xiao *et al.* (2009) reconstructed image sequences using multi-semantic image segmentation and structure from motion (SfM) algorithms and generated a set of semidense point clouds. However, the employed linear structure hypothesis has limitations for more complex buildings. Lee (2009) estimated the rotation parameters from the motion of sky region in panoramic photos and used them to increase the robustness of camera's trajectory estimation. They subsequently used a combination of the SfM algorithm and bundle adjustment for 3D building reconstruction. Their method is, however, not applicable to large-scale reconstruction. Fan and Zipf (2016) proposed a method which used OpenStreetMap data and volunteered geographic information photo data for 3D reconstruction. However, the photo data used in this method had very limited coverage and cannot provide views from different angles. In addition, such data are inadequate for large-scale reconstruction of urban buildings.

Proposed Method

Figure 1 shows the workflow of the proposed 3D reconstruction method. In this study, we focus on the integration of technologies. There are three steps in the entire technical framework, including selecting and grouping of crowd-sourced photos, 3D reconstruction using crowd-sourced photos, and point cloud registration based on 2D vector data. The 3D reconstruction step was conducted in Agisoft Photoscan software.

Selecting and Grouping of Crowd-Sourced Photos

In this section, the crowd-sourced photos of the buildings are grouped to reconstruct buildings separately. The other-source photos are unstructured and unordered. They have different illumination, resolution, and quality. Therefore, they are grouped together with the street view images before 3D reconstruction. In addition, the street view images contain different scenes. The reconstruction can be affected by proportion of building in the images, overlapping degree of adjacent images, and distribution of cameras. As the main data source, these images are first checked to remove invalid data and reduce volume before grouping, which can speed up the subsequent processing.

Extraction of Green Vegetation and Sky Areas from Street View Images

The street view images contain a lot of green vegetation or sky areas which make it difficult for 3D reconstruction, as shown in Figure 2. Green vegetation and sky areas are the main nonbuilding parts and have significant influences on 3D point cloud generation. Therefore, this section will try to remove images that contain large green and sky areas.

Due to the acquisition time, imaging conditions, and location, street view images usually contain a lot of noise. Consequently, a Gaussian filter is used to preprocess the origin images. A Gaussian filter is a linear, smoothing filter that can effectively eliminate noise and improve quality of images.

Extraction of green area: The green view index (GVI) of an image is the ratio of green area in the image to the total area, which is proposed by Yang *et al.* (2009):

$$\mathrm{GVI} = \frac{\mathrm{Area}_{\mathrm{green}}}{\mathrm{Area}_{\mathrm{total}}} \tag{1}$$

where $\mathrm{Area}_{\mathrm{green}}$ is the number of green pixels in the street view image, and $\mathrm{Area}_{\mathrm{total}}$ is the number of all pixels.

The calculation of GVI involves the following two steps:

1. Coarse extraction of green pixels: The green area is extracted using a band calculation algorithm (Li *et al.* 2015), which utilizes the following formula:

$$G - R = \mathrm{diff1} \tag{2}$$

$$G - B = \mathrm{diff2} \tag{3}$$

$$\mathrm{diff1} \times \mathrm{diff2} = \mathrm{diff3} \tag{4}$$

where diff1 and diff2 are the difference images among different bands. For each pixel (i, j), if it satisfies diff3>0 and diff1>0, the pixel is regarded as a green pixel. Then we assigned a value of 1 to the green pixel and a value of 0 to the nongreen pixel.

2. Optimization: This step mainly involves morphological filtering and image reconstruction. Though the foreground region is extract in step (1), there are still many spurious points in the image (Blaschke *et al.* 2000). Morphological filtering is an effective way to remove these points (Jayaraman *et al.* 2009). A morphological opening operation is used for an image's erosion followed by dilation. According to a morphological reconstruction algorithm, the street view image can be restored, and the green area will be extracted.

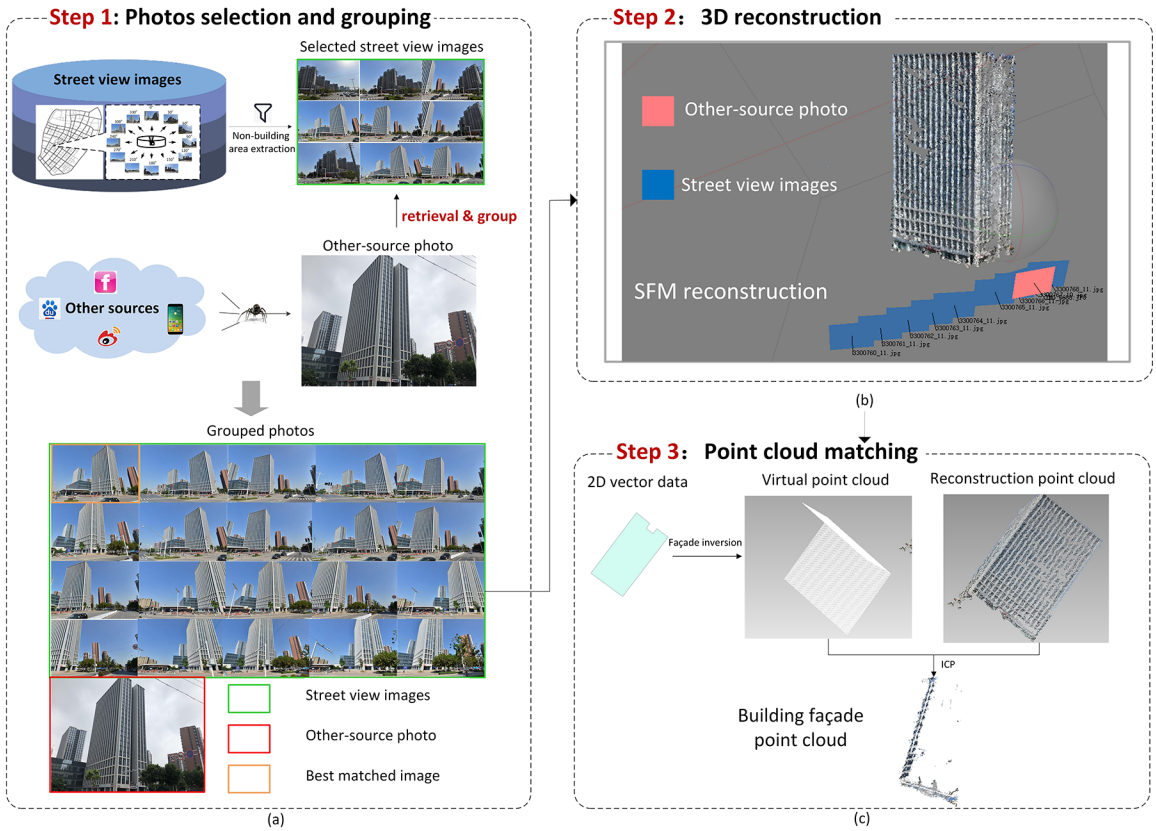

Figure 1. Technical flow diagram of the proposed method (example of a single building): (a) photos selection and grouping; (b) 3D reconstruction; (c) point cloud matching.

Figure 2. Street view images contain a lot of green vegetation or sky areas.

Extraction of sky area: The extraction of the sky area requires the initial segmentation of the street view image. This is performed by a color image segmentation algorithm proposed by Ye *et al.* (2004). The algorithm combines color and spatial information and enables accurate splitting of the sky area. The specific process includes (1) color quantization, (2) initial segmentation using a region growing algorithm, (3) similarity region merging, and (4) regional merging termination rule by measuring the inhomogeneous degrees of the colors in merged regions.

After the image segmentation, the sky area in street view image is then extracted using the sky-openness index (SOI) proposed by Cheng *et al.* (2017). The SOI is defined as the sky's proportion of a visual cone from some certain observation points. The formula of SOI is as follows:

$$\mathrm{SOI} = \frac{\sum_{i=0}^{N_{\mathrm{sky}}} |r_i|}{N} \times 100\% \tag{5}$$

where N_{sky} is the number of regions classified as sky in the image after segmentation, r_i is the number of pixels in the ith sky region, and N is the total number of pixels in the image. Thus, the sky area in the street view image is extracted.

Initial selection of street view images: The green and sky areas in each street view image are first extracted, which will greatly influence the effect of 3D point cloud generation. If the area ratio of the green and sky areas in a particular image is higher than a certain threshold, it will be removed before 3D reconstruction. This process is followed by further retrieval and grouping, as described below. Figure 1a shows a set of street view images obtained after the initial selection for a sampling point.

Photos Retrieval and Grouping

Grouping photos based on sharing buildings: Due to the large number of street view images and the disorderliness of other-source photos, it takes a lot of time to group them directly. We therefore adopt an image retrieval method proposed by Cheng *et al.* (2018), which uses the other-source photos to group selected street view images in order to shorten processing time. Specifically, we use other-source photos as queried photos and street view images as reference data set. The detailed process is as follows: (1) For each other-source photo and reference data set, the scale-invariant feature transform (SIFT) descriptor (Lowe 1999; Lowe 2004; Vedaldi and Fulkerson 2010) is first used for feature extraction. A nearest neighbor feature retrieval is then conducted to query each feature. According to a voting method and dynamic trimming and smoothing (Zamir and Shah 2010), the street view image that best matches each other-source photo can be identified, as shown in Figure 1a. (2) A buffer zone with 200 m radius is generated at the sampling point where the best-match street view image is located. The street view images within this range are grouped together, along with the corresponding other-source photo.

Each group of photos is selected before 3D building reconstruction: (1) The target building in each other-source photo should be less sheltered. If not, those photos should be removed before 3D reconstruction, while their corresponding street view images retained. (2) Further images are selected based on their location, pose, and overlap between each other. The overlap between two adjacent images should be >60%. Any image that is too far from, or too close to the target should be removed. In addition, the images must contain two sides of the building. It is difficult to realize the stereoscopic reconstruction based on images acquired from the same station. Therefore, in this study, we selected images from different stations with sufficient degrees of overlap. After this step, each group of photos will be considered as a data source for the building reconstruction, as shown in Figure 1a.

3D Reconstruction Using Crowd-Sourced Photos

In the proposed 3D reconstruction method, an SfM algorithm is used to recover 3D information (Snavely *et al.* 2008; Wu 2013). The SfM technology is able to reconstruct 3D scenes, camera positions, and orientations from a set of 2D images with low cost (Snavely *et al.* 2008). During the movement of the camera, image pairs can be captured to establish a set of corresponding features, which can recover the 3D coordinates of points. The SfM procedure requires internal parameter matrix of cameras. Thus, it is necessary to conduct camera calibration on all selected photos.

Camera Calibration

A camera model needs to be used to transform the camera coordinate system to the pixel coordinate system in the photo. The most commonly used camera model is the pinhole model. To obtain the relationship between a point in the real world and the corresponding pixel in the image, an internal parameter matrix of a camera is presented as follows:

$$\mathrm{K} = \begin{bmatrix} f & 0 & c_x \\ 0 & f & c_y \\ 0 & 0 & 1 \end{bmatrix}$$

where f is the focal length, and c_x and c_y are the main point positions. For street view images without Exchangeable Image File Format information and photos from social media, f was set as 50 mm, while it was 33 mm for mobile photos.

Although the pinhole model is an ideal camera model, cameras always have lens distortion in reality. Therefore, it is necessary to perform camera calibration on all photos selected for 3D reconstruction. Lens distortion includes radial and tangential distortions. Because the curve of light away from the center of lens is greater than that close to the center, radial distortion is often greater than tangential distortion. Thus, only radial distortion was corrected in this study. Brown's distortion model was used with a fixed set of parameters, namely, f, c_x, and c_y and three radial distortion coefficients (K1, K2, and K3).

Feature Extraction and Matching

Feature extraction: The feature extraction is performed using the current optimal maximally stable extremal region (MSER) operator (Matas *et al.* 2004) and the SIFT descriptor (Lowe 1999; Lowe 2004; Badri *et al.* 2016). The MSER operator uses different gray thresholds to binarize an image in order to obtain the most stable region and achieve affine invariance. In the case of SIFT algorithm, it calculates (x, y) positions of the feature points using Difference of Gaussians filter. It can obtain a 128-dimensional feature vector to extract high-quality local invariant features effectively.

Matching and building tracks: Nearest neighbor matching is conducted based on kd-tree data structure using an approximate nearest neighbors (ANN) algorithm (Har-Peled *et al.* 2012). There is an image pair I and J. For each feature i in image I, we can find nearest neighbor feature vector j among the features in image J. We define the distance to the nearest neighbor as $d1$, and to the second nearest neighbor as $d2$. If the ratio of $d1$ to $d2$ is less than a certain threshold, the matching of the image pair is acceptable. However, the matching results of ANN algorithm contain error-matched pairs, which needs to be checked further. Hence, the random sample consensus algorithm and the eight-point algorithm (Zheng *et al.* 2013) are used to calculate the f-matrix to remove the matched pairs that do not satisfy the matrix.

After the successful matching of all photo pairs, the feature matching points that appear in multiple photos are traced to form a track.

Structure from Motion and Generation of Sparse Point Cloud

The pair of photos $I1$ and $I2$ with the highest number of matching pairs is used as the initial photo pair. Then the five-point algorithm (Nister 2003) is used to calculate the initial camera parameters. After triangulation of the track, the initial 3D point cloud is obtained and a bundle adjustment (BA) is performed on the initial photo pair (Lourakis and Argyros 2009). BA is an iterative solution process that utilizes non-linear least squares. After each iteration, all the 3D points are back-projected to the pixel coordinates of the corresponding photos and compared with the initial coordinates. If the difference exceeds a certain threshold, the point will be removed from its track. If less than two points are left in a track, this track will be entirely removed. The optimization is continued until there is no point need to be removed. Whenever a new photo is included, BA should be performed again. The pose of the photo and geometric details are estimated and optimized by minimizing the reprojection error. Thus, a sparse 3D point cloud of the building can be obtained.

Generation of Dense Point Cloud

The objective of the proposed method is to reconstruct a point cloud of building facades effectively. Therefore, a sparse point cloud cannot be satisfying. To generate a dense point cloud, a clustering multi-view stereo algorithm is first used to classify the image clusters and optimize the SfM algorithm input. A patch-based multi-view stereo algorithm (Furukawa and Ponce 2008) is then used to complete the final dense matching. The detailed process includes initial feature matching, seed patch expansion, and filtering. The generated dense point cloud is shown in Figure 1b.

Point Cloud Registration Based on 2D Vector Data

The reconstructed point clouds are in the local coordinate system. Therefore, we need to match them to the 2D building outline vector data to obtain their absolute orientation and real geographic coordinate. The point cloud registration will be based on a rotation matrix **R**, a translation parameter T, and a scale difference λ relative to the real geographic coordinate system.

In this section, we describe the registration of reconstructed point cloud based on the 2D contour data in details. The process is illustrated in Figure 3.

Before the registration, the vector data is used to measure the length of building contour edge, which can adjust the scales of 3D reconstruction point cloud by comparison. In addition, to speed up the data processing and reduce the required amount of data inversion, we extract the building's outline from Tencent satellite image map to trim the corresponding 2D building outline vector data. The satellite image of the original building (the Olympic Mingzuo) and the 2D building vector contours before and after the trim are shown in Figure 3a.

Virtual Facade Point Cloud Inversion Based on 2D Vector Contour

Division of the building vector outline: The building outline on the Gaode map is based on polygonal features which need to be conversed to line features. The line features are divided into points with interval of 0.5 m and the X-Y coordinates of each point are recorded on meters (m).

Facade inversion: Assuming that the height of building's top is 0 m, the set of 2D outline plane points extend downward to a certain height h at certain steps. To improve the accuracy of subsequent point cloud registrations, the inversion point cloud should be close to the true scale of the building. Therefore, in this study, the floor information (*floor*) available in the Gaode data was used as a reference, and we assumed the height of each floor to be 3 m. Thus, the height h can be given by *floor* × 3 m. In the case of the Olympic Mingzuo, assuming that the height of building's roof is 0 m, the virtual facade point cloud was obtained through extension in the downward direction to 50 m in steps of 0.2 m.

The top views of the virtual facade point cloud, 3D reconstruction point cloud after scale adjustment and positional relationship between the two point clouds are shown in Figure 3b.

Registration of 3D Reconstruction Point Cloud and Virtual Facade Point Cloud

The iterative closest point (ICP) algorithm (Cheng *et al.* 2015; Cheng *et al.* 2017) is used to match the 3D reconstruction point cloud and the virtual point cloud. The ICP algorithm is an optimal registration method based on the least squares method, which is characterized by good stability and robustness. However, ICP algorithm requires a more exact initial state of point cloud; otherwise, the global convergence would fail because of a large initial error. Thus, an initial registration is used to make two cloud positions closer.

Initial registration: Three pairs of homologue points are selected for a rough registration. The selected points should have obvious features such as turning points or corner points of the target. The 3D reconstruction point cloud may miss its top or bottom. Therefore, the selected homologue points should be distributed as much as possible in the middle part of the entire facade point cloud. After the rough registration, the two point clouds would have good initial positions and the ICP algorithm can then be applied effectively.

Fine registration using ICP algorithm: The ICP algorithm repeatedly selects corresponding point pairs and calculates the optimal rigid transformation until the convergence accuracy meets the requirements. Regarding the virtual facade point cloud (P) as reference point cloud, we can calculate the error of reconstructed facade point cloud (Q) as follows:

$$f(R,T,\lambda)=\sum_{i}^{n}\left\|P_i-(\lambda RQ_i+T)\right\|^2 \tag{6}$$

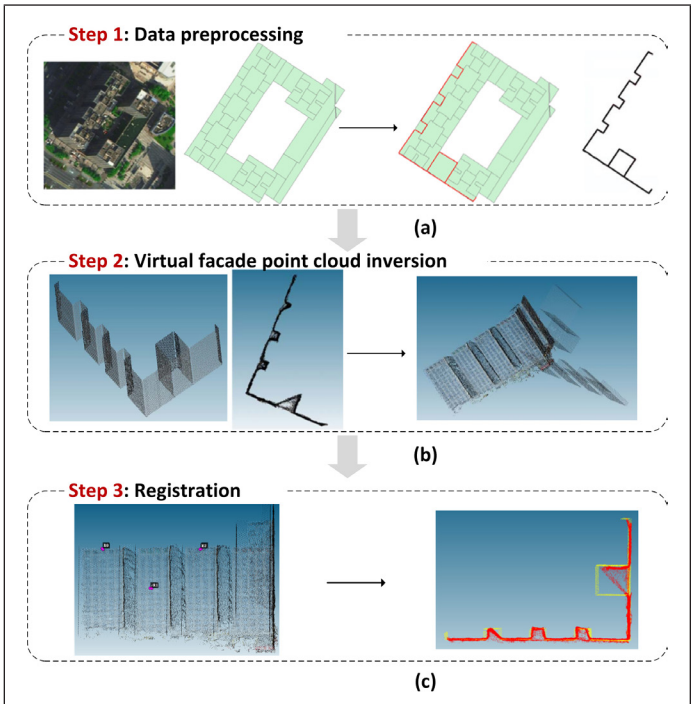

Figure 3. Illustration of point cloud registration (the red point is the reconstructed point cloud, and the yellow point is the virtual facade point cloud): (a) data preprocessing; (b) virtual facade point cloud inversion; (c) registration.

The essence of the ICP algorithm is repeated iterations to determine the rotation matrix **R**, translation matrix **T**, and scale parameter λ between Q and P that minimize the above error function.

The selection of the homologue points and top views of the two point clouds after registration are shown in Figure 3c. The reconstructed facade point cloud has been registered with the building vector data.

Experiment

Study Area and Data

To evaluate the performance of proposed 3D building reconstruction method, we applied it to an area in Jianye District in Nanjing, China. A schematic diagram of the study area is shown in Figure 4. Jianye District is one of the main urban areas in Nanjing and located in the southwest. The Jianye District contains both old towns with lower and denser buildings, and new urban construction areas with many modern high-rise buildings. The buildings are of different types and with diverse facade structures, which makes this district suitable for a 3D building reconstruction experiment. The study area is typical and representative. The coverage area is about 29.0 km². The total number of buildings in the study area is about 14 274.

Two data sets were used for the 3D building facade reconstruction experiment, namely, crowd-sourced photo data (mainly Tencent street view images, supplemented with other-source photos) and vector data of the top profiles of buildings obtained from Gaode map. Vehicle lidar data was further used for accuracy verification. A total of 200 000 street view images and 655 other-source photos were used in the experiment, which covered 286 km of urban roads. The study area and some of the utilized data are shown in Figure 4.

Street View Image Data

Street view maps are real-view map services that provide users with panoramic street view images of cities, streets, and other environments. The services offer users immersive map-browsing experiences. Tencent Maps, a high-resolution street view map service in China, cover practically all prefecture-level cities in China. Tencent also provides several types of maps including electronic maps, satellite images, and topographic map. Tencent street view maps were the source of street view images used in this study, while the road networks are also obtained from Tencent digital maps. The parameters used to download the Tencent street view images are presented in Table 1.

It can be seen from Table 1 that it is necessary to obtain the latitude and longitude coordinates of street view sampling points first. The road network data was preprocessed. We then

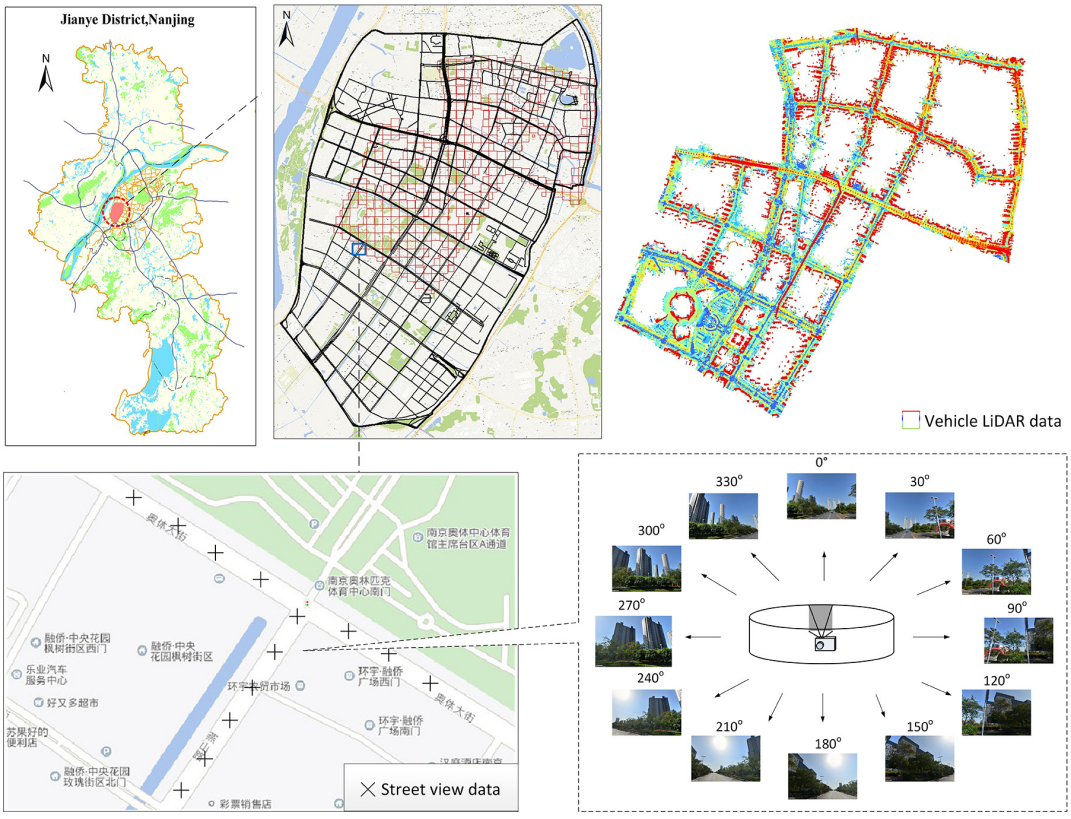

Figure 4. Study area and data (blue to red coloring is used to depict the point cloud elevation from low to high).

Table 1. Parameters of the street view crawl.

Parameter	Explanation	Example
Size	The size of images, width × height	Size = 960 × 640
Location	Coordinates, used to find the nearest image from that location	Location = 39.11, 116.84
Heading	The yaw angle, formed by rotation from true north.	True north: Heading = 0
Pitch	The pitch angle, above or below the horizontal line from the street view camera relative to the acquisition equipment.	Pitch = 0: horizontal view Pitch = 90: vertically upwards Pitch = –90: vertically downwards
Key	Developer key	Key = NXRBZ-62YW6-JPTSW-MHYFF-JYM2V-LHB3G:

divided each processed street into discrete points at 12-meter intervals, which was guaranteed to be consistent with the sampling intervals of street view images. The pitch of the street view camera was set to 20°. At each sample point, we crawled photos at 30° clockwise intervals beginning from the initial yaw angle, which produced 12 images per sample point as shown in Figure 3. This procedure not only ensured the overlap of adjacent street view images, but also reduced the storage greatly. Java programming was used to download street view image automatically. The images were collected in 2014.

Other-Source Photos Data

The street view images used in this study were obtained under spherical projection and spliced by panoramic cameras. Therefore, the employed mathematical models were different from the collinear equations for ordinary digital image plane projection. As a result, the generated building models sometimes contained deformations such as tilting. Moreover, some images with low resolution and some buildings with few images selected will affect reconstruction greatly. Consequently, other-source photos were employed as auxiliary data to improve the quality of the point cloud for 3D building reconstruction.

These other-source photos were collected from three platforms, including search engines, social media, and mobile phones. The search engines include Google search and Baidu search which is popular in China. We searched different combinations of keywords to get the photos and eliminated duplicate or incorrect results. Social media platforms include WeChat official accounts and Sina Weibo. There were also plenty of photos taken in the study area by the authors using mobile phones.

In total, 655 other-source photos were collected. These photos had different perspectives, resolutions, dimensions, and scenes.

2D Building Vector Data

The top-view 2D vector contour data of the buildings provided by Gaode maps was used to transform the coordinate system of reconstructed 3D point cloud. The data attributes included the geographical position of the buildings and the numbers of floors. Figure 5a shows the overall display of the data, while Figure 5b shows the data of the Olympic Mingzuo building (Figure 5d) in the Jianye District as an example. Figure 5c shows the corresponding top view contour in the satellite image.

Vehicle Lidar Data

Vehicle lidar sensor is mounted on a moving vehicle and can acquire information of roads and objects on both sides of roads with high accuracy and point cloud density. In this study, a set of vehicle lidar data was used to evaluate the accuracy of reconstructed building point cloud. The employed data was acquired on 12 October 2011 using an Optech Lynx SG1 system. This data had a coverage of approximately 4800 × 4380 × 330 m, as shown in Figure 4.

Reconstruction and Performance Evaluation Experiments

To evaluate the performance of proposed 3D building facade reconstruction method, the experiment included the following groups:

1. Group A: Building facade point cloud generation based on multi-sourced data.
2. Group B: Comparative experiments were performed to analyze the contribution of the other-source photos. Six representative buildings were selected for this purpose. In this group, other-source photos were removed and only street view images were used for 3D reconstruction (Group B-1).
3. Group C: Calculation of the heights of buildings based on reconstructed facade point cloud (see Table 2). The accuracy of building height extraction can reflect the quality of reconstructed building facade point cloud. Because the facade point cloud was converted into the real geographic coordinate system, the height of building can be directly obtained from the Z value of point cloud or based on the highest and lowest points.

Further, the accuracy assessment included the following steps: (1) Height extraction accuracy: 20 buildings within the coverage of the lidar data were selected (Group D) for comparison with the *floor* value provided by Gaode maps. (2) Facade point

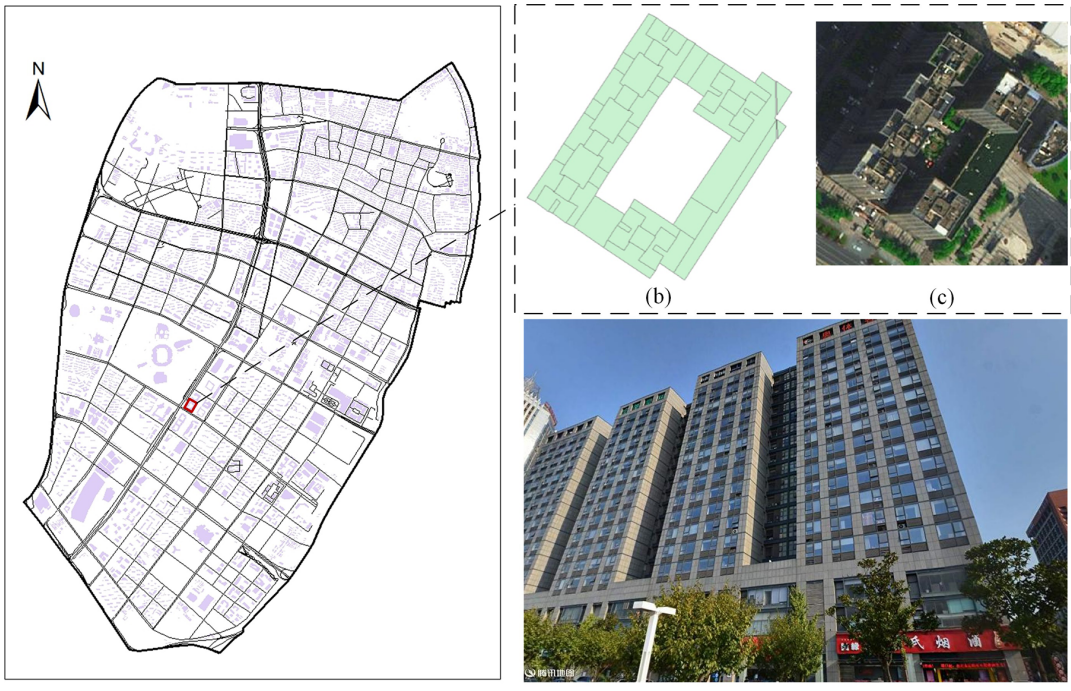

Figure 5. Two-dimensional vector contour data of buildings: (a) overall display of the vector data; (b) the vector data of the Olympic Mingzuo building; (c) the top view contour in the satellite image of the Olympic Mingzuo building; (d) the photo of the Olympic Mingzuo building.

Table 2. Groups of buildings for reconstruction experiments and performance evaluation.

Group	Number	Description
A	112	Buildings be reconstructed
B	6	Buildings in Group A chosen to product comparative experiment
B-1	6	Buildings in Group B that remove other-source photos
C	53	Buildings with relatively complete façade point cloud
D	20	Buildings in Group C that covered by lidar data
E	16	Buildings in Group D with the same reconstructed facades as the lidar scanning facades

cloud: 16 buildings were selected for comparison of reconstruction facades with vehicle lidar facades (Group E) (see Table 2).

Evaluation Indicators

The façade point cloud evaluation indicators comprised the following two aspects:

1. Cloud to cloud: We calculated the absolute offset distance between the 3D model point cloud and the true value data for each building. As shown in Figure 6, we calculated the distance d_i between each point R_i in the 3D point cloud R and the nearest neighbor point T_i in the truth point cloud T. The average absolute error, minimum distance, and maximum distance were determined as the bases of accuracy evaluation.
2. Cloud to mesh: Because point clouds are discrete, the cloud-to-cloud distance may not represent a true distance. The cloud-to-mesh distance provides a more accurate assessment of each point's nearest neighbor. Hence, as shown in Figure 7, we generated a Delaunay 2.5D triangular grid on the X-Y plane from the lidar point cloud, and searched for the nearest triangular P_i to R_i. Then we calculated the absolute distance deviation $|d_{P_i}|$ between R_i and P_i, and recorded the number of points that satisfied $|d_{P_i}|<0.8$m. The mean error and root-mean-square error d_{RMS} were subsequently calculated using Equation 7 to evaluate the accuracy.

$$d_{\mathrm{RMS}} = \sqrt{\frac{\sum_{i=1}^{n} d_{Pi}^2}{n}} \tag{7}$$

where n is the number of points in 3D model point cloud.

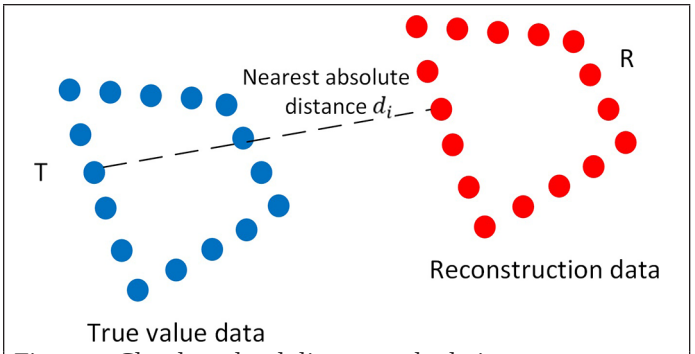

Figure 6. Cloud-to-cloud distance calculation.

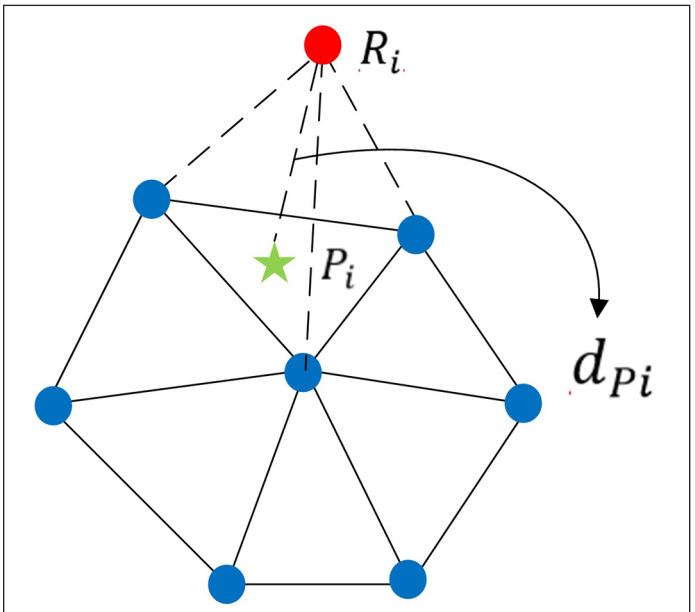

Figure 7. Calculation of cloud-to-mesh distance.

Results and Discussion

Threshold Determined from Street View Images

The initial selection of street view images for the experiment was an iterative process. First, 260 street view images were randomly selected for 3D reconstruction. The green and sky areas from all the 260 selected images were extracted. The buildings that were completely reconstructed were then

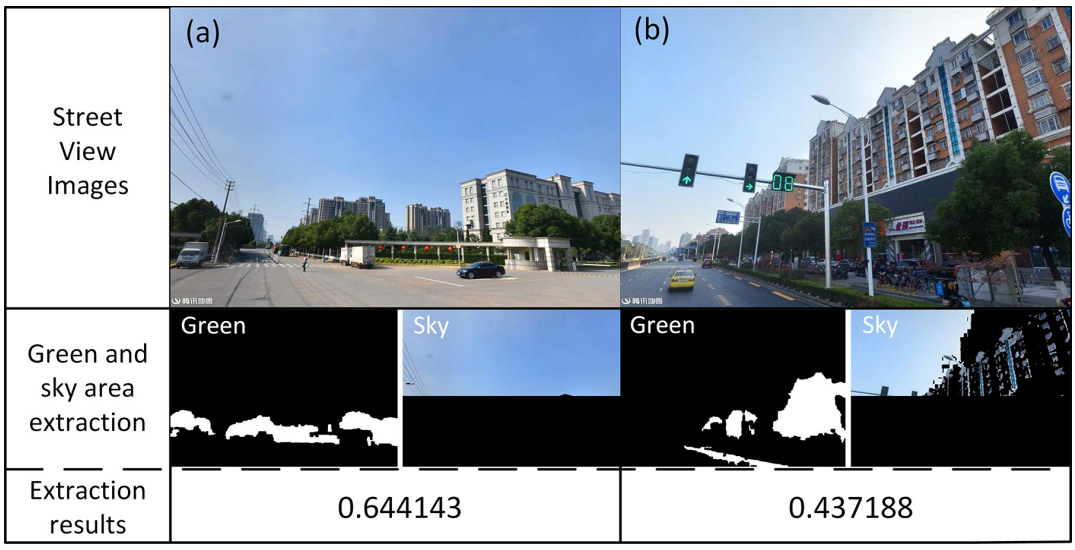

Figure 8. Results of nonbuilding region extraction.

separated. Considering the two images in Figure 8 as examples, the 3D reconstruction of the building in image (a) failed, while reconstruction in image (b) was completed. The green and sky areas in the two images were successfully extracted. Figure 8 includes the extraction results of green and sky regions and total sizes of green and sky areas. As we can see, the green and sky areas in image (a) is larger than image (b).

As shown in Figure 9, when the green and sky area threshold is set to 0.5, it is easier to select street view images that would ensure complete 3D reconstruction. This can reduce the number of photos used for the reconstruction, which will make grouping easier.

In the early stage of the study, we have downloaded street view images of 62 cities over the world, as shown in Figure 10. As a result, many buildings are built on concrete streets without any green vegetation periphery. In this case, only the sky area in the image was extracted. The images where the sky area is larger than the set threshold will be eliminated. In addition, it is rare that the building itself is green. Although this method has limitation of green buildings, the proportion of green buildings is too small to affect the result.

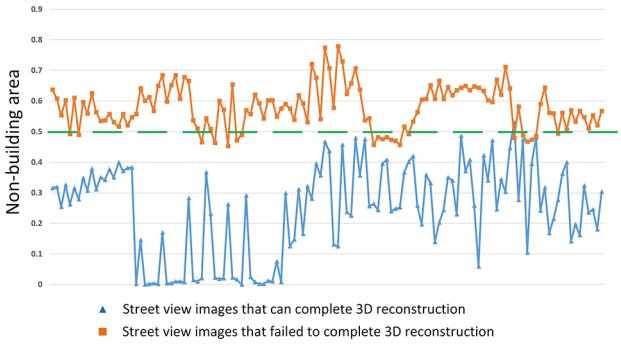

Figure 9. Threshold determined from street view images.

Facade Reconstruction Results and Visual Quality Evaluation

In this experiment, 3673 street view images were selected for 3D building reconstruction, supplemented by 46 other-source photos. The number of reconstructed buildings was 112 (Group A). Noise that included sky, points, roads, and other surrounding objects was removed from all generation models for subsequent analysis and accuracy evaluation. However, complete denoising is impossible. There were outliers that required further removal during the accuracy evaluation.

The results of the 3D reconstruction are shown in Figure 11. Figure 11a shows the buildings with better restoration of facade and reconstruction point clouds, while Figure 11b shows the buildings with unsatisfactory point cloud recovery and reconstruction point clouds. The latter group of buildings can be roughly divided into three classes: (1) Buildings that the central part of the point cloud is missing: An example is the building in street view image (7) in Figure 11b. Because the algorithm uses 2D photos to develop a 3D model, it involves automatic identification of matching parts from adjacent photos. The original shape of object is calculated based on its deformation observed from different angles. Hence, a building with smooth and reflective surfaces would not be properly modeled by this technique. (2) Buildings that the point cloud of upper or lower part is missing: An example is the building in image (8) in Figure 11b. This may be because that the building is too tall or the data collection vehicle was too close to it, which will make the street view images not completely capturing the top of building or bottom part such as vegetation, vehicles, and other objects. (3) Buildings with tilted point clouds, such as that in image (9) in Figure 11b.

After eliminating models with poor recovery of the point clouds, the number of building models was reduced to 53


Figure 10. Street view images of 62 cities around the world.

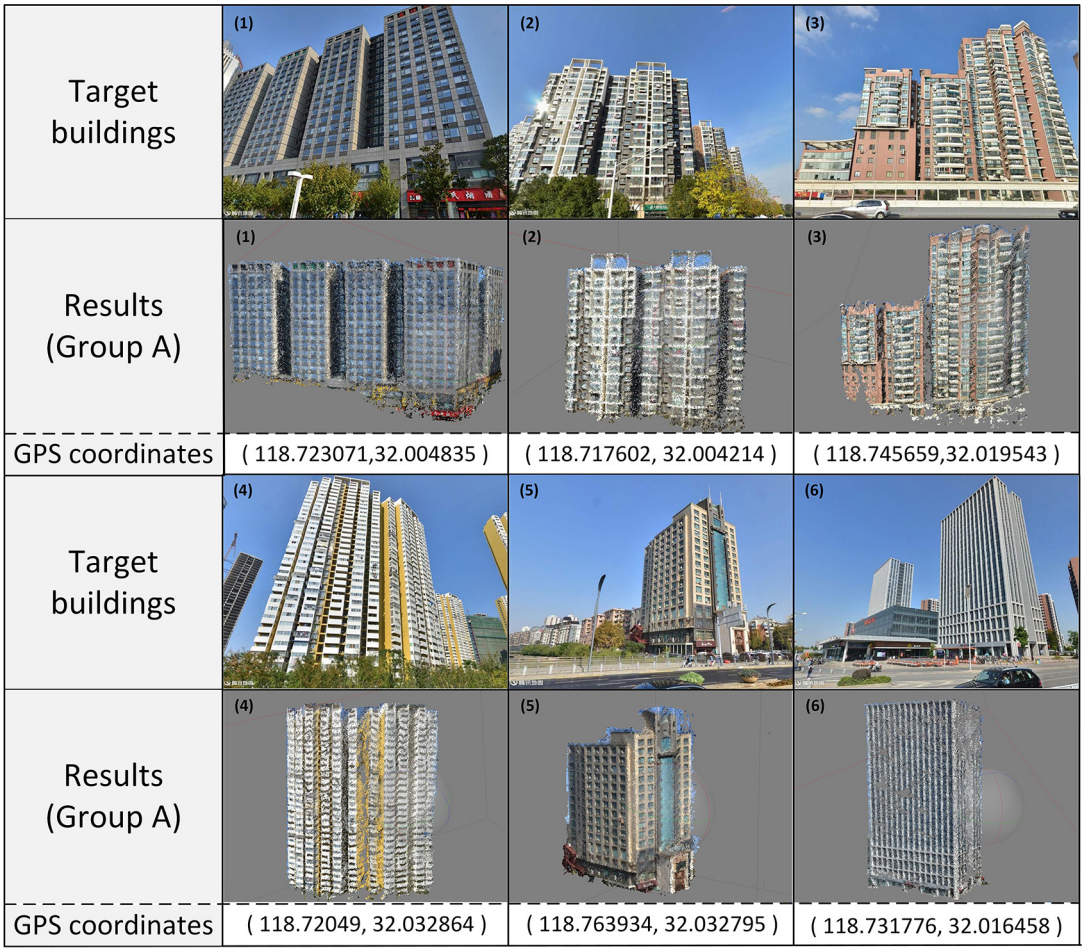

Figure 11. Results of buildings' 3D reconstruction: (a) the buildings with better restoration of the façade and reconstruction point clouds; (b) the buildings with unsatisfactory point cloud recovery and the reconstruction point clouds.

(Group C). As shown in Figure 12, the red marks indicate the locations of those 53 buildings that finely completed 3D reconstruction. The buildings are evenly distributed over the study area. Among them, 25 buildings were reconstructed with the aid of other-source photos.

Based on the above classification of buildings and indicators of the geographical national conditions census (GDPJ 01-2013), the buildings with completed 3D reconstruction were divided into four groups according to their height, as presented in Table 3. It can be seen that the proposed 3D reconstruction method is suitable for middle high-rise and super high-rise buildings.

Contribution of Other-Source Photos

The reconstruction results of comparative experiment described in the section "Reconstruction and Performance Evaluation Experiments" are shown in Figure 13a. The effects of adding the other-source photos on 3D reconstruction results

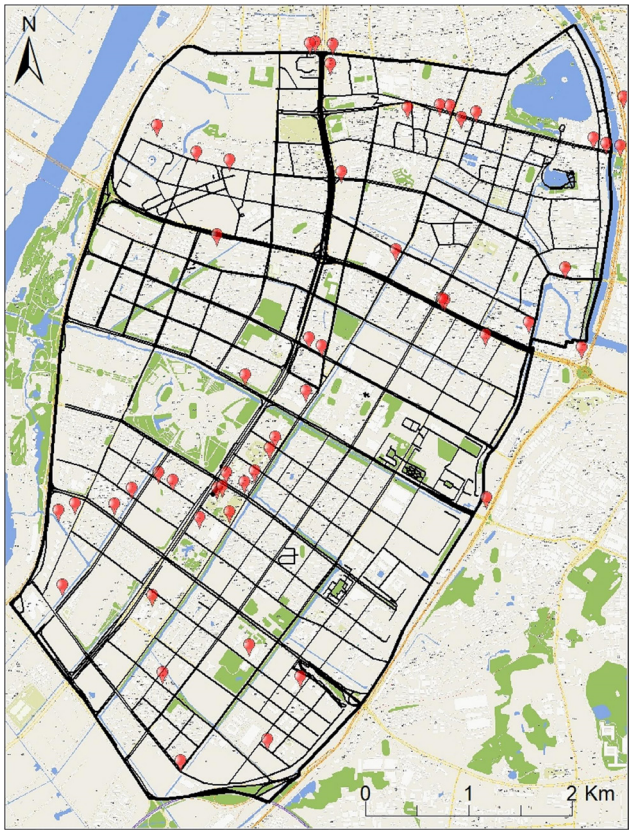

Figure 12. Distribution of the finely completed 3D building reconstruction.

Table 3. Classification of buildings with completed 3D reconstruction.

Level	Height	Building Classification	Number
One	1~3floors height < 10m	Low or abandoned buildings	0
Two	4~9floors 10 < height < 25m	Multi-floor buildings	0
Three	10~18floors 25 < height < 50m	Middle high-rise buildings	12
Four	19~38floors height > 50m	Super high-rise buildings	41

can be roughly divided as follows: (1) Case of Group B(1): Improved deformation of building and integrity of point cloud, as highlighted by red frames and reflected by the clearer texture of blue windows. (2) Case of Group B(2): Improved tilting condition of the dense point. (3) Group B(3) and B(4): Improved point cloud integrity at the bottom and upper parts of building, respectively, as highlighted by red frames. (4) Group B(5) and B(6): Good point cloud quality with no obvious change when other-source photos are applied. It is noteworthy that the number of dense points of building in (5) in Figure 13a was increased only from 54 313 to 55 355. Regarding the building in (6) in Figure 13a, the other-source photos significantly increased the number of dense points from 47 562 to 88 118.

Figure 14 shows the point cloud densities of buildings in Group B-1(6) and Group B(6). It can be seen that the other-source photos significantly increase the volume density, with the density peak increasing from 10.5 to 25, as indicated by the red line in the figure.

As a result, other-source photos can improve the reconstruction of most point clouds. When the camera position cannot be correctly restored with other-source photos, only street view images will be used for 3D reconstruction. In Figure 13b, the red frame shows a newly introduced Internet photo. Because the left and right sides of the building are highly symmetrical, the street view image and other-source photos have no additional public parts apart from the building. In addition, the angle of the Internet photo is different from selected street view images, which results in failure to recover the correct photo camera position.

Quantitative Analysis of Facade Point Cloud Quality

As shown in Figure 15, it was necessary to extract vehicle lidar point cloud first. The nontarget points such as ground, streetlights, and trees were filtered out. The different parts of ground objects between lidar data and reconstructed data needed to be removed as well (considering the time difference between the data of the two phases). As shown in Figure 15(1), it was necessary to crop the points in the red box. The point cloud extraction result was thus obtained for comparison, as shown in Figure 15(2). In addition, the reconstructed point cloud contained noise points that affected the calculation of absolute distance. Therefore, it was necessary to filter out the noise from the reconstructed point cloud, as shown in the red frame in Figure 15(3).

Cloud-to-Cloud Facade Point Cloud Accuracy

The statistical details of absolute distance results are presented in Table 4. The minimum error is 0.005 m, while the maximum error is 3.272 m. Overall, the average error is only 0.391 m, which shows that the recovery of building point clouds has a good fit with the true value. However, the maximum error is slightly high. We will use three single buildings (E13, E5, E15) to analyze the cause of this error. The average errors of these three cases are 0.29 (small), 0.358 (medium), and 0.69 (large), respectively.

Table 4. Absolute distances of the building point clouds.

Building Number	Statistical Points	Average Error (m)	Minimum Distance (m)	Maximum Distance (m)
E1	85 532	0.314	0.003	2.841
E2	43 154	0.473	0.006	4.711
E3	77 180	0.475	0.003	3.732
E4	33 956	0.468	0.007	3.184
E5	35 776	0.358	0.008	2.563
E6	60 074	0.865	0.004	4.245
E7	51 452	0.350	0.002	2.916
E8	51 899	0.492	0.004	3.805
E9	49 989	0.303	0.005	1.859
E10	52 688	0.184	0.003	2.725
E11	72 247	0.183	0.003	2.940
E12	57 775	0.586	0.007	6.750
E13	47 702	0.290	0.006	2.307
E14	17 600	0.077	0.002	1.011
E15	19 565	0.690	0.010	4.746
E16	31 261	0.140	0.006	1.382
Average value	49 241	0.391	0.005	3.272

Figure 16a shows the offset distances of building E13, with the magnitude of errors colored from blue (small) to red (large). The overall error distribution is relatively uniform,

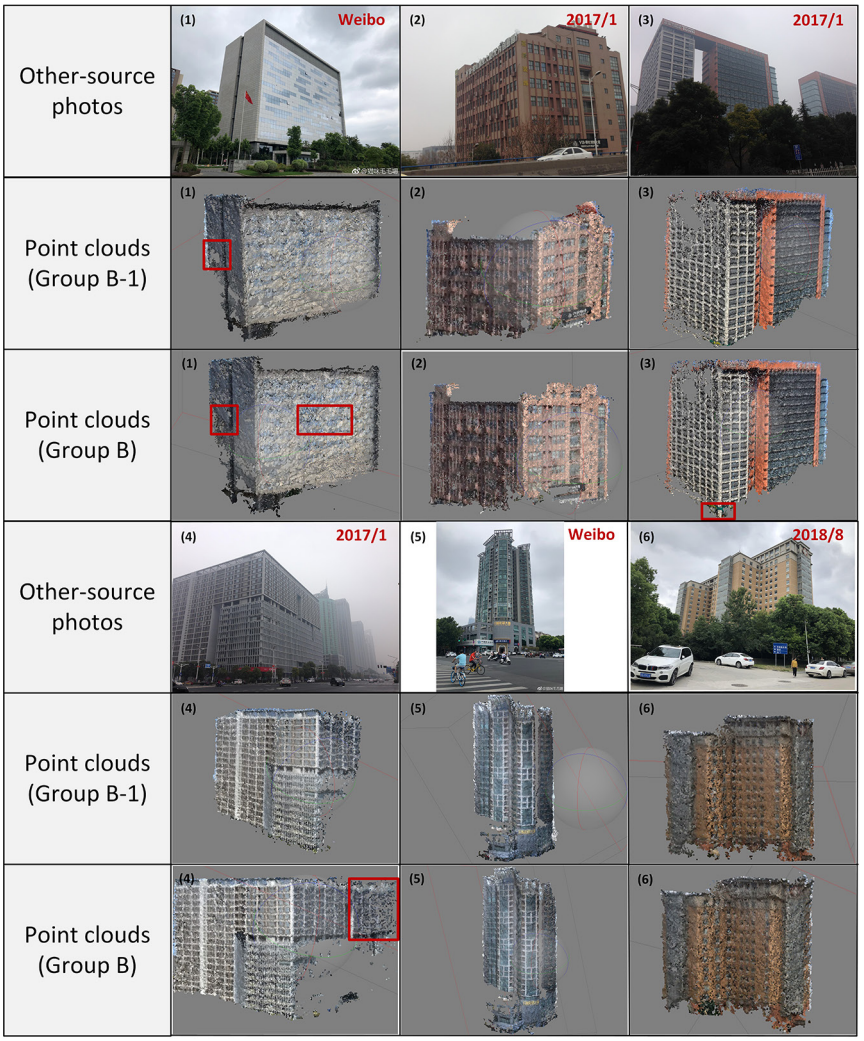

Figure 13. Comparative analysis of the impact of introducing other sources photos: (a) cases that the point cloud was improved after the introduction of the other sources photos; (b) case that the camera position cannot be correctly restored after introduction of the other sources photos.

with most of errors being small. Larger errors mainly occur in the top and bottom parts of building. The errors in the top (region 1) were due to the sky points and residual noise after filtering. In addition, as shown in region 2 in Figure 16b, the vehicle lidar data scan was affected by trees, vehicles, and other objects that located in the bottom part of building. The errors in the middle part of building (region 3) is mainly due to the complex structure of walls. The building has an intrusion about 4.8 m, and the data contains noise. In such cases, the reconstructed point cloud data has a positional shift, as shown in Figure 16c.

A histogram of absolute error of building E13 is shown in Figure 17, where the color code is the same as in Figure 16. The histogram reveals that absolute distance error follows is

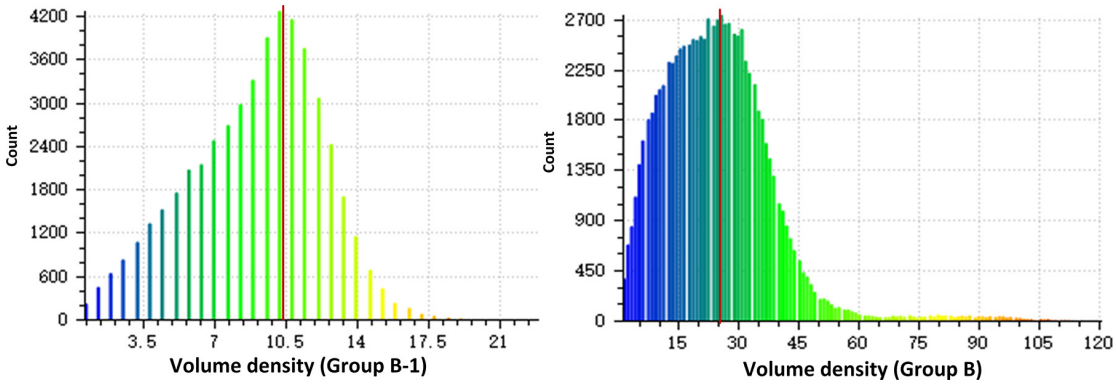

Figure 14. Distribution of the point cloud density.

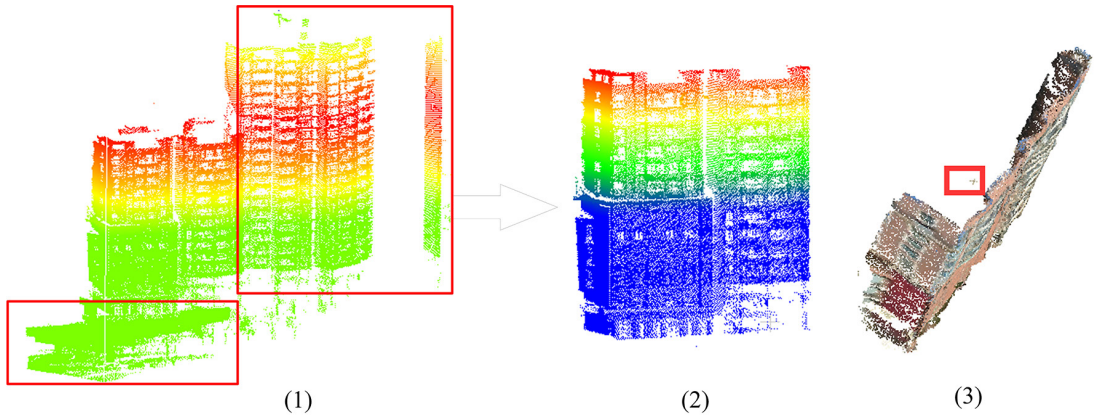

Figure 15. Point cloud denoising: (1) schematic diagram of vehicle lidar point cloud denoising; (2) lidar point cloud building extraction result; and (3) filtering diagram of the reconstruction point cloud outlier data.

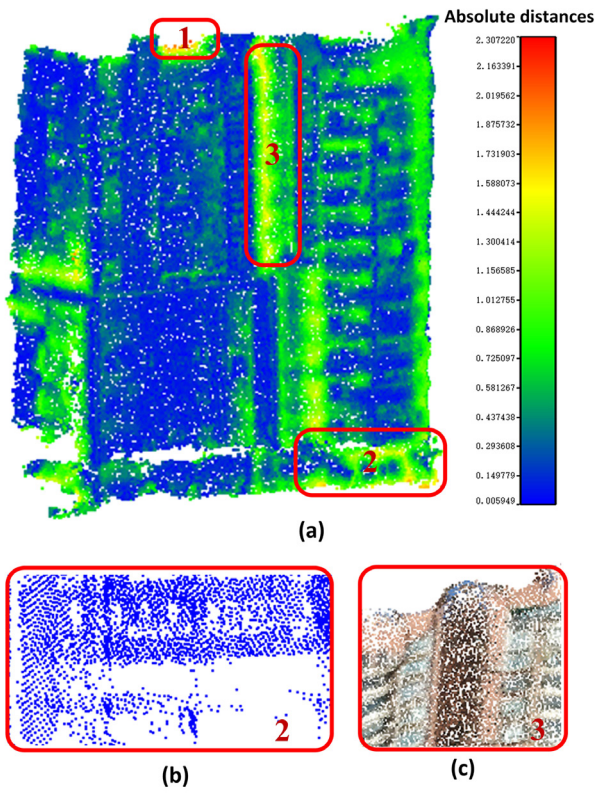

Figure 16. Absolute distance error of building E13: (a) offsets between the 3D model and the lidar points; (b) lidar points in region 2; and (c) reconstructed points in region 3.

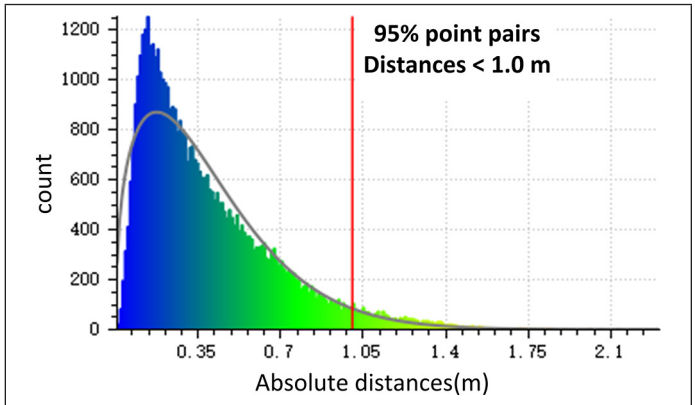

Figure 17. Histogram of absolute distance errors of building E13.

a Weber distribution. About 95% of point pairs have error distances less than 1.0 m, while mostly about 0.15 m. With increasing absolute distance, the number of point pairs exponentially decreases. It can be intuitively observed from the histogram that the building point cloud generated by proposed method is accurately spatially positioned.

Similarly, as shown in Figure 18a, the overall error distribution of building E5 is relatively uniform, with most of errors being small. In region 1, the residue noise after the filtering caused the errors in the top. In addition, as shown in region 2 in Figure 18b, the bottom of reconstructed point cloud was missing because of vegetation, vehicles, and other objects, which resulted in large errors. The error in region 3 is mainly due to the building that has an intrusion about 5.5 m, and the reconstructed point cloud data has a positional shift, as shown in Figure 18c.

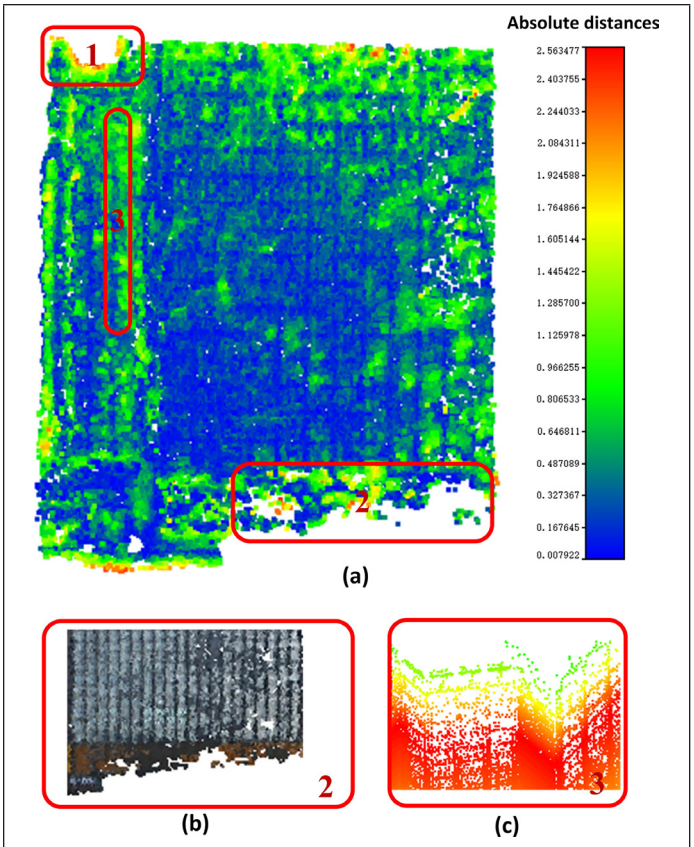

Figure 18. Absolute distances error analysis of building E5: (a) offset distances between the 3D model and lidar points; (b) the reconstructed points of region 2; (c) the lidar points of region 3.

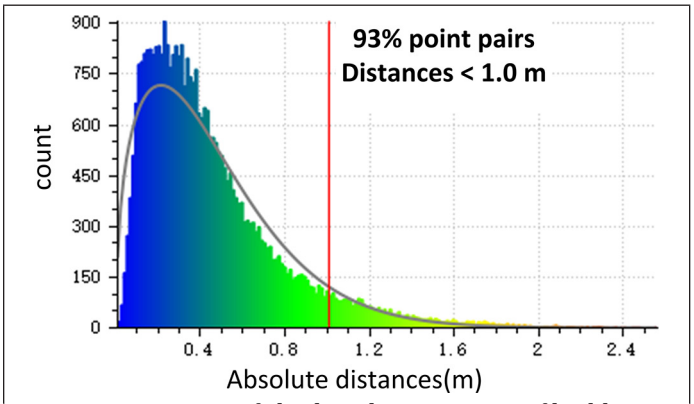

Figure 19. Histogram of absolute distance errors of building E5.

The absolute error histogram of building E5 is shown in Figure 19, where the color code is the same as in Figure 18. Similar to Figure 17, the absolute distance error follows a Weber distribution. About 93% of point pairs have error distances less than 1.0 m, while mostly about 0.2 m. With increasing absolute distance, the number of point pairs exponentially decreases.

For buildings with larger offset errors, we choose a typical case (E15) for description. Figure 20a shows the offset distances, with the magnitude of errors colored from blue (small) to red (large). The whole errors are almost located in the low value and median value regions. The greatest error is located at the top (region 1). The building has an intrusion about 6 m. Due to scanning limitations, the lidar point cloud was missing, which resulted in larger errors, as shown in Figure 20b. The error in region 2 is mainly due to the complex structure of the wall. The building has a curved wall, and the reconstructed point cloud data may have a positional shift in such cases.

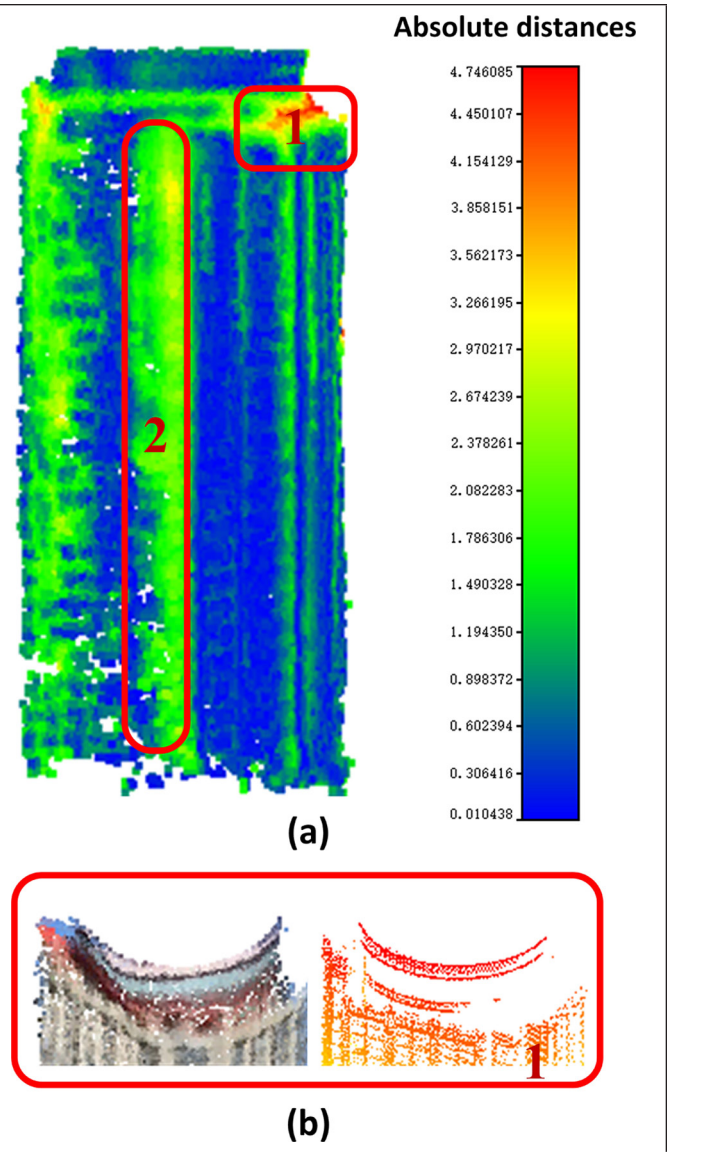

Figure 20. Absolute distances error analysis of building E15: (a) offset distances between the 3D model and lidar points; (b) the reconstructed points and the lidar points of region 2.

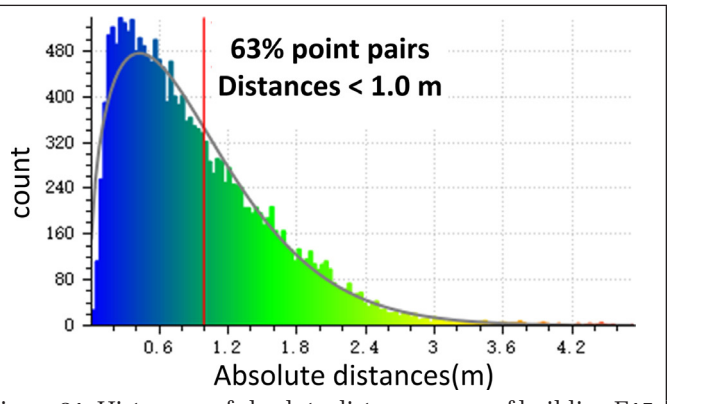

Figure 21. Histogram of absolute distance errors of building E15.

A histogram of absolute error of building E15 is shown in Figure 21, where the color code is the same as in Figure 20. The absolute distance error also follows a Weber distribution. About 63% of point pairs have error distances less than 1.0 m, while mostly about 0.4m. As the absolute distance increases, the number of point pairs decreases exponentially.

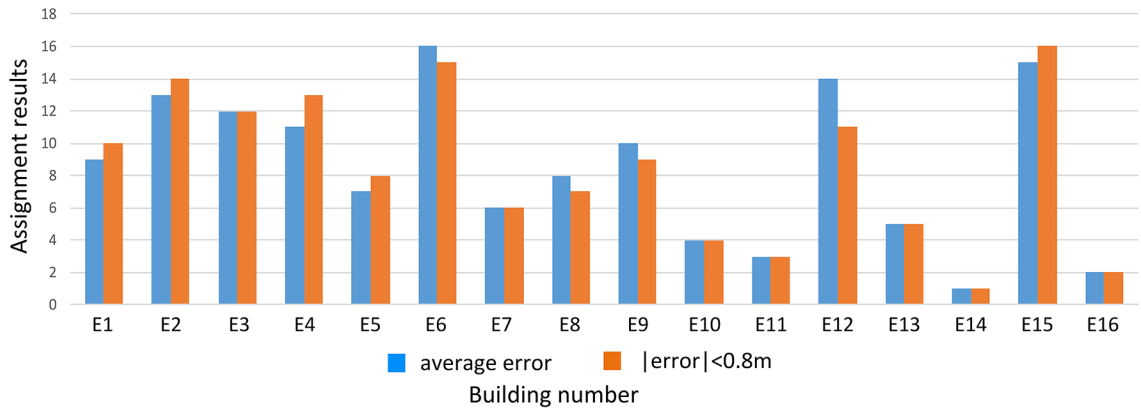

Figure 22. Ranking chart for accuracy of building reconstruction.

Table 5. Cloud-to-mesh distances.

Building Number	Statistical Points	Average Error (m)	Standard Deviation (m)	–0.8 m < error < 0.8 m (%)
E1	85 532	0.372	0.021	93.81
E2	43 154	0.527	0.295	89.87
E3	77 180	0.475	0.067	92.22
E4	33 956	0.416	0.279	91.28
E5	35 776	0.325	0.389	95.66
E6	60 074	0.901	0.252	81.10
E7	51 452	0.277	0.066	97.07
E8	51 899	0.346	0.088	96.80
E9	49 989	0.373	0.164	94.41
E10	52 688	0.188	0.150	98.67
E11	72 247	0.171	0.393	98.98
E12	57 775	0.629	0.021	92.85
E13	47 702	0.267	0.021	97.80
E14	17 600	0.056	0.026	100
E15	19 565	0.631	0.360	80.61
E16	31 261	0.135	0.237	99.57
Average value	49 241	0.381	0.177	93.79

Cloud-to-Mesh Facade Point Cloud Accuracy

The evaluation results are shown in Table 5, from which it can be seen that the reconstructed point clouds have a good fit with true point clouds. The average error is 0.381 m. The absolute error distances of about 93.8% point pairs are within 0.8 m. Using the method presented by Chen *et al.* (2015), all 16 buildings (Group E) were assigned and ranked according to their average errors, from 1 (small error) to 16 (large error). The ratios of points with errors less than 0.8 m are also ranked. The buildings with smaller ranks were positioned more accurately. The ranking chart is shown in Figure 22.

From Figure 22, the average error ranking is strongly positively correlated with the ratio ranking. That is, the buildings with smaller average errors also have a larger proportion of points with absolute distance errors less than 0.8 m.

Figure 23a shows the facade point clouds of buildings E5, E10, E13, and E16. These buildings have small error distances, which is because that the facade structures are relatively regular and top contours are approximately rectangular. Therefore, the locations of reconstructed point clouds could be restored more accurately. With increasing complexity of facade structures of buildings, the errors of model point clouds increase. As shown in Figure 23a, there is a partial recessed structure on the facade of building E13, and a curved wall on building E5. The order of contour complexity of building facades is E16 < E10 < E13 < E5, which reveals a strong positive correlation with the error ranking.

Figure 23. Facade point clouds of different buildings: (a) buildings with high fit, and (b) buildings with slightly lower fit.

Buildings E2, E6, and E15 have larger offset errors, as shown in Figure 23b. Building E15 is a ring structure and the wall of building E6 has many recessed parts, which will easily cause great errors during point cloud reconstruction.

Although the contour of building E2 is relatively regular, it is very high and misses a significant part of its top in vehicle lidar data, which results in an increased offset distance.

Facade Height Accuracy

The height extraction results are shown in Figure 24. Owing to the great height of building in Figure 24, image (1), its top was missing from reconstructed point cloud. Therefore, a low-rise building next to it was selected to verify the accuracy. The differences between estimated and true values is much smaller in panels (1), (2), (3), and (4) in Figure 24, which indicates that ICP registrations are more accurate in these panels. In the case of buildings with complex top contours, such as in panels (5) and (6) in Figure 24, the 2D vector data have some deviations. This will result in large ICP registration errors between inversion point clouds and reconstruction point clouds, which may affect accuracy of estimated building heights.

Figure 25a shows scatter plots of the estimated building heights in Group D versus the true values. The height data obtained from 3D reconstruction is strongly correlated with true values, which indicates that extraction of height information for both high and low buildings is accurate. Figure 25b shows a histogram of relative errors between estimated heights and true values. In the figure, the buildings are numbered from 1 to 20 according to their heights from low to high. The heights estimated by proposed method for lower buildings are mostly lower than true values, whereas those for higher buildings are significantly higher than true values. It is mainly due to the incomplete vehicle lidar data for tall buildings.

The error value E and absolute precision P are defined by Equations 8 and 9, respectively. For the 20 data sets, the E values are within 0.03–10.2 m, the P values are within 81.54%–99.91%, and the average absolute accuracy is 96.67%. Thus, it can be indicated that the proposed method enables accurate estimation of building heights.

$$E = |S - T| \tag{8}$$

$$P = 1 - E/T \tag{9}$$

where S is the estimated value, and T is the true value.

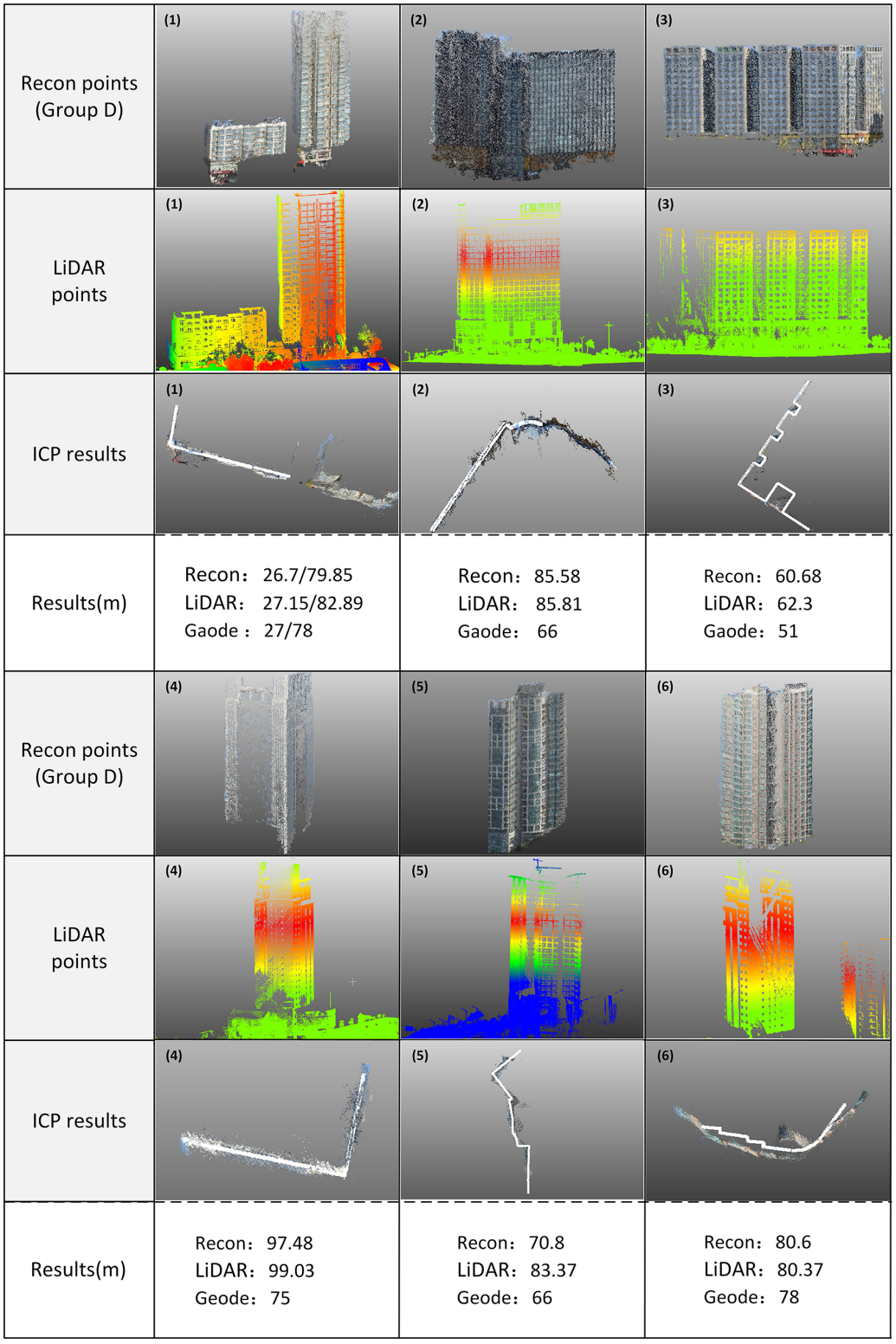

Figure 24. Extracted building height information ("recon" indicates reconstruction).

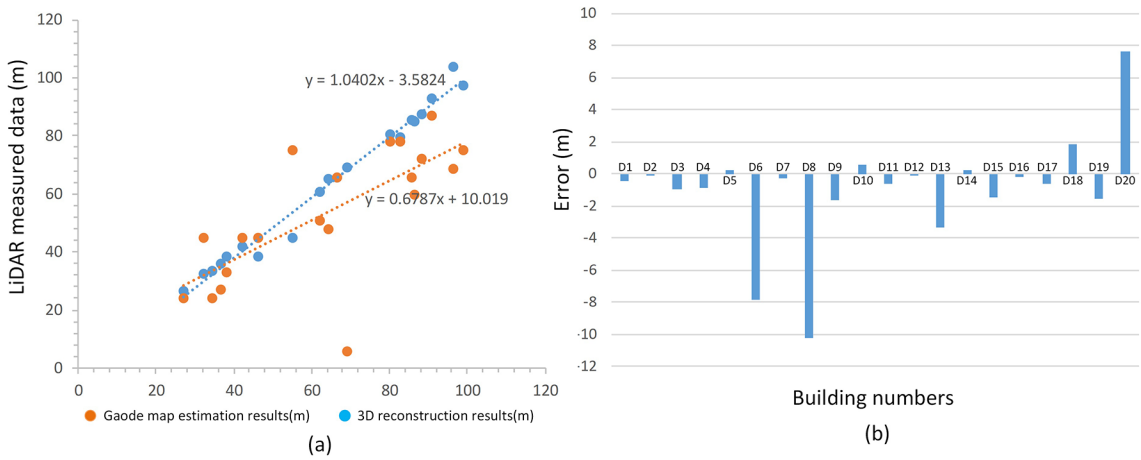

Figure 25. Errors of estimated building heights: (a) scatter plots of the heights of the Group D buildings estimated from the reconstructed point cloud and the Gaode data versus the true values; (b) the relative errors between the heights estimated by the reconstructed point cloud and the true values.

Conclusions

In this paper, we proposed a method for integrating crowd-sourced photos and 2D vector data for 3D reconstruction of building facades in large urban areas. In the present demonstration of proposed method, the utilized photos were mainly Tencent street view images, which were supplemented by photos obtained from other sources. The method was qualitatively and quantitatively evaluated by experiments in Jianye District in Nanjing. In the experiment, 53 buildings were finely reconstructed, and 25 of them were reconstructed with the aid of other-source photos. Using vehicle lidar data in study area as true values, the height estimation accuracy of proposed method was determined to be 96.67%, with average absolute cloud-to-cloud and cloud-to-mesh errors of 0.391 and 0.381 m, respectively. These results show that the method can be effectively used to combine different source data for high-precision building facade modeling.

The main innovation of this study is a new technical framework to generate 3D building facade information. The data used in this study (i.e., street view images and 2D vector contour data) are open source and low-cost. According to the experiments, the accuracy of obtained building facade information is verified. The proposed framework represents a novel 3D reconstruction method that utilizes multi-sourced data through a three-step strategy: selection and grouping of crowd-sourced photos, 3D reconstruction using the selected photos, and point cloud registration based on 2D vector data.

The proposed 3D reconstruction method, however, has some limitations. It is applicable to most high-rise buildings, while it may fail to conduct a complete reconstruction for low buildings, especially in densely built areas. Further development is required to overcome this limitation. Besides, we will attempt to solve the problem of missing point cloud data because of moving objects around buildings. We will also try to collect more kinds of photo sources and focus on photo processing including removing indoor image. In addition, we will study on feature matching of nontextured regions to improve the quality of subsequent 3D reconstruction. Moreover, we have not taken into account the case that the building itself was green, although the conclusion is still reliable, the solution will be discovered in future studies.

Acknowledgments

This work was supported by the National Key Research and Development Plan (Grant No. 2017YFB0504205), the National Natural Science Foundation of China (Grant No. 41622109, Grant No. 41901401), and the Natural Science Foundation of Jiangsu Province (Grant No. BK20190743).

References

Aicardi, I., F. Chiabrando, N. Grasso, A. M. Lingua, F. Noardo and A. Spanò. 2016. UAV photogrammetry with oblique images: First analysis on data acquisition and processing. Pages 835–842 in *Proceedings of ISPRS—International Archives of the Photogrammetry, Remote Sensing and Spatial Information Sciences*, Volume XLI-B1.

Badri, F., E. M. Yuniarno and S.N.S. Mardi. 2016. 3D point cloud data registration based on multiview image using SIFT method for Djago temple relief reconstruction. Pages 191–195 in *Proceedings of the International Conference on Instrumentation.*

Blaschke, T., S. Lang, E. Lorup, J. Strobl and P. Zeil. 2000. Object-oriented image processing in an integrated GIS/remote sensing environment and perspectives for environmental applications. In *Environmental Information for Planning, Politics and the Public, vol 2,* edited by A. Cremers and K. Greve, 555–570. Marburg, Germany: Metropolis.

Chen, Y. M. 2015. *Multi-View Reconstruction of* 3D *Building Models Based on Airborne and Mobile LiDAR Data.* Ph. D. Dissertation, Nanjing University, Jiangsu, China, 120 pp.

Chen, Y., M. Li, L. Cheng, H. Xu, S. Li and X. Liu. 2017. Three-dimensional reconstruction and solar energy potential estimation of buildings. *American Geophysical Union* GC33E-1132.

Cheng, L., S. S. Chu, W. W. Zong, S. Y. Li, J. Wu and M. C. Li. 2017. Use of Tencent street view imagery for visual perception of streets. *International Journal of Geo-Information* 6:265. doi: 10.3390/ijgi6090265.

Cheng, L., Y. Wu, S. Chen, W. W. Zong, Y. Yuan, Y. F. Sun, Q. Z. Zhuang and M. C. Li. 2017. A symmetry-based method for LIDAR Point registration. *IEEE Journal of Selected Topics in Applied Earth Observations and Remote Sensing* 11 (1):285–299.

Cheng, L., Y. Wu, L. H. Tong, Y. M. Chen and M.C. Li. 2015. Hierarchical registration method for airborne and vehicle LIDAR point cloud. *Remote Sensing* 7 (10):13921–13944.

Cheng, L., Y. Yuan, N. Xia, S. Chen, Y. M. Chen, K. Yang, L. Ma and M. C. Li. 2018. Crowd-sourced pictures geo-localization method based on street view images and 3D reconstruction. *ISPRS Journal of Photogrammetry and Remote Sensing* 141 (2018):72–85.

Christian, F. and Z. Avideh. 2004. An automated method for largescale, ground-based city model acquisition. *International Journal of Computer Vision* 60 (1):5–24.

Cornelis, N., B. Leibe, K. Cornelis and G. L. Van. 2008. 3D urban scene modeling integrating recognition and reconstruction. *International Journal of Computer Vision* 78 (2):121–141.

Elberink, S. O. and V. George. 2011. Quality analysis on 3D building models reconstructed from airborne laser scanning data. *ISPRS Journal of Photogrammetry and Remote Sensing* 66 (2):157–165.

Fan, H. C. and A. Zipf. 2016. Modelling the world in 3D from VGI/Crowdsourced data In *European Handbook of Crowdsourced Geographic Information*, 435–446. doi: http://dx.doi.org/10.5334/bax.ae.

Furukawa, Y. and J. Ponce. 2008. Accurate camera calibration from multi-view stereo and bundle adjustment. *International Journal of Computer Vision* 84 (3):257–268.

Hartl, P. and F. Cheng. 1995. Delimiting the building heights in a city from the shadow in a panchromatic SPOT-image—Part 2: Test of a complete city. International Journal of Remote Sensing 16 (15):2829–2842.

Har-Peled, S., P. Indyk and R. Motwani. 2012. Approximate nearest neighbor: Towards removing the curse of dimensionality. *Theory of Computing* 8 (1):321–350.

Hu, J. H., S. Y. You and U. Neumann. 2006. Automatic pose recovery for high-quality textures generation. In *IEEE Computer Society Proceedings 18th International Conference on Pattern Recognition (ICPR 2006)*, held in Hong Kong, China, 20–24 August 2006.

Huang, X. J. and L. K. Kwoh. 2007. 3D building reconstruction and visualization for single high resolution satellite image. In *Proceedings IEEE International Geoscience and Remote Sensing Symposium*,held in Barcelona, Spain, 23–28 July 2007.

Jayaraman, S., S. Esakkirajan and T. Veerakumr. 2009. *Digital Image Processing*. India: Tata McGraw Hill Education.

Lee, T. 2009. Robust 3D street-view reconstruction using sky motion estimation. Pages 1840–1847 in *Proceedings IEEE International Conference on Computer Vision Workshops*.

Li, X. J., C. R. Zhang, W. D. Li, R. Ricard, Q. Y. Meng and W. X. Zhang. 2015. Assessing street-level urban greenery using Google Street View and a modified green view index. *Urban Forestry & Urban Greening* 14 (3):675–685.

Liasis, G. and S. Stavrou. 2016. Satellite images analysis for shadow detection and building height estimation. *ISPRS Journal of Photogrammetry and Remote Sensing* 119:437–450.

Lourakis, M.I.A. and A. A. Argyros. 2009. SBA: A software package for generic sparse bundle adjustment. *ACM Transactions on Mathematical Software* 36 (1):2.

Lowe, D. G. 1999. Object recognition from local scale-invariant features. In *Proceedings of the Seventh IEEE International Conference on Computer Vision*, held in Kerkyra, Greece, 20–27 September 1999.

Lowe, D.G. 2004. Distinctive image features from scale-invariant keypoints. *International Journal of Computer Vision* 60 (2):91–110.

Malihi, S., M.J.V. Zoej and M. Hahn. 2018. Large-scale accurate reconstruction of buildings employing point clouds generated from UAV imagery. *Remote Sensing*, 10:1148.

Matas, J., O. Chum, M. Urban and T. Pajdla. 2004. Robust wide-baseline stereo from maximally stable extremal regions. *Image Vision Computing* 22 (10):761–767.

Mayer, H. and S. Reznik. 2007. Building facade interpretation from uncalibrated wide baseline image sequences. *ISPRS Journal of Photogrammetry and Remote Sensing* 61 (6):371–380.

Nina, D., S. Mihail and C. Spartak. 2018. Smart city: Automatic reconstruction of 3D building models to support urban development and planning. *MATEC Web of Conferences*, 251:03047.

Nister, D. 2003. An efficient solution to the five-point relative pose problem. *IEEE Transactions on Pattern Analysis & Machine Intelligence*. doi: 10.1109/CVPR.2003.1211470.

Pollefeys, M., D. Nistér, J.-M. Frahm, A. Akbarzadeh, P. Mordohai, B. Clipp, C. Engels, D. Gallup, S.-J. Kim, P. Merrell, C. Salmi, S. Sinha, B. Talton, L. Wang, Q. Yang, H. Stewénius, R. Yang, G. Welch and H. Towles. 2008. Detailed real-time urban 3D reconstruction from video. *International Journal of Computer Vision* 78 (2):143–167.

Shi, P. and V. George. 2009. Knowledge based reconstruction of building models from terrestrial laser scanning data. *ISPRS Journal of Photogrammetry and Remote Sensing* 64 (6):575–584.

Snavely, N., S. M. Seitz and R. Szeliski. 2008. Modeling the world from internet photo collections. *International Journal of Computer Vision* 80 (2):189–210.

Soergel, U., E. Michaelsen, A. Thiele, E. Cadario and U. Thoennessen. 2009. Stereo analysis of high-resolution SAR images for building height estimation in cases of orthogonal aspect directions. *ISPRS Journal of Photogrammetry and Remote Sensing* 64 (2009):490–500.

Stilla, U., U. Soergel and U. Thoennessen. 2003. Potential and limits of InSAR data for building reconstruction in built-up areas. *ISPRS Journal of Photogrammetry and Remote Sensing* 58 (2003):113–123.

Tian, Y. X., M. Gerke, G. Vosselman and Q. Zhu. 2010. Knowledge-based building reconstruction from terrestrial video sequences. *ISPRS Journal of Photogrammetry and Remote Sensing* 65 (2010):395–408.

Toschi, I., M. M. Ramos, E. Nocerino, F. Menna, F. Remondino, K. Moe, D. Poli, K. Legat and F. Fassi. 2017. Oblique photogrammetry supporting 3D urban reconstruction of complex scenarios. *The International Archives of the Photogrammetry, Remote Sensing and Spatial Information Sciences* XLII-1/W1:519–526.

Varney, N. M. and V. K. Asari. 2015. Volume component analysis for classification of LiDAR data. P*roceedings of SPIE 9477*. doi: 10.1117/12.2179268.

Vedaldi, A. and B. Fulkerson. 2010. *VLFeat* 2010:1469.

Wang, L., S. Y. You and U. Neumann. 2007. Semiautomatic registration between ground-level panoramas and an orthorectified aerial image for building modeling. Pages 1–8 in *Proceedings IEEE 11th International Conference on Computer Vision,* held in Rio de Janeiro, Brazil, 14–20 October 2007.

Wu, B., L. F. Xie, H. Hu, Q. Zhu and E. Yau. 2018. Integration of aerial oblique imagery and terrestrial imagery for optimized 3D modeling in urban areas. *ISPRS Journal of Photogrammetry and Remote Sensing* 139:119–132.

Wu, C. 2013. Towards linear-time incremental structure from motion. Pages 127–134 in *Proceedings International Conference on* 3D *Vision*-, held in Seattle, Washington, 29 June–1 July 2013.

Xiao, J. X., T. Fang, P. Zhao, M. Lhuillier and L. Quan. 2009. Image-based street-side city modeling. *ACM Transactions on Graphics* 28 (2009).

Yang, J., L. S. Zhao, J. McBride and P. Gong. 2009. Can you see green? Assessing the visibility of urban forests in cities. *Landscape and Urban Planning* 91 (2):97–104.

Ye, L. and B. Wu. 2018. Integrated image matching and segmentation for 3D surface reconstruction in urban areas. *Photogrammetric Engineering & Remote Sensing* 84 (3):135–148.

Ye, Q. X., W. Gao, W. Q. Wang and T. J. Huang. 2004. A color image segmentation algorithm by using color and spatial information. *Journal of Software* 15 (4):522–530.

Zamir, A. R. and M. Shah. 2010. Accurate image localization based on Google maps street view. In *Proceedings 11th European Conference on Computer Vision*, held in Heraklion, Crete, Greece, 5–11 September 2010.

Zhang, X. M., G. J. He, W. Wang, W. L. Jiao and Q. J. Wang. 2011. Extracting buildings height and distribution information in Tianjin City from the shadows in ALOS images. *Spectroscopy & Spectral Analysis* 31 (7):2003–2006.

Zheng, Y., S. Sugimoto and M. Okutomi. 2013. A practical rank-constrained eight-point algorithm for fundamental matrix estimation. *Computer Vision & Pattern Recognition* 9 (4):1546–1553.

Zhu, L., A. Shortridge, D. Lusch and R. Shi. 2011. Feature extraction from 3D Lidar point clouds using image processing methods. *Proceedings of SPIE—The International Society for Optical Engineering* 8159.

Zhu, Z. S., A. Su, H. B. Liu, Y. Shang and Q. F. Yu. 2015. Vision navigation for aircrafts based on 3D reconstruction from real-time image sequences. *Science China Technological Sciences* 58:1196–1208.

VNIR-SWIR Superspectral Mineral Mapping: An Example from Cuprite, Nevada

Kathleen E. Johnson and Krzysztof Koperski

Abstract

Cuprite, Nevada, is a location well known for numerous studies of its hydrothermal mineralogy. This region has been used to validate geological interpretations of airborne hyperspectral imagery (AVIRIS HSI), Advanced Spaceborne Thermal Emission and Reflection Radiometer (ASTER) imagery, and most recently eight-band WorldView-3 shortwave infrared (SWIR) imagery. WorldView-3 is a high-spatial-resolution commercial multispectral satellite sensor with eight visible-to-near-infrared (VNIR) bands (0.42–1.04 µm) and eight SWIR bands (1.2–2.33 µm). We have applied mineral mapping techniques to all 16 bands to perform a geological analysis of the Cuprite, Nevada, location. Ground truth for the training and validation was derived from AVIRIS hyperspectral data and United States Geological Survey mineral spectral data for this location. We present the results of a supervised mineral-mapping classification applying a random-forest classifier. Our results show that with good ground truth, WorldView-3 SWIR + VNIR imagery produces an accurate geological assessment.

Introduction

WorldView-3, launched in August 2014 by DigitalGlobe (now Maxar Technologies), is the only 16-band commercial high-resolution Earth-imaging satellite currently in orbit. In addition to the eight visible and near-infrared (VNIR; 0.42–1.04 µm) bands, *WorldView-3* has the expanded capability of eight shortwave infrared bands (SWIR; 1.2–2.33 µm). The *WorldView-3* SWIR sensors (Figure 1) were carefully selected to provide remote mineral-mapping and material-identification capabilities not available in any other spaceborne multispectral system (Kruse, Baugh, and Perry 2015).

Previous studies by Kruse *et al.* (2015) and Kruse and Perry (2012) have tested *WorldView-3* SWIR bands only. Both studies applied the mixture-tuned matched filtering method commonly used in Airborne Visible/Infrared Imaging Spectrometer (AVIRIS) classifications. Prior to the launch of *WorldView-3*, Kruse and Perry (2012) compared simulated *WorldView-3* data to Cuprite AVIRIS hyperspectral imagery and Advanced Spaceborne Thermal Emission and Reflection Radiometer (ASTER) six-band 30-m-resolution SWIR imagery. Their findings suggested that *WorldView-3* SWIR bands could be a significant tool for geological mapping. We presented a preliminary study of the Cuprite location using *WorldView-3* superspectral data (Johnson and Koperski 2017). Our experiments showed that some of the VNIR bands also make a significant contribution to mineral identification (Figure 2). Of particular interest are VNIR bands 6, 7, and 8, the red-edge and infrared bands. Here we expand upon that study, providing more detailed statistical modeling and confirmation of the accuracy of the results. The minerals studied are presented in Table 1.

Previous *WorldView-3* studies (Longbotham *et al.* 2014; Longbotham *et al.* 2015) have applied first- and second-order statistical methods, and mutual information estimates, to the

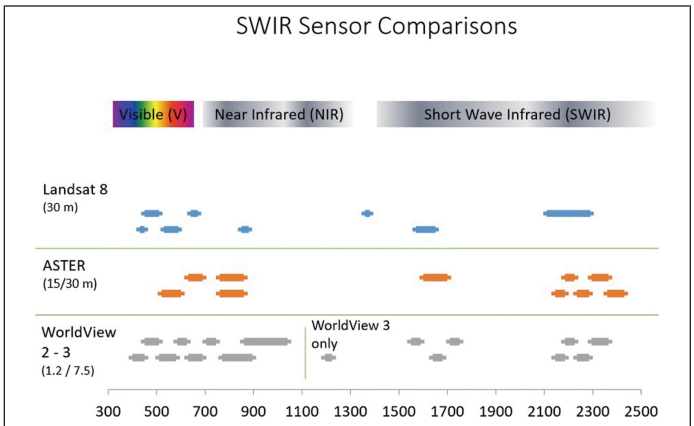

Figure 1. Shortwave infrared sensor comparison for *WorldView-3*, Advanced Spaceborne Thermal Emission and Reflection Radiometer, and *Landsat 8* (Maxar, Inc. 2015). *WorldView-3* has a broader visible-to-near-infrared spectrum (0.42–1.04 µm) and shortwave infrared spectrum (1.2–2.33 µm).

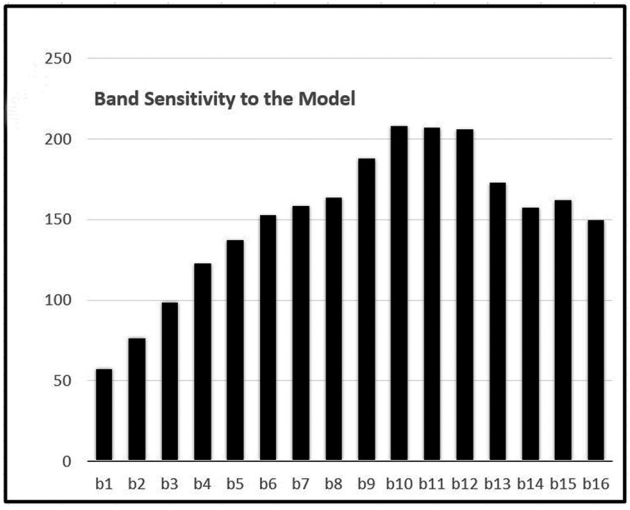

Figure 2. In an exploratory mineral-mapping study (Johnson and Koperski 2017), we found that Bands 6–8 also contribute significantly to the identification of geological materials, being above the detection threshold. This graph represents individual predictor importance calculated using IBM SPSS functionality. Bands at a level of 150 or above are contributing the most to the image spectra (IBM SPSS 2017).

Kathleen E. Johnson and Krzysztof Koperski are with Maxar Technologies, Westminster, CO 80234 (kathleen.johnson@digitalglobe.com).

Photogrammetric Engineering & Remote Sensing
Vol. 86, No. 11, November 2020, pp. 695–700.
0099-1112/20/695–700

doi: 10.14358/PERS.86.11.695

spectral content of the simulated *WorldView-3* sensor data relative to AVIRIS hyperspectral imagery. Longbotham *et al.* (2015), in particular, included an evaluation of Cuprite, Nevada, geological data yielding a an overall accuracy value of 0.85. This article presents a geologically focused application of the landuse/landcover capabilities of *WorldView-3* superspectral data specifically for mineral mapping. Summaries of mineral-mapping applications are given by Abrams and Yamaguchi (2019) and Porwal and González-Álvarez (2019).

We examine in detail the application of the Maxar-LULC (landuse/landcover) model to *WorldView-3* 16-band superspectral imagery for mineral identification and mapping. Specifically, we describe the method (Marchisio *et al.* 2015) and present a map of key minerals from the Cuprite Mineral District, Nevada (Table 1, Figure 3). As already summarized, previous *WorldView-3* mineral-identification studies have focused on the eight SWIR bands. This article presents the results of 16-band superspectral mineral-mapping analysis of the Cuprite Mineral District, Nevada, for a low-resolution (SWIR 7.5 m) data set. Prior experience applying Maxar-LULC to *WorldView-2* eight-band VNIR imagery suggested that there might also be some value in using VNIR bands in the classification analysis of geological materials (Koperski 2012).

Table 1. Minerals studied.

Mineral	Description	Formula
Alunite	Hydrous potassium sulfate	$(KAl_3(SO_4)_2(OH))_6$
Palagonite	Amorphous weathering product of basaltic glass	N/A
Calcite	Calcium carbonate	$(CaCO_3)$
Iron oxides	Goethite, hematite	(α-FeOOH), (Fe_2O_3)
Kaolinite	Clay mineral	$(Al_2Si_2O_5(OH)_4)$
Muscovite	Sheet silicate related to clays	$(KAl_2(AlSi_3O_{10})(F,OH)_2)$
Silica	Chalcedony variant	(SiO_2)

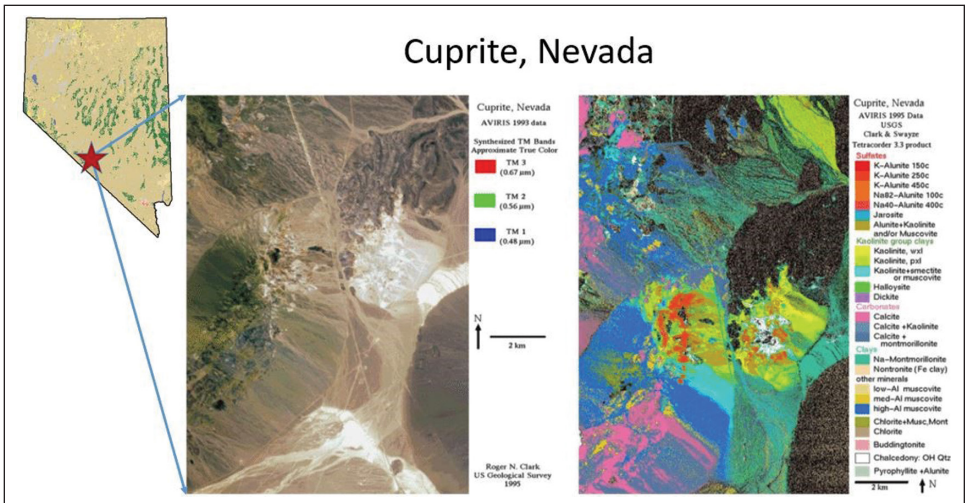

Figure 3. Example mineral map and data used to determine ground truth for this study (derived from Clark and Swayze 1996), and inset map showing study-area location. The mineral species are located visually on the maps and sampled by regions of interest on the computer.

Materials and Methods

Data Acquisition

We use the *WorldView-3* imagery referenced by Kruse *et al.* (2015). The VNIR and SWIR images were collected simultaneously on September 19, 2014, at a native resolution of 1.24 m for VNIR and 3.7 m for SWIR. A proprietary layer-stacking algorithm performed atmospheric compensation and regridded both the VNIR and SWIR data sets to 1.2 m. According to US regulations at the time, only 7.5-m SWIR data could be released, so the SWIR data were processed by our automated image-delivery system, which regridded the SWIR bands to 7.5 m for the most direct comparison to results from previous *WorldView-3* studies. Therefore, the results published here incorporate 1.2-m VNIR and 7.5-m SWIR in the layer-stack process producing the final superspectral data set for analysis.

Supervised Spectral Sampling and Ground Truth

Ground truth was determined following Kruse *et al.* (2015) and Swayze (1997). Mineral maps derived from United States Geological Survey (USGS) AVIRIS data were the primary source of ground truth. Additionally, spectral data collected in situ by Swayze (1997) were applied. The USGS mineral maps provide a detailed compilation of surface minerals supported by field validation, X-ray diffraction, and laboratory spectral measurements (Kruse *et al.* 2015). We evaluate general mineral classes here, such as alunites, muscovites, kaolinites, and silica, since satellite data average the effects of mineral composition, crystallinity, and spectral mixing, and cannot reproduce the detailed mineralogical information available for the Cuprite District.

The Mineral-Mapping Workflow

The mineral-mapping workflow, summarized in Figure 4, is taken from our landuse/landcover algorithm (Maxar-LULC). Ten basic steps are required to complete the classification workflow. The first step is material selection, for which there are two possible data sources: *Landsat 8* and the Maxar sensors—in this study, *WorldView-3*. Once this imagery has been acquired, it must be preprocessed through atmospheric compensation, mosaicking, setting the extent to be analyzed, and finally orthorectification. The processed imagery is then uploaded to the web user interface server. In the web user interface, one creates an image group, adds the image, selects the classes, and sets the feature-extraction options. These options include Gabor texture, histogram, mean, and band ratios. The following summary descriptions of these features are based on those of Achtziger and Johnson (2018).

Gabor texture enables detection of edges and textures from repetitive patterns such as row crops and vineyards. It is also helpful in classifying narrow and small features, such as roads and buildings. Gabor texture is extracted by default from NIR Band 7, which shows a strong vegetation response.

Histogram is a texture feature that accounts for the color response in the neighborhood of a pixel. It enables detection of classes with strong color texture (e.g., orchards that are a mix of trees and grass/barren, docks that are bright areas surrounded by water, forests that are a mix of shadows and illuminated trees, and so forth.)

Mean normalizes and smooths out pixels by averaging values in the neighborhood of a pixel. It is especially helpful for classes with a lot of texture from shadows, such as in a forest. The mean kernel defines the size of the neighborhood. The kernel size applied here is 3 × 3.

Once these features are set, this step is carried through the iterative training and validation process automatically. Step seven initiates the supervised classification process. Independent training and validation region-of-interest (ROI) sets are collected. A total of 610 ROIs were collected for this study.

Once an acceptable mineral map has been determined by the validation process, the training and validation ROI sets are exported and saved. The map raster can also be downloaded.

After classification, export of the raster data and optional vectorization are the final steps.

Figure 5 shows the Maxar-LULC web user interface and examples of ROI selection, shown here as rectangles. Sample ROIs indicated for the mineral alunite are shown in RGB natural color in Figure 5a. A mineral-identification raster (Figure 5b) is produced and tested through the iterative process already described until the accepted accuracy thresholds are met or exceeded (Marchisio *et al.* 2015). The accuracy is evaluated in a confusion-matrix format according to the overall accuracy, the user accuracy, and the κ coefficient.

SWIR band ratios can be used to predict how well the selected classes can be defined and separated one from another (Figure 6). Ideally the mineral classes would form compact spectral clusters, indicating a well-defined chemical composition (e.g., calcite). However, most of the minerals in a hydrothermally altered region are solid solution series and will display a range of chemical (and therefore spectral) compositions, such as kaolinite, alunite, and iron oxides, or bimodal clustering, such as muscovite. Band ratios are always included in the model calculations.

Results

The accuracy of the Maxar-LULC algorithm has been validated in a number of studies using eight-band VNIR imagery and 16-band superspectral imagery (Koperski 2012; Johnson *et al.* 2013; Longbotham *et al.* 2015; Marchisio *et al.* 2015; Johnson and Koperski 2017). The classification results were assessed by the overall accuracy per class, the user accuracy, and the kappa (κ) coefficient (Cohen 1960). The confusion matrix for

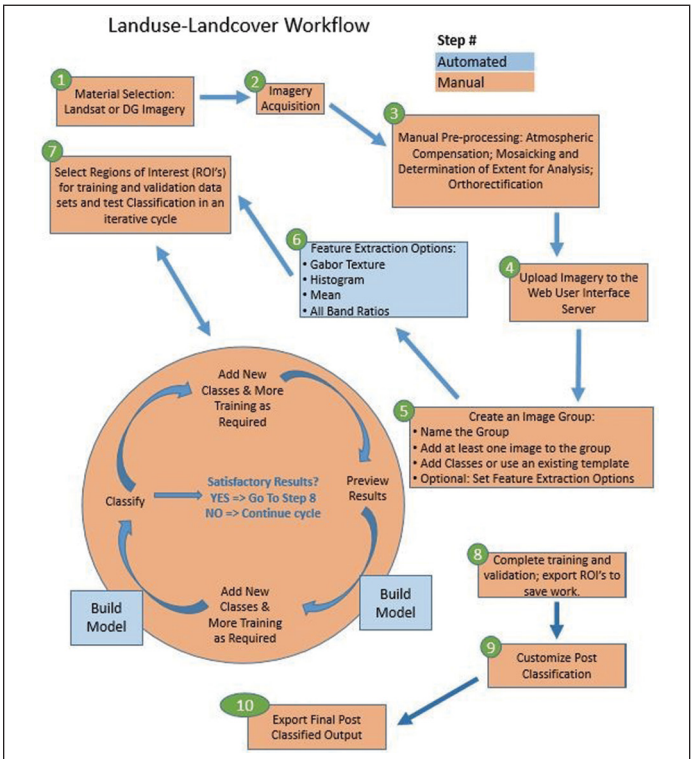

Figure 4. Diagram of the landuse/landcover workflow (Maxar-LULC) that has been applied here to mineral mapping. The workflow is an iterative process, with step 7 repeated until the model yields acceptable statistical results. In step 7, new regions of interest for training and validation can be added to improve the results. Conditions for the model features (mean, Gabor texture, histogram) can also be adjusted.

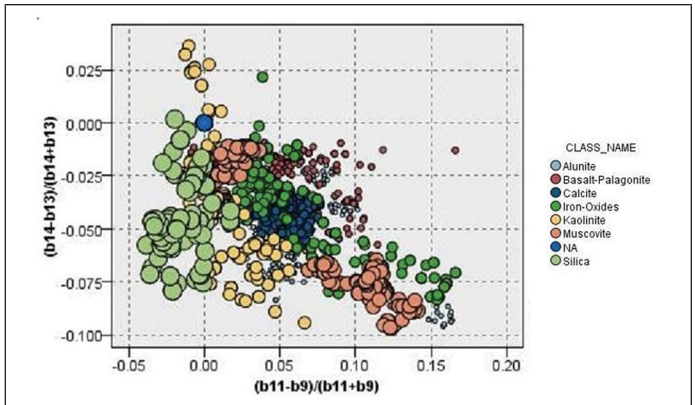

Figure 6. Mineral compositions defined by band ratios. The vertical axis represents the ratio of Band 14 – Band 13 to Band 14 + Band 13; the horizontal axis represents the ratio of Band 11 – Band 9 to Band 11 + Band 9. Silica and calcite plot in clusters, whereas mineral compositions defined by solid solutions form either a range (e.g., kaolinite, alunite) or a bimodal cluster (e.g., muscovite).

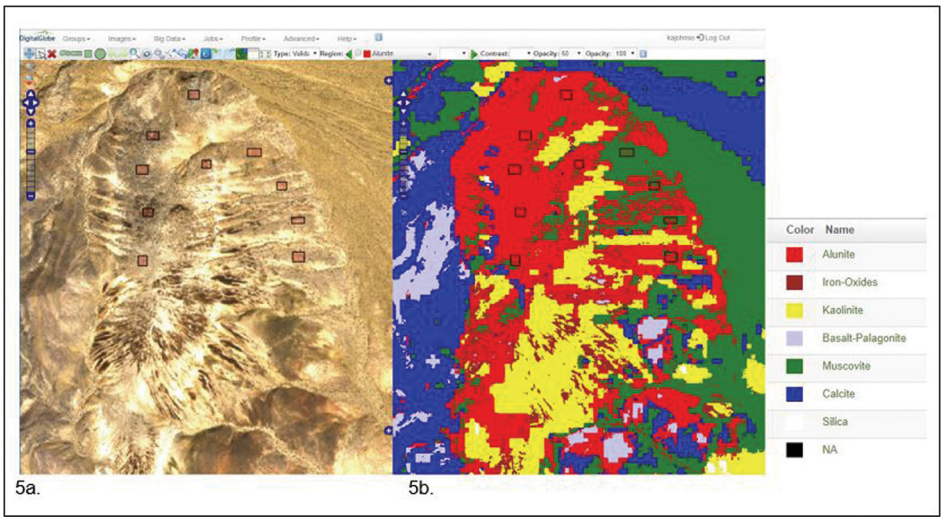

Figure 5. Supervised classification spectral sampling within the Maxar-LULC web user interface. Rectangles represent validation regions of interest for alunite. (a) Spectral sampling of alunite mineral region shown in RGB. (b) Red mineral shown is alunite in the classified image.

Table 2. Maxar-LULC confusion matrix: Random Forest with 100 trees.

Class	Alunite	Iron Oxides	Kaolinite	Palagonite	Muscovite	Calcite	Silica	Mineral Accuracy
Alunite	**58.26**	0.60	0.00	9.13	0.51	6.83	0.00	66.01
Iron oxides	22.13*	**98.43**	1.45	1.13	0.20	0.05	1.26	67.73
Kaolinite	2.17	1.00	**91.72**	0.00	0.00	0.00	30.84*	85.41
Palagonite	5.66	0.00	0.00	**89.71**	0.15	0.00	0.00	93.13
Muscovite	11.28	0.00	0.00	0.00	**94.19**	4.00	0.00	85.42
Calcite	0.01	0.00	4.09	0.00	0.33	**88.50**	3.48	93.52
Silica	0.00	0.00	2.73	0.00	0.00	0.00	**64.41**	91.53
Total	5164	2955	11655	5664	16500	8121	3325	100.00

Overall accuracy per class = 83.25%; user accuracy = 0.85; κ coefficient = 0.82. All features are included: mean, histogram, and Gabor texture. Column totals represent pixel values per mineral. Boldface indicates within-class accuracy.
* There are special mineralogical relationships between alunite and iron oxides and between kaolinite and silica, described in the text.

the best results from this study is presented in Table 2, and the mineral map produced by the classification is presented in Figure 7. The accuracy is based upon running an independent validation data set against the training data set. The confusion matrix allows visualization of the algorithm accuracy. Each row represents an instance in the predicted class, and each column represents an instance in the actual class (Viera *et al.* 2005). The results for this classification have an overall accuracy of 83.25%, user accuracy of 0.85, and κ coefficient of 0.82 (Table 2). The κ coefficient is a measure of precision which takes into account the case where two independent observers (the training and validation data sets) may agree or disagree simply by chance (Viera *et al.* 2005). A value of $\kappa = 1$ represents perfect agreement between the observers, and $\kappa = 0$ represents agreement simply by chance. The confusion matrix should show a high percentage for overall accuracy, since this represents an average of the percentages for the accuracy of each class. An overall accuracy approaching 85% or higher is considered very good. Compare the result with 100 trees to those with 40 and 20 trees (Table 3).

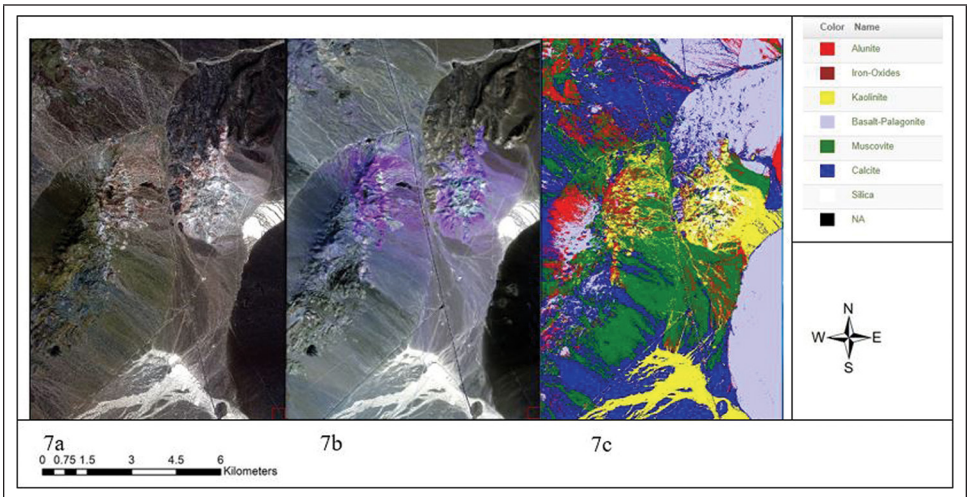

Figure 7. Mineral-mapping results for this study produced by the Maxar-LULC algorithm. (a) Natural color; (b) shortwave infrared Bands 15-13-12 highlighting the mineral kaolinite. Salt flats are also classified as kaolinite (southeast corner), because the two minerals are likely to be mixed here. In the future we will examine salt. (c) Maxar-LULC superspectral classification results.

The confusion matrix also shows whether any classes were problematic. The numbers in the rows and columns depict confusion between *different* classes—that is, where instances of misclassified pixels occurred. The numbers in the rows and columns of the same name depict accuracy within classes (bold diagonal numbers), where instances of correctly classified pixels occurred. Therefore, ideally the matrix should show very low numbers where one class intersects with other classes, and high numbers where a class in a row intersects with the column for that same class. In the case of alunite versus iron oxides this is not true. Iron oxides, especially goethite (Table 1), can occur as fine coatings on other minerals. Here it is likely that the alunite has a coating of iron oxide, thereby confusing the spectral signature. Kaolinite and silica also show more confusion, with silica a major weathering breakdown product of the clay mineral.

The user accuracy is determined by dividing the number of correctly classified pixels in each category (the minerals) by the total number classified in that category (sometimes shown as the row total in the confusion matrix). It represents the probability that a classified pixel in a given category actually represents what is on the ground. In contrast, the overall accuracy is determined by dividing the number of correctly classified pixels in each category (those on the major diagonal) by the number of reference pixels (total number of pixels per class). The overall accuracy simply represents correct versus incorrect classification.

Discussion

The results of testing several classifiers and various parameter combinations as mineral identifiers are presented in Table 3. The model parameters and data imported from Maxar-LULC are eight-band VNIR, eight-band SWIR, separate VNIR and SWIR normalized band ratios, Gabor texture, histogram, and mean. The Maxar-LULC results are stored as .arff files that were imported to IBM SPSS Modeler (version 17) for modeling. The data shown in Table 2 were calculated using a Random Forest with 100 trees based on an overall accuracy of 83.25%. We have chosen to compare the overall accuracies in Table 3 because that is the output for the SVM and C5.0 models (discussed later). The model outputs test the influence of different combinations of modeling features (mean, histogram, Gabor texture) and band combinations.

Maxar-LULC Classification Algorithm

The Maxar-LULC algorithm applies the Weka open-source Java data-mining process to classify images (Marchisio *et al.* 2015). Weka (Waikato Environment for Knowledge Analysis) accesses a variety of statistical methods for sample analysis through machine learning (Williams 2010; Frank, Hall, and Witten 2016). For the novice analyst, the common practice is to begin with decision-tree methods because they are the most robust to outliers generated during the training process (e.g., Quinlan

Table 3. Model accuracy comparisons (%).

Model Comparisons	SVM[a]	C5.0 20 Boosted Trees[b]	WEKA Random Forest 20 Trees[c]	WEKA Random Forest 40 Trees[c]	WEKA Random Forest 100 Trees[c]
All LULC parameters included	76.58	79.80	81.99	82.22	83.25
VNIR, SWIR, mean, and Histogram	76.67	79.91	80.73	81.18	82.20
VNIR, SWIR, and mean	**84.00**	**81.44**	**82.20**	**83.28**	**84.69**
VNIR and SWIR	83.73	82.92	80.54	82.79	83.68
VNIR only	61.64	64.43	64.14	64.54	64.67
SWIR only	76.98	74.55	75.30	76.08	76.86

For the Maxar-LULC VNIR + SWIR model with a 100-tree Random Forest, overall accuracy = 83.25% and κ coefficient = 0.82. LULC parameters as defined by the Maxar-LULC model: eight-band VNIR, 28 VNIR normalized band ratios, eight-band SWIR, 28 SWIR normalized band ratios, Gabor texture, histogram, 16 spectral 3×3 mean values. Boldface indicates the best-performing model.
SVM = support vector machine; VNIR = visible to near-infrared; SWIR = shortwave infrared.
[a] IBM SPSS support vector machine model.
[b] IBM SPSS C5.0 model.
[c] WEKA Machine Learning Suite (http://www.cs.waikato.ac.nz/ml/index.html).

1986; Breiman 2001; Grossmann *et al.* 2010; Williams 2010; Biau 2012). Decision trees are recursive, i.e., they apply the same rule at each node split (Quinlan 1986; Breiman 2001). The decision tree-based method applied here is a random forest with 100 trees. The classification results for Maxar-LULC VNIR + SWIR (superspectral) random-forest 100 trees are visualized in Figure 8. Shown also are the natural-color RGB image (Figure 8a) and SWIR bands 15-13-12 image (Figure 8b).

Random Forest uses a bootstrapping method optimized for large data sets with a large number of variables (classes), and is a good starting place for the novice analyst because it provides a stable model builder with minimal data preprocessing, does not require a normal distribution, is less sensitive to outliers than a single-decision-tree method, and is competitive with nonlinear classifiers such as neural networks (Breiman 2001).

The training data set is used to initiate each node. Once a tree is completed, the next tree is initiated, until all have reached a conclusion. Each node is tested by the percent error of misclassification of the validation data set (Breiman 2001). The number of decision trees must be specified and can range up to 1000 for very large data sets, with 500 as an average number of trees (Grossmann *et al.* 2010; Williams 2010). For the small data set in this study, 20, 40, and 100 trees were specified for seven mineral classes. In image classification, the Random Forest method can be subject to bias if care is not taken to select balanced sample sizes among the training classes and for both training and validation data sets (Grossman *et al.* 2010). The random-forest method has been applied to Landsat data to generate the USGS GAP land cover layers (Grossmann *et al.* 2010). For details of the Random Forest method, refer to Breiman (2001).

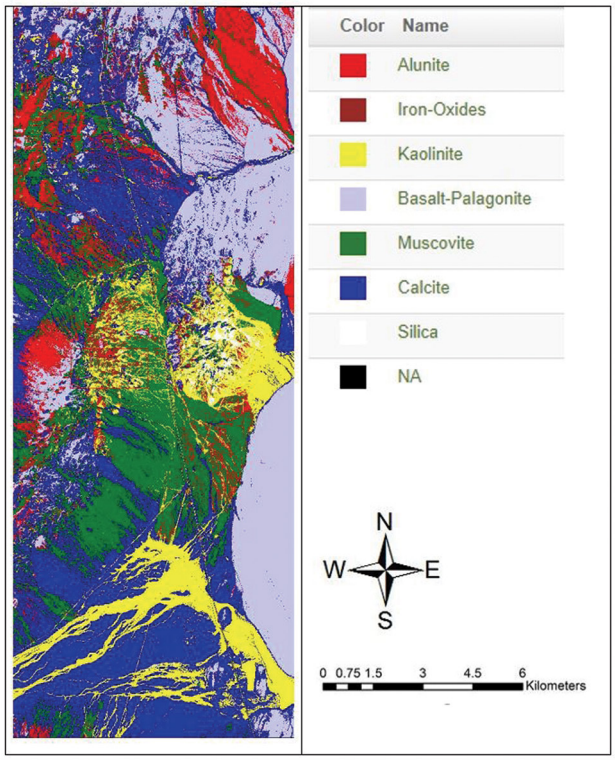

Figure 8. Final mineral map produced from the *World-View-3* superspectral data set of visible to near-infrared + shortwave infrared + mean.

SPSS Support Vector Machine and C5.0 Analysis

A support vector machine (SVM) is a supervised classification algorithm. It works by mapping data to a high-dimensional feature space so that data points can be categorized even when the data are not otherwise linearly separable (IBM SPSS Modeler 2017). A separator between the categories is found, and the data are then transformed in such a way that the separator could be drawn as a hyperplane. Following this, characteristics of new data can be used to predict the group to which a new record should belong (IBM SPSS Modeler 2017). As a classifier, SVM models analyze data and can recognize patterns that distinguish classes for small sample sets (Pandya and Pandya 2015). The results are compared in Table 3. As with all of the models, VNIR + SWIR + mean yields the strongest result.

C5.0 is a classification method that can produce two types of models: a decision tree or a rule set. In either mode, it splits the sample based on the fields that provide the maximum normalized information gain (IBM SPSS Modeler 2017). As a classifier it can anticipate which attributes are relevant in the classification and which are not (Pandya and Pandya 2015). Large decision trees can be pruned and simplified using rule sets which retain most of the information of the original decision tree (IBM SPSS Modeler 2017). Given that our model inputs the data from the Maxar-LULC Random Forest of 100 trees, only the decision-tree mode was applied.

Classifiers can be boosted to potentially improve predictive performance. Boosting works by successively reweighting the training data set based on the classifier's previous performance. Boosting is most successful when applied to unstable classifiers, such as decision trees. In this case, boosting was applied to the C5.0 classifier, showing slight improvement over SVM for the three models (Table 3) that include all LULC features, histogram + mean, and VNIR only. Although VNIR Bands 6–8 do contribute significantly to the classification results, the accuracy of the VNIR-only result is significantly decreased compared to the VNIR + SWIR models. This reinforces the importance of the SWIR bands to the overall classification results, as the VNIR-only accuracies fall outside the accepted range for Maxar-LULC (Koperski 2012).

Outside of mean, other texture features (Gabor texture and histogram) do not improve accuracy, because mineral mapping

is based on spectral properties. We believe that adding the mean feature improves the results due to better averaging of spectral differences that may result from sparse vegetation in the area.

Conclusions

Maxar-LULC was used to produce a supervised Random Forest mineral map from a superspectral data set for the Cuprite Mineral District, Nevada. Seven geological materials were tested for identification, with an accuracy of 83.25% and a κ coefficient of 0.82. Imagery data for this study were collected by *WorldView-3*, which has 16-band superspectral (VMIR + SWIR) capability. Previous experimental (Kruse and Perry 2012; Longbotham *et al.* 2014) and empirical studies (Kruse *et al.* 2015; Longbotham *et al.* 2015) of the SWIR bands have demonstrated the potential for mineral mapping. Our final mineral map is presented in Figure 8.

Our preliminary superspectral study (Johnson and Koperski 2017) applied all 16 bands to the mineral-mapping problem, and additionally identified three VNIR bands (6–8) that appear to contribute to mineral identification. This study applied a Random Forest model, because it is more robust to outlier values (Grossman *et al.* 2010; Biau 2012). It was also demonstrated through predictive statistical analysis in IBM SPSS Modeler (2017) that VNIR Bands 6–8 (red edge, NIR1, NIR2) do contain valuable spectral information, and are comparable in sensitivity to some of the SWIR bands, such as Bands 14–16.

Although we have selected the 100-tree solution as the most accurate, the results for 20 and 40 trees indicate that increasing the number of trees for the random-forest model does not significantly improve the results. The IBM SPSS models using only the mean feature have an accuracy comparable to that with 100 random-forest trees using the same features. Additionally, our SWIR-only results (76.98% accuracy) demonstrate an improvement over the 63% mixture-tuned matched filtering classification of Kruse *et al.* (2015). The overall findings show that Maxar-LULC classification analysis using all 16 *WorldView-3* bands provides a quick and accurate solution for mineral/geological mapping. As with any supervised classification method, accuracy of mineralogical classification depends on high-quality ground truth.

Acknowledgments

We would like to acknowledge the indispensable support and assistance of our fellow Maxar employees past and present, without whom this study could not have been completed: Giovanni Marchisio (project director), Carsten Tusk (lead developer), Lubos Pochman (web user interface developer), Rachana Ravi (training and testing initial versions of the algorithm), Chuck Chaapel (data preprocessing), and Amy Povak (guidance through the Maxar approval process). This manuscript has benefited from insightful comments by two anonymous reviewers and our colleagues B. Bader, A. Povak, D. Stark, and C. Danforth.

The distribution of SWIR data is regulated by NOAA (15 CFR 960). Sharing of data must be reviewed by the legal department at Maxar Technologies on a case-by-case basis. Please contact the corresponding author for further information.

References

Abrams, M. and Y. Yamaguchi. 2019. Twenty years of ASTER contributions to lithologic mapping and mineral exploration. *Remote Sensing* 11 (11):1394.

Achtziger, H. and K. E. Johnson. 2018. *Maxar Land-Use/Land-Cover Classification User's Guide 1.0*. Westminster, Colo.: Maxar LLC.

Biau, G. 2012. Analysis of a random forests model. *The Journal of Machine Learning Research* 13 (1):1063–1095.

Breiman, L. 2001. Random forests. *Machine Learning* 45 (1):5–32.

Clark R. N., and G. A. Swayze. 1996. Evolution in imaging spectroscopy analysis and sensor signal-to-noise: An examination of how far we have come. Pages 49–53 in *Summaries of the Sixth Annual JPL Airborne Earth Science Workshop, March 4–8, 1996. Vol. 1: AVIRIS Workshop*, held in Pasadena, Calif., 4–6 March 1996. Edited by R. O. Green. Pasadena, Calif.: Jet Propulsion Laboratory, California Institute of Technology.

Cohen, J. 1960. A coefficient of agreement for nominal scales. *Educational and Psychological Measurement* 20 (1):37–46.

DigitalGlobe. 2014. WorldView-3. <http://worldview3.digitalglobe.com> Accessed 07 August 2014.

Frank, E., M. A. Hall and I. H. Witten. 2016. *The WEKA Workbench: Online Appendix for "Data Mining: Practical Machine Learning Tools and Techniques, 4th ed*." <https://www.cs.waikato.ac.nz/ml/weka/Witten_et_al_2016_appendix.pdf> Accessed 12 December 2018.

Grossmann, E., J. Ohmann, J. Kagan, H. May and M. Gregory. 2010. Mapping ecological systems with a random forest model: Tradeoffs between errors and bias. *Gap Analysis Bulletin* 17:16–22.

IBM SPSS Modeler [Version 15.0], 2017. IBM Knowledge Center, https://www.ibm.com/support/knowledgecenter/

Johnson, K. E., K. Bol, G. Hammann, R. Ravi and B. Morey. 2013, Monitoring ponderosa pine health in White Ranch Park and Elk Meadow Park, Jefferson County, Colorado, parks and open space. Pages PP–PP in *GIS in the Rockies* 2013, held in Denver, Colo., 9–10 October 2013. Edited by J. Editor. City, St.: Publisher. <https://www.researchgate.net/publication/323178674> Accessed 01 October 2017.

Johnson, K. E. and K. Koperski. 2017. WorldView-3 SWIR land use-land cover mineral classification: Cuprite, Nevada. Pages PP–PP in *Pecora 20: Observing a Changing Earth*, held in Sioux Falls, S.D., 13–16 November, 2017. Edited by J. Editor. City, St.: Publisher. <https://www.researchgate.net/publication/323178662> Accessed 18 November 2019.

Koperski, K. 2012. *IARPA Finder Project Phase I*. Report to Intelligence Advanced Research Projects Activity. <https://www.iarpa.gov/index.php/research-programs/finder/> Accessed 12 July 2017.

Kruse F. A., W. M. Baugh and S. L. Perry. 2015, Validation of DigitalGlobe WorldView-3 Earth imaging satellite shortwave infrared bands for mineral mapping. *Journal of Applied Remote Sensing* 9 (1):096044.

Kruse, F. A. and S. L. Perry. 2012. Mineral mapping using simulated short-wave-infrared bands planned for DigitalGlobe WorldView-3. Paper RM3E.4 in *Imaging and Applied Optics Technical Papers, Optical Remote Sensing of the Environment*, held in Monterey, Calif., 24–28 June 2012. Edited by J. Editor. Washington, D.C.: Optical Society of America.

Longbotham N., F. Pacifici, B. Baugh and G. Camps-Valls. 2014. Prelaunch assessment of WorldView-3 information content. Pages PP–PP in *2014 6th Workshop on Hyperspectral Image and Signal Processing: Evolution in Remote Sensing (WHISPERS)*, held in Lausanne, Switzerland, 24–27 June 2014. Edited by J. Editor. City, St.: Publisher.

Longbotham N., F. Pacifici, S. Malitz, W. Baugh and G. Camps-Valls. 2015. Measuring the spatial and spectral performance of WorldView-3. Paper HW3B.2 in *Fourier Transform Spectroscopy and Hyperspectral Imaging and Sounding of the Environment*, held in Lake Arrowhead, Calif., 1–4 March 2015. Edited by J. Editor. City, St.: Publisher.

Marchisio G. B., C. Tusk, K. Koperski, M. D. Tabb and J. D. Shafer. 2015. Classification of land based on analysis of remotely-sensed Earth images. U.S. patent 9,147,132 B2.

Pandya, R. and J. Pandya. 2015. C5.0 algorithm to improved decision tree with feature selection and reduced error pruning. *International Journal of Computer Applications* 117 (16):18–21.

Porwal, A and I González-Álvarez. 2019. Reprint of: Introduction to special issue on geologic remote sensing. *Ore Geology Reviews* 108:1–7.

Quinlan, J. R. 1986. Induction of decision trees. *Machine Learning* 1 (1):81–106.

Swayze, G. A. 1997. *The hydrothermal and structural history of the Cuprite Mining District, southwestern Nevada: An integrated geological and geophysical approach* (PhD dissertation). University of Colorado at Boulder.

Williams, G. 2010 Data Mining Desktop Survival Guide. <https://www.togaware.com/datamining/survivor/> Accessed 04 October 2017.

A New Approach to Land Registry System in Turkey: Blockchain-Based System Proposal

Arif Furkan Mendi, Önder Demir, Kadir Kaan Sakaklı, and Alper Çabuk

Abstract

Blockchain is an emerging technology whose extraordinary advantages make it popular. Blockchain applications are not limited to cryptocurrencies; it can be used in many areas, including smart ownership. Blockchain-based land registry systems have great potential thanks to their advantages of high-level security and no intermediary transactions. Although the requirements of land registry systems vary by country, common to all of them are the eye-catching advantages and conveniences that a blockchain-based system brings. We examined the process used in Turkey, which consists of eight steps, identified the participants of the system, and generated a blockchain-based land registry system for Turkey. This article explains that proposed blockchain-based land registry system, configured for the local requirements of Turkey.

Introduction

Blockchain is a popular technology of today; it was discovered in 1992, but its name became widely heard with Bitcoin's sensational explosion. The capabilities offered by this technology began to emerge with the spread of Bitcoin. Blockchain is a decentralized distributed database system. Data are collected in blocks and united as an integral chain that stores them from the first block.

Geographic information systems (GIS) have made many improvements since they were invented by Roger Tomlinson in 1960; they have been used in many different fields, such as cartography, resource management, and land management (Li and Shao 2009). In all these broad application areas, the important issue to be addressed is data. Data are a vital element for GIS to achieve successful results (Shan 1998). The accuracy and security of the data are key to making the analyses and simulations accurate and healthy. On the other hand, the amount of data in the world that forms the basis of GIS is scaling up, increasing the need for good data management (Wang and Shan 2005). The advantage that characterizes blockchain technology is that data stored in the system are precise and cannot be manipulated. Blockchain is not only for financial transactions; it is a technology that can be programmed to record anything of value and importance, where transactions are stored in an intact digital distributed ledger. This value can be anything that can be expressed in code. Values such as food tracking, supply-chain management, and land registration can all be easily managed this way. Blockchain technology can be used together with the Internet of Things, allowing objects to communicate directly and securely with each other and providing an important solution for people to communicate with each other without intermediaries. With the widespread use of these Internet of Things devices, important concepts such as the smart city appear (Li *et al.* 2013). Smart homes, cities, health systems, agriculture, and energy conservation are also areas where blockchain technology. With this extensive range of application fields and examples, attention to blockchain technology is growing. Moreover, with its eye-catching advantages and sensational popularity, some technologists have described blockchain technology as the greatest invention since the Internet. Just as the Internet provides a structure for communication, it is argued that blockchain will have a similar meaning for information sharing. This assertive approach originates from the technology's revolutionary features. The key attribute is the distributed ledger, a structure created from the moment the system was installed, distributed to all stakeholders in the network installed in the system, where recorded data cannot be manipulated. Each transaction that occurs in the network is recorded and stored in this structure and shared with all participating computers, so that the need for any trusted third parties is eliminated and the distributed database structure acts as a digital notary. Although blockchain is a relatively new technology, the number of studies on it has increased considerably thanks to the fact that it offers such a safe structure. Large companies are investing heavily in this technology to gain real use and benefit from these eye-catching advantages.

When investing in technology, a market analysis of the product to be produced with the relevant technology is of great importance in terms of achieving successful outputs. The preparation of such reports requires significant experience, knowledge, and market monitoring. Since technology companies do not have the opportunity to do such deep analysis in their daily routines and do not have sufficient depth of knowledge, some research companies conduct such research and provide various reports. When big technology companies make technological investments, they follow this type of external analysis and make investment decisions after analyzing their outputs. Gartner is one of these firms; it is known as one of the leading companies in the world for technology and market analysis. It is a prestigious company that especially follows new-generation technologies and offers many detailed analyzes. As expected, Gartner did not remain insensitive to the remarkable advantages offered by blockchain technology, and researched this trend. In the' "Top Trends in the Gartner Hype Cycle for Emerging Technologies" report (Panetta 2017), when we look at the "Hype Cycle" curve for blockchain technology, it is seen that the technology has passed the "Peak of Inflated Expectations" and progressed to the "Trough of Disillusionment" (Figure 1). It is emphasized that this does not have a negative meaning; on the contrary, the number of studies related to the technology will increase, and it will be take five to 10 years for the technology to reach efficiency.

Arif Furkan Mendi and Kadir Kaan Sakaklı are with HAVELSAN A.Ş., Ankara, Turkey (afmendi@havelsan.com.tr).

Önder Demir is with the Computer Research and Application Center, Anadolu University, Eskisehir, Turkey.

Alper Çabuk is with the Faculty of Architecture and Design, Eskişehir Technical University, Eskisehir, Turkey.

Photogrammetric Engineering & Remote Sensing
Vol. 86, No. 11, November 2020, pp. 701–709.
0099-1112/20/701–709

doi: 10.14358/PERS.86.11.701

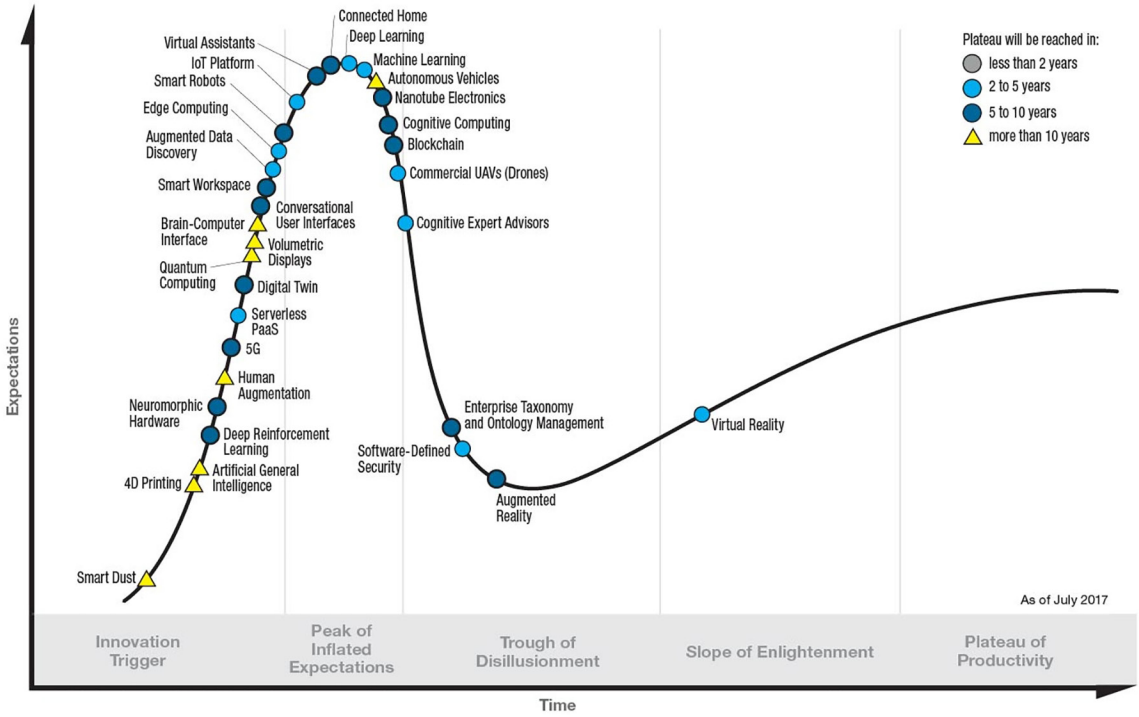

Figure 1. Gartner Hype Cycle for Emerging Technologies (Panetta 2017).

Many applications using blockchain technology have been developed since 2015, including GIS. Many experts argue that blockchain applications are not limited to cryptocurrency applications and that the smart property concept enabled by blockchain can be used in various areas. It is anticipated that diversity will be provided and knowledge about technology will be increased by using the concept of smart property in different areas (Yli-Huumo *et al.* 2016). There are many applications where GIS and blockchain technology can be used together. Land registration is one of the most popular and potential rising stars of those usages. Land registration generally describes systems by which matters concerning ownership, possession, or other rights in land can be recorded to provide evidence of title, facilitate transactions, and prevent unlawful disposal. This process is usually controlled by government agencies. Although the requirements of land registry systems vary by country, common to of all are the eye-catching advantages and conveniences that such a system would bring. In this article, creating a land registry system with Turkey's requirements will be explained.

Materials and Methodology

Materials

Within the scope of the study, a literature review related to blockchain technology was carried out. Many academic articles with detailed explanations of technology and application examples have been examined. Sample applications of blockchain-based real estate hand-exchange systems in the world have been examined and user guides created. In order to successfully establish a blockchain-based real estate hand-exchange system suitable for current law in Turkey, the real estate hand-exchange process guide of Turkey was used as primary material. The resources from market and technology analysis were also used as primary materials.

In the system to be created, the infrastructure offered by blockchain technology will be used as material. Several infrastructure suppliers provide such a platform for users to build their applications. After evaluating various alternatives that offer blockchain smart-contract infrastructure to their users, we decided to use Hyperledger Fabric. Details of the research are explained later in this article.

Methodology

A literature review was carried out and application examples in the world were examined. After the literature review was completed, it was time to start building the application. In order to do this, the real estate hand-exchange process in Turkey needed to be investigated. As a result of the examination, the requirements were prepared and the system was designed. In the next stage, appropriate infrastructure options were evaluated for the development of the blockchain-based system, and implementation of the application on the most suitable infrastructure was completed. The detailed methodology is given in Figure 2.

Literature Summary

Yli-Huumo *et al.* (2016) argue that with increasing blockchain research, the maturity level of the technology will increase, and thus it will have a positive effect on the development of the system. For this, they give an example of using a blockchain-GIS, proposing the idea that companies can sell their properties in a virtual environment by using the decentralized database.

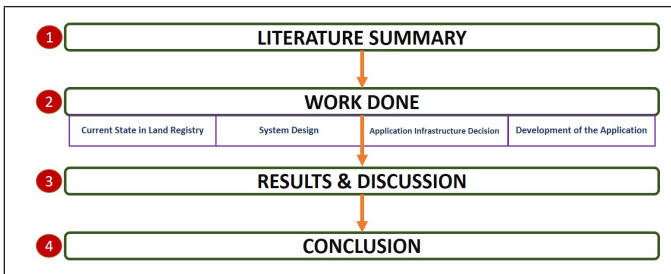

Figure 2. Methodology.

Spielman (2016) claims that land registry systems based on blockchain technology are the future of land registration, and their advantages over the current land registry system will be evident. Blockchain-based land registration systems can increase processing efficiency, prevent fraud in property exchange, add security levels, accountability, and transparency, and lower sensitivity to natural or created disasters.

Lemieux (2017) also argues that blockchain technology has the potential to radically change the registration of land and real-property transactions, describing blockchain-based land registration applications in Brazil, Georgia, Ghana, Japan, India, and Sweden. It is stated that different providers have developed several different blockchain-based applications for the local needs of these countries.

Honduras is the first country to invest in a blockchain-based land registration system. The Honduran government made a radical decision to eliminate irregularities in the land registration process after seeing that its efforts toward changing the laws to prevent irregularities during land registration did not work; it signed a deal with Factom, a US-based firm, to establish a blockchain-based real estate hand-exchange system (Lemieux 2017).

Similar to the need in Honduras, the Brazilian government has also invested in a blockchain-based solution to improve the security of existing processes and address property and land disputes in order to prevent fraud in land registration. The land registration system, which was previously carried out in 13 steps, was moved to a blockchain-based system and put into pilot use in the state of Rio Grande do Sul, Pelotas and Morro Redondo Municipalities between May and July 2017 (Lemieux 2017). The data obtained as a result of the pilot application showed that errors in the recording system were significantly reduced, and archiving was facilitated significantly (Allison 2017).

Sweden is another country that have moved its land registration process to a blockchain-based system. Sweden ranks at the top of the World Bank Business Index, which indicates that it is one of the countries where the real estate hand-exchange process operates most reliably and healthily. Therefore, Sweden's transition to a blockchain-based real estate registration system was not due to fraud or irregularity in processes, unlike in Brazil and Honduras. In Sweden, the transfer of real estate is completed in seven steps. A blockchain-based land registry system was created by ChromaWay and is still in use (Lemieux 2017). A sample screenshot of the application, showing the transaction between the buyer and seller, is seen in Figure 3.

After evaluating all these blockchain-based application usages, even with the advantages of the technology, some issues need to be clarified before a land registry system is built using blockchain. One of the most critical points is that transactions performed through the system need to be counted as legal evidence in case of dispute, to ensure the accuracy and consistency of the system. To address this concern, issues such as how old records are moved into the newly developed system and how legislation is managed through the system should be clarified. Otherwise, the widespread use of the system will be limited and its use will decrease over time [14].

Work Done

The requirements of land registry systems vary by country. Therefore, creating a generic system is not possible. In order to create a land registry system for Turkey, a road map was determined. First, the current state of the land registry system in Turkey was examined and the requirements decided. With these requirements, the system design was determined. With the system design, the best blockchain infrastructure to satisfy the needs was chosen. Then the development phase was started, and in the end a blockchain-based land registry system for Turkey was created.

Current State of Land Registry

Land registry is a multi-stakeholder process and is created according to the laws and operations of the country. In some countries, transactions have to be done with the approval of a notary, while in others the land registry offices carry out this task. Hence, real estate change processes vary by country. In Turkey, after the verbal agreement between the buyer and seller parties for the real estate, the real estate change process is carried out in eight steps (Figure 4):

1. On the application of the real estate owner, the municipality where the property is located determines the fair value of the property.
2. An official letter is obtained from the same municipality stating that the property subject to sale is not in debt.
3. On acknowledgment of fair value by the buyer and seller, separately a 3% title deed is deposited to the bank where the title deed is agreed, together with the revolving capital fee.
4. If the buyer is to perform the payment using bank credit, mortgage documents are prepared by negotiating with the bank.
5. Both the buyer and the seller for the transfer transaction prepare the required documents, such as an identity card with a photocopy and passport photographs. The seller also physically provides the original deed and a photocopy.
6. Documents such as the fee receipt, mortgage documents, identities, deed, and other necessary documents for the

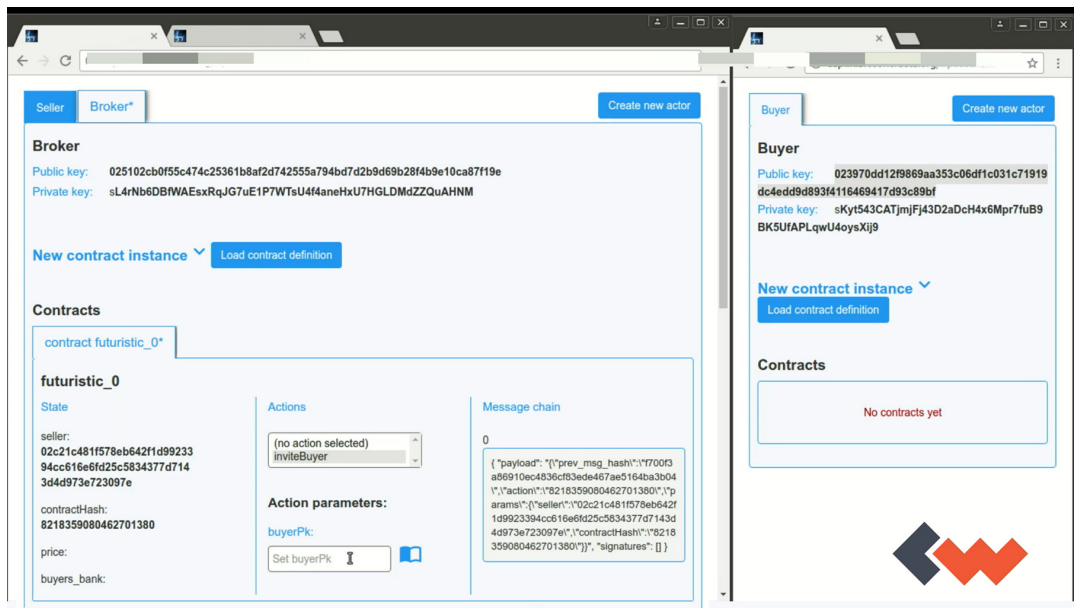

Figure 3. ChromaWay land registry system (ChromaWay n.d.).

transfer, obtained in the previous steps, are collected and delivered to the land registry office.

7. An appointment is made with the land registry office to officially carry out the transfer.
8. If no obstacles are detected as a result of the examinations carried out in the land registry office, the buyer and seller physically go to the office. After the money delivery, the official deed documents are signed and the transfer of the property is completed.

In the current situation, it takes an average of 2 or 3 days for all these steps to take place. During this period, the land registry office performs the work for confirming the eligibility of the exchange of the property in question, and if there is no negative result, the exchange is carried out. Following the laws in force in Turkey, owners of property who sell within five years are obliged to pay a value-added tax on the difference between the sale price and the purchase price. This tax is a mechanism established to provide for financial collection of the effect of public investments made by the state on the value increase of the relevant property owner and to invest this income in other regions. The correct determination of this tax is of great importance for the state to provide equal service to citizens. Unfortunately, to minimize or avoid this tax, sometimes house sale values are declared lower than they actually are. In the present circumstance, after the buyer and seller decide the property sale price between them during the real estate transaction, they inform the land registry office, together with the fair value determined by the municipality. During this application, the buyer and seller also inform the land registry office of the number of sales they have agreed upon as a result of the bargaining between them. Since generally the money exchange is made between the parties physically, the land registry office cannot check the accuracy of the declared sales price. Since sales prices are not displayed in a permanent way, correct sales values and data cannot be obtained. The land registry office cannot check the accuracy of the declared sales price, since generally the money exchange is made between the parties physically. The value-added tax needs to be determined correctly to return public investments fairly to all citizens. Hence, obtaining the actual sales value has great importance for public welfare. It is also necessary to make physical applications to many institutions and prepare lots of physical documents in order to complete a real estate transaction. It should be also be noted that a high amount of physical activity is required in the current situation.

System Design

There is a need to establish a high-security system that will meet all the needs in the current state. Considering that we are in the age of digital transformation, and considering the new-generation technologies emerging in this period, blockchain stands out for its eye-catching advantages:

- By having a distributed database structure, the parties easily operate without the need for mutual trust.
- Transactions are carried out transparently and automated with a smart contract structure.
- Transactions are protected with high security.
- No records can be deleted.

Due to the revolutionary advantages it offers, blockchain technology stands out in comparison to systems to be installed in a central structure, which becomes the reason to install our new system. Although all these advantages are reasons to choose blockchain to build a system on, considering the widespread use of central databases, it would not be logical to choose blockchain without any detailed comparison. When we compare blockchain and central database solutions, we encounter many points. Whereas there is no dependence on third parties with blockchain, there is a need for a central authority or manager in the central database approach. Data are protected against modification or deletion in blockchain technology, but in a central database an authorized manager has control over the data, since the control is in a single center. While it is not necessary to change the system architecture to add or remove parties or change the transaction flow with blockchain's smart-contract structure, in a central database the system architecture must be changed and the data adapted to this process. While there is a high level of verification with blockchain, thanks to its certificate-verified log-in structure, in a central database approach traditional controls are carried out with the user-management mechanism. Thanks to blockchain's open ledger structure, the data are available to all users, thus ensuring security and consistency, whereas the data in a central structure are stored in a single point. In blockchain technology, the data are kept in a block structure with time stamps and transaction flow, while in a central structure time stamps can only be added manually, and the transaction flow cannot be kept. In addition to all these compaisons, one of the most important elements is that blockchain technology is suitable for the steps of the current deed-exchange process and for situations where trust between the parties is not required. Especially when this and other points are considered, we can say that blockchain is one step ahead of central database approaches (Figure 5).

After analyzing the current land registry process in Turkey, the operation steps were determined and the design steps for the blockchain-based system prepared in line with these needs. In the proposed system, the real estate hand-exchange process begins after the owner decides to put property on sale and after the agreement with the buyer who wants the property. Following this agreement, the management of the hand-exchange process will be carried out through the system.

The buyer will be included in the system via the sale code that will be created when the seller party puts the property on sale in the system. Using the sale code, buyers will have the ability to examine the spatial, attribute, and sales information of the property. The consistency of the verbally understood property and the spatial information in the system can be checked so that the seller cannot defraud the buyer by selling a different property.

After the buyer checks and approve the information of the property in question, the agreement between the buyer and seller will be finalized. After the buyer is included in the system, he or she approves the sale and the agreement between the buyer and seller is recorded in the system.

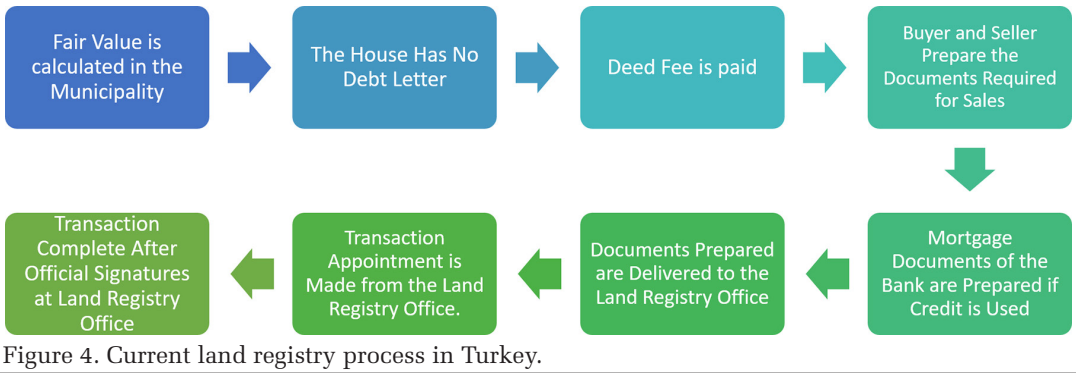

Figure 4. Current land registry process in Turkey.

Afterward, the municipality will approve that there is no debt attached to the property, and then the fair value will be determined. After the transaction fees are paid, confirmation of the correct transfer of housing sale prices through the banks of the buyer and seller parties will be ensured. With the involvement of the banks in the system, the process of the money transfer takes place digitally. Therefore, physical money transfer will be excluded from this proposed system.

In the current situation, it seems that the parties frequently tend to show sales prices lower than they are to avoid the value-added tax. This problem will be eliminated with the involvement of banks in the system.

Following confirmation from the banks, the land registry office will check the steps taken within the process and check that there is no problem with the sale of the property. If no problems are found during this check, transfer of the property and the money will be carried out at the same time following the signatures of the buyers and sellers at the land registry office. In any of these steps, if the party with the approval order does not approve the transaction, the whole transaction will be canceled.

Performing all these steps through software will speed up the process, reduce physical hustle, and eliminate the problem of manipulating residential sales prices. After building a logical software model, it is necessary to synthesize an implementation that runs on a given target platform. At this point, determining the flow of this software model is important to ensure success (Gu and He 2005). The flow diagram of the proposed system is shown in Figure 6.

Application Infrastructure Decision

Concepts such as smart contracts and smart property indicate value ownership in the digital environment. Smart contracts define the rules and flow that enable the cases to which we

Blockchain	VS	Centralized Database
There is no dependence on third parties.		Databases have central controls and administrators.
The data cannot be changed / deleted.		Authorized users can change / delete data.
Adding / removing parties; no change in system architecture is required.		Adding / removing parties; requires a change in system architecture.
Database management / maintenance costs are low.		Database management / maintenance costs are high.
High level verification is done with certificate verification.		User authentication; provided with username and password.
The process flow is determined without the need for changes in the system architecture.		Changing process flow requires a change in system architecture.
All users have «Open Ledger», where data is held.		The data are kept in a single centre.
It is compatible with the deed transfer process steps in the existing structure.		It is necessary to adapt the deed transfer process steps of the existing structure.
Users are provided to manage transactions in groups (Smart Contracts).		There is no structure like grouping transactions.
The blocks are stored with time stamp.		The timestamp can be added only manually.
Suitable where trust between parties is not required.		Central reliable authority is needed.
The process flow is kept together with the data in the blocks.		Process flow can be added manually with the logging mechanism.

Figure 5. Comparison between blockchain and centralized database.

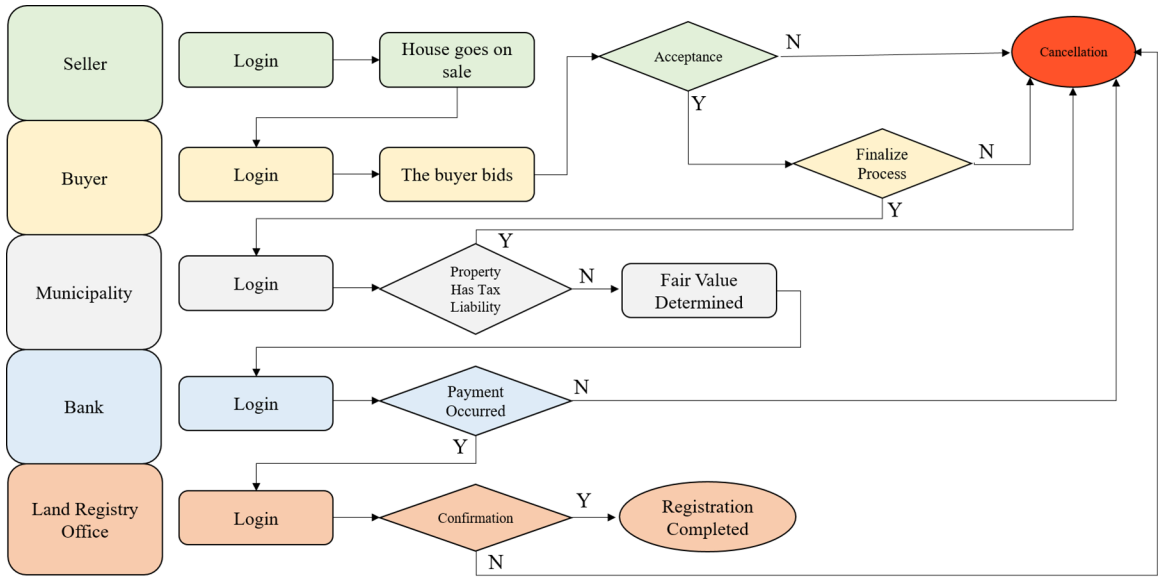

Figure 6. Flow diagram of the proposed system.

attach value to operate automatically as determined without the need for an external trigger mechanism. The smart-contract structure is a critical concept to achieve all the advantages offered by blockchain technology. It not only defines the rules and penalties around a contract like a traditional contract does but also automatically enforces those obligations. The flow is carried out completely automatically and no manual intervention is possible. This means that there is no need for any authority to manage the flow, that is, to run the flow with consensus between the parties. With this extraordinary structure, blockchain technology stands out and becomes the preferred system. When we look at the idea of smart contracts, we see that it was proposed in 1997 by Nick Szabo (Szabo 1997), who argues that through smart contracts, a structure in which digital contracts can be triggered can be established and set up digitally. The idea of smart property was initially proposed in 2012 by Mike Hearn ("Smart Property" n.d.), who argues that property status and the transfer process can be monitored. Smart property and smart ownership concepts can find a place with the smart-contract structure offered by blockchain technology. It is crucial to use the most appropriate smart-contract infrastructure to create a strong blockchain-based system. Currently there are few important blockchain smart-contract service providers in the market; the most prominent among the popular and powerful are Ethereum, Hyperledger, and Corda.

Ethereum is one of the most popular smart-contract providers. Announced by Vitalik Buterin in 2015, Ethereum is a smart-contract infrastructure platform where many cryptocurrencies currently operating in the market are developed. Apart from cryptocurrencies, it offers its users a structure to create a smart-contract protocol and provides the opportunity to develop different applications using this infrastructure (Wood 2017). Ethereum allows its users to develop their smart contract-based applications using the Solidity language.

Similar to Ethereum, R3 Corda offers smart-contract infrastructure for the development of blockchain applications. Corda is a blockchain platform developed by R3; its first version was released in 2016. R3 has entered the blockchain world with a different product by working with more than 200 members and partners in the development process, revealing the permissioned blockchain architecture for financial services, insurance, and the business world. With its smart-contract infrastructure, R3 Corda allows its users to develop their applications using the Java and Kotlin languages. With the infrastructure provided by R3 Corda, users can establish their own permissioned-type blockchain networks (Brown *et al.* 2016).

Hyperledger is another alternative we considered. It was founded by the Linux Foundation in 2016, adopting the principle of developing an open-source infrastructure and setting standards for blockchain-based application development. It is an organization with more than 50 members in total, with many companies from the financial sector as well as important companies in the world of technology, such as IBM and Fujitsu. With the basic principle of establishing a standard for distributed databases, it aims to develop blockchain technology by creating an open-standard platform across industries and institutions for distributed databases. With this platform, the way of developing applications in different fields can be opened, and thus a new setup will emerge that will include different actors on a global basis. Unlike its competitors, which currently offer blockchain-based smart-contract infrastructure, the Hyperledger project has targeted areas of application outside of cryptocurrencies since its first appearance. It produces a wide range of solutions for different needs for incubation at all development stages for enterprise-class blockchain. This infrastructure aims at creating awareness in the Internet world which will constitute an infrastructure quality for smart contracts (Cachin 2016).

When determining the infrastructure service provider to use in developing our application, we considered two basic criteria. First, the field of application is one of the topics evaluated. If we were developing a financial application, Corda's smart-contract infrastructure could be used. However, when we consider that the application we will develop is not in this field of activity, we have to remove Corda from the alternatives. At this point, two alternatives remain: Ethereum and Hyperledger. The second criterion is the need to be able to determine how and with what authority users will participate in the blockchain network to be created. Currently, a blockchain network can be set up as public or private. In a public network, users can freely join the system as a writer or reader node without permission. Bitcoin and some other cryptocurrencies are the best-known examples of this usage. Conversely, a private network is a structure that only authorized writers and readers can join. Authorization of the nodes to be included in the system is determined in advance, and those that are not found are not included in the system (Wüst and Gervais 2018). While Ethereum offers a public blockchain, where users can join without needing any authorization, Hyperledger offers, in addition to a public blockchain infrastructure, a special structure in which users must have authority to read and write on the network. In addition, Hyperledger is more flexible than the others, so the configuration could be almost totally decided by the users. Since the nodes that will be included in the application we will develop need to be included in the system with certain authorities, we need to establish a private and flexible network. Evaluating these reasons, we decided to use Hyperledger infrastructure in our application.

There are many solutions proposed by Hyperledger, such as Fabric, Indy, and Sawtooth. Fabric is the most active and preferred Hyperledger project among these alternatives. It is a distributed ledger application platform that allows the implementation of smart contracts with its modular and flexible architecture. It supports several different consensus protocols that enable the system to be designed according to different usage scenarios and models instead of the costly mining-verified consensus models used in cryptocurrencies. In addition, it is the first blockchain infrastructure to run applications written to a certain standard in general programming languages without systematic dependency on cryptocurrency. Therefore, Hyperledger Fabric is a revolutionary solution that can be used independent of industry. It is supported by advantages such as flexibility, performance optimization, and low resource consumption. With its modular architecture, it offers a permissioned (private) structure and provides a high level of privacy, keeping relevant transactions in the system in line with each other and isolated from other transactions (Androulaki *et al.* 2018).

After the blockchain structure is built with Fabric, an additional tool is needed to create and distribute the network. Hyperledger Composer, which can work in harmony with Fabric, provides an advanced and user-friendly interface for network creation and distribution. It allows changes to the network to be seen simultaneously, no matter how large the network. Thanks to REST service compatibility, it provides integration with different databases and systems. When all these considerations were evaluated, we decided to use the Hyperledger Composer tool to display the network.

Development of the Application

After analyzing the current land registry process in Turkey and determining the software infrastructure to be used, at the next stage the system parties need to be decided. Blockchain is a technology that provides communication between stakeholders, and since verifications will be made between the parties, these must be determined during the installation of the system. There are six stakeholders in the proposed system; the completion of

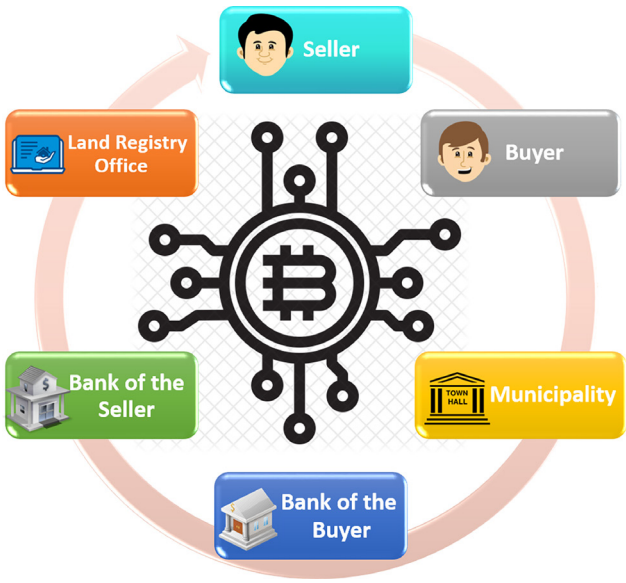

Figure 7. Nodes of the blockchain-based system.

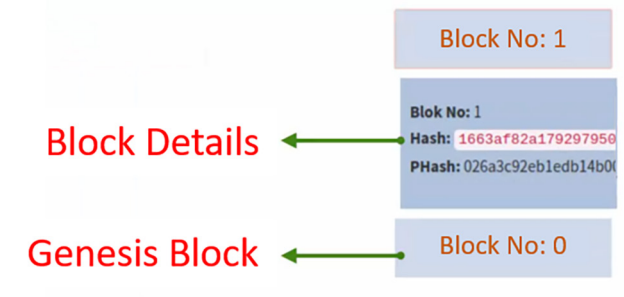

Figure 8. An example of block structure in the system.

the process flow is carried out with sequential approvals from these participants. Therefore, we decided to use the proof-of-authority (PoA) consensus method. This is a consensus method that gives a specified number of blockchain actors the power to validate transactions or interactions with the network and update its more or less distributed registry. Compared to other consensus methods, PoA is less computationally intensive, more secure, and more predictable, and provides lower transaction latency (He *et al.* 2018). PoA is one of the most suitable ways for private blockchain. Since we are offering a private blockchain, the PoA consensus method is chosen.

There are six participants (Figure 7) in our proposed blockchain-based land registry system, whose sequential approvals are necessary for the completion of the process flow:

- Seller
- Buyer
- Municipality with which the property is affiliated
- Bank of the buyer
- Bank of the seller
- Land registry office

In the system whose stakeholders are determined, the smart-contract template needs to be created through which real estate hand-exchange transactions should be carried out. For this purpose, the parties must be determined for inclusion in the blockchain network created using Hyperledger Fabric and Composer. After the stakeholders are added to the system, it is necessary to define in what order and in what structure transactions will be carried out between them. Smart-contract conditions such as the order of stakeholders and minimum and maximum approval period were determined with the smart-contract template. The blockchain network is established in line with the determined consensus method, nodes, and smart-contract terms (Figure 8).

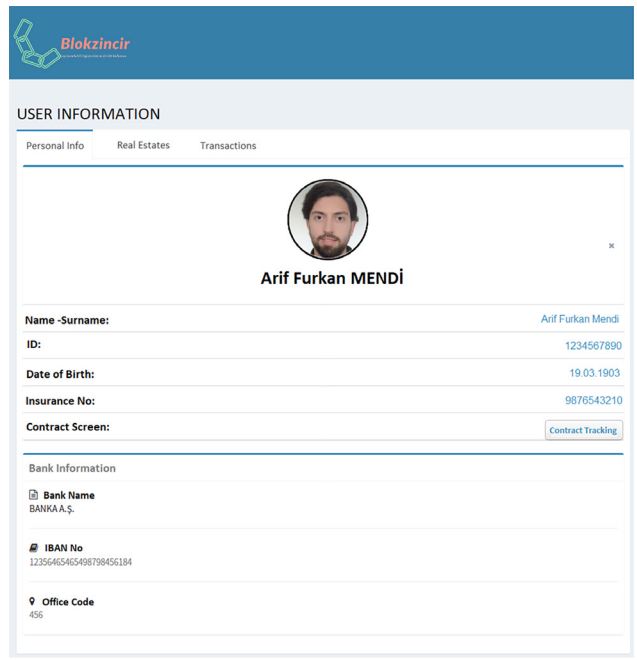

Figure 9. Seller-information screenshot.

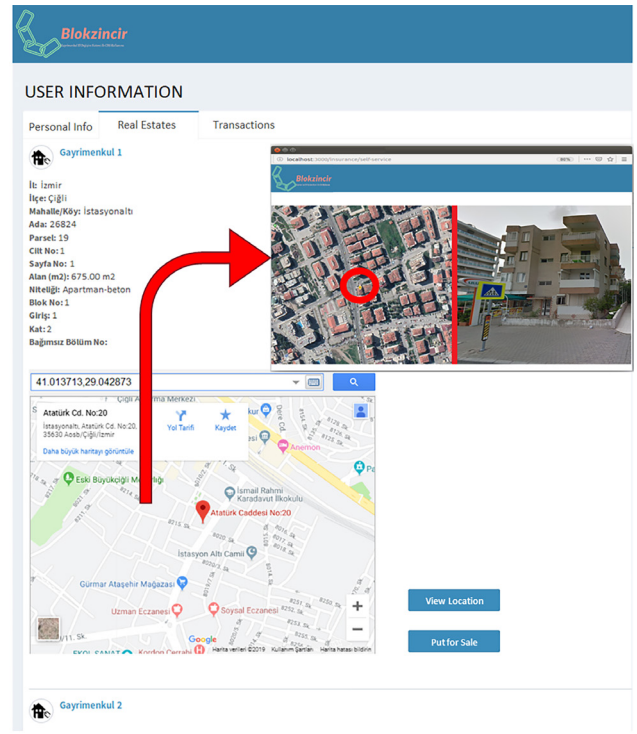

Figure 10. Estate-information screenshot.

In the first step of the application, the owner of the property logs into the system, which lists the properties that belong to that owner, and makes a selection from the listed properties (Figure 9).

The spatial and attribute data of the selected real estate are displayed on the real estate list (Figure 10). After the sale price of the real estate subject to sale, the information of the buyer, and the contract terms are determined, the house is put up for sale. When the sale is registered, a sales code is generated, which the buyer will use when entering the system.

The buyer logs into the system with the sales code and displays the spatial and attribute information of the property that the seller has offered for sale. The sales price agreed upon between them is also displayed here. After viewing all the information about the sale, the buyer approves the price and smart-contract information, if appropriate (Figure 11). If changes are requested in the terms of the contract or if the offer is rejected, the flow is canceled and sent to the seller for preparation of the contract again.

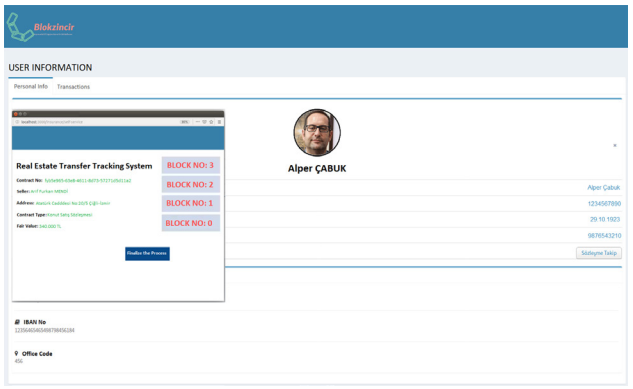

Figure 11. Screenshot where the buyer displays the property information and approves the sale.

After the buyer finalizes the transaction, the municipality is included in the system to determine the fair value of the house. In the next stage, the buyer's bank is involved in the process, paying the agreed-upon amount of the money to the seller's bank. After the seller's bank confirms that there is a payment order from the buyer's bank, the last step in the flow proceeds, including the land registry office in the system. The land registry office examines the related real estate hand-exchange request and approves the flow if it does not encounter any negative information. Following the approval of the land registry office, the real estate hand exchange and money transfer take place and the flow is completed.

Results and Discussion

After evaluating the requirements in the existing land registry process in Turkey, a blockchain-based land registry application was developed which is carried out in six steps. The proposed system aims to allow buyers and sellers to perform hand exchange safely with less physical effort. If the system is put into use across the country, a useful method will be obtained to determine the value-added tax correctly. For this purpose, Hyperledger—one of the most popular, flexible, and useful providers of blockchain smart-contract infrastructure—was preferred. With the system prepared using Hyperledger, which provides an open-source infrastructure, a system was prepared to meet the needs of Turkey.

While we were creating the system, we met some problems in the development stage. Lack of resources is the main problem encountered, since Hyperledger is a relatively new organization (established in 2016). The number of projects developed with and using a Hyperledger infrastructure is limited, and there are not enough projects completed to transfer the experience gained to new projects. The development of the Hyperledger project is still ongoing. The organization has released many versions. As a result of experience and feedback, the release of successive versions continues periodically. User manuals for Hyperledger services are available to everyone over the Internet. However, since the history of the services provided is not very long, the number of studies in the literature carried out using Hyperledger is very limited. When a problem is encountered during the development phase, research is done on the Internet, and the problem is solved quickly by using resources that have encountered similar problems and produced solutions. Since there are a limited number of Hyperledger applications in the literature, it causes difficulties in quickly overcoming problems encountered during the application development phase. During the development process, when it was not possible to solve some problems with existing documents, it was possible to find solutions by examining the source code and performing various trials. This process took more time than expected and cost high effort.

Innovation is an important concept in increasing the acceleration of development, especially in emerging countries like Turkey. With the use of a system where innovation takes place and new-generation technologies are used, the development level of the country will also be positively affected. It is of great importance to increase the number of such innovative projects in order to increase the development level of the country.

Conclusion

Blockchain technology is an emerging technology that stands out thanks to advantages such as agentless transaction, high-level security, and transparency in data tracking. Even though the advantages of blockchain technology look brilliant, the maturity level is a bit low—as expected—because the history of the technology is not very long. This fact is also valid for our proposed solution for Turkey, a blockchain-based land registry system application. This emerging technology-based, innovative application proposes high-level security, no intermediary transactions, and a low level of physical effort for the whole process. In addition, it proposes an important solution for the problem of not being able to determine value-added taxes to fairly return public investments to all citizens. However, to put the system into use throughout the country, it is necessary to make legal arrangements and adapt the processes according to the application. Even if the application has important advantages, in order to ensure the continuity of the system and expand usage, the sales transactions made using the application must qualify as legal evidence. Globalization of the application is another issue. The needs mentioned are mostly subject to regional regulations, so the claim that a single solution can be produced in the international market with the blockchain-based land registration system application developed is unrealistic. Although the local laws of all countries are different from each other, implementation can be easily customized for different countries through regional regulations. With such dissemination, the advantages of blockchain land registry applications will begin to emerge concretely. In addition to all of these, the importance of digitalization has emerged with the global COVID-19 epidemic. Daily physical life is largely restricted because of this pandemic, and people have been unable to perform work that requires physical application and effort. Blockchain technology is the safest and fastest example of digitalization, and free of intermediaries. Since the existing land registration process in Turkey involves many steps requiring physical exertion, it has been greatly affected by the physical restrictions imposed by the pandemic. Thus, there has been a great decrease in the number of house-sale transactions. If the application we developed were put into use throughout the country, there would not be such a big decrease in the land registry process. When we think of the technology era we are in, we have once again experienced the necessity of developing innovative approaches by going beyond traditional solutions.

References

Allison, I. 2017, April 5. Blockchain-based Ubitquity pilots with Brazil's land records bureau. *International Business Times*. <https://www.ibtimes.co.uk/blockchain-based-ubitquity-pilots-brazils-land-records-bureau-1615518> Accessed 1 April 2018.

Androulaki, E., A. Barger, V. Bortnikov, C. Cachin, K. Christidis, A. De Caro, D. Enyeart, C. Ferris, G. Laventman, Y. Manevich, S. Muralidharan, C. Murthy, B. Nguyen, M. Sethi, G. Singh, K. Smith, A. Sorniotti, C. Stathakopoulou, M. Vukolić, S. Weed Cocco and J. Yellick. 2018. Hyperledger Fabric: A distributed operating system for permissioned blockchains. Article 30 in *EuroSys '18: Proceedings of the Thirteenth EuroSys Conference*, held in Porto, Portugal, 23–26 April 2018. Edited by J. Editor. City, St.: Publisher. https://doi.org/10.1145/3190508.3190538

Brown, R. G., J. Carlyle, I. Grigg and M. Hearn. 2016. Corda: An Introduction. <https://doi.org/10.13140/RG.2.2.30487.37284> Accessed DD Month YYYY.

Cachin, C. 2016. Architecture of the Hyperledger blockchain Fabric. https://doi.org/10.1080/00131880701200781

ChromaWay. n.d. Solutions. <https://chromaway.com/landregistry> Accessed 26 May 2018.

Gu, Z. and Z. He. 2005. Real-time scheduling techniques for implementation synthesis from component-based software models. Pages 235–250 in *CBSE 2005: Component-Based Software Engineering*, held in St. Louis, Mo., 14–15 May 2005. Edited by G. T. Heineman, I. Crnkovic, H. W. Schmidt, J. A. Stafford, C. Szyperski and K. Wallnau. Lecture Notes in Computer Science vol. 3489. Berlin, Germany: Springer.

He, Q.,N. Guan, M. Lv and W. Yi. 2018. On the consensus mechanisms of blockchain/DLT for Internet of Things. Pages PP–PP in *2018 IEEE 13th International Symposium on Industrial Embedded Systems*, held in Graz, Austria, 6–8 June 2018. Edited by J. Editor. City, St.: Publisher.

Lemieux, V. L. 2017. Evaluating the use of blockchain in land transactions: An archival science perspective. *European Property Law Journal* 6 (3):392–440.

Li, D., J. Shan, Z. Shao, X. Zhou and Y. Yao. 2013. Geomatics for smart cities—concept, key techniques, and applications. *Geo-Spatial Information Science* 16 (1):13–24.

Li D. and Z. Shao. 2009. The new era for geo-information. *Science in China Series F: Information Sciences* 52 (7):1233–1242.

Panetta, K. 2017, August 15. Top trends in the Gartner Hype Cycle for emerging technologies, 2017. <https://www.gartner.com/smarterwithgartner/top-trends-in-the-gartner-hype-cycle-for-emerging-technologies-2017/> Accessed 2 March 2020.

Shan, J. 1998. Visualizing 3-D geographical data with VRML. Pages PP–PP in *Proceedings: Computer Graphics International*, held in Hannover, Germany, 26 June 1998. Edited by J. Editor. City, St.: Publisher.

Smart Property. n.d. <https://en.bitcoin.it/wiki/Smart_Property> Accessed 31 March 2018.

Spielman, A., 2016. Blockchain: Digitally Rebuilding the Real Estate Industry.

Szabo, N. 1997. The Idea of Smart Contracts. <http://www.fon.hum.uva.nl/rob/Courses/InformationInSpeech/CDROM/Literature/LOTwinterschool2006/szabo.best.vwh.net/idea.html> Accessed 31 March 2018.

Wang, J. and J. Shan. 2005. Lidar data management with 3-D Hilbert space-filling curve. Pages 1123–1129 in *ASPRS 2005 Annual Conference*, held in Baltimore, Md., 7–11 March 2005. Edited by J. Editor. City, St.: Publisher.

Wood, G. 2017. Ethereum: A Secure Decentralised Generalised Transaction Ledger, EIP-150 Revision. <http://gavwood.com/paper.pdf> Accessed DD Month YYYY.

Wüst, K. and A. Gervais. 2018. Do you need a blockchain? Pages 45–54 in *2018 Crypto Valley Conference on Blockchain Technology*, held in Zug, Switzerland, 20–22 June 2018. Edited by J. Editor. City, St.: Publisher.

Yli-Huumo, J., D. Ko, S. Choi, S. Park and K. Smolander. 2016. Where is current research on blockchain technology?—A systematic review. *PLoS One* 11 (10):e0163477.

PE&RS Media Kit 2021

PE&RS 2021 Advertising Rates & Specs

THE MORE YOU ADVERTISE THE MORE YOU SAVE! *PE&RS* offers frequency discounts. Invest in a three-times per year advertising package and receive a 5% discount, six-times per year and receive a 10% discount, 12-times per year and receive a 15% discount off the cost of the package.

	Corporate Member Exhibiting at a 2021 ASPRS Conference	**Corporate Member**	**Exhibitor**	**Non Member**
All rates below are for four-color advertisments				
Cover 1	$1,850	$2,000	$2,350	$2,500
In addition to the cover image, the cover sponsor receives a half-page area to include a description of the cover (maximum 500 words). The cover sponsor also has the opportunity to write a highlight article for the journal. Highlight articles are scientific articles designed to appeal to a broad audience and are subject to editorial review before publishing. The cover sponsor fee includes 50 copies of the journal for distribution to their clients. More copies can be ordered at cost.				
Cover 2	$1,500	$1,850	$2,000	$2,350
Cover 3	$1,500	$1,850	$2,000	$2,350
Cover 4	$1,850	$2,000	$2,350	$2,500
Advertorial	1 Complimentary Per Year	1 Complimentary Per Year	$2,150	$2,500
Full Page	$1,000	$1,175	$2,000	$2,350
2 page spread	$1,500	$1,800	$3,200	$3,600
2/3 Page	$1,100	$1,160	$1,450	$1,450
1/2 Page	$900	$960	$1,200	$1,200
1/3 Page	$800	$800	$1,000	$1,000
1/4 Page	$600	$600	$750	$750
1/6 Page	$400	$400	$500	$500
1/8 Page	$200	$200	$250	$250
Other Advertising Opportunities				
Wednesday Member Newsletter Email Blast	1 Complimentary Per Year	1 Complimentary Per Year	$600	$600

A 15% commission is allowed to recognized advertising agencies

Ad Size	**Width**	**Height**
Cover (bleed only)	8.625"	11.25"
Full Page (bleed)	8.625"	11.25"
Full Page (trim)	8.375"	10.875"
2/3 Page Horizontal	7.125"	6.25"
2/3 Page Vertical	4.58"	9.625"
1/2 Page Horizontal	7.125"	4.6875"
1/2 Page Vertical	3.4375"	9.625"
1/3 Page Horizontal	7.125"	3.125"
1/3 Page Vertical	2.29"	9.625"
1/4 Page Horizontal	7.125"	2.34"
1/4 Page Vertical	3.4375"	4.6875"
1/8 Page Horizontal	7.125"	1.17"
1/8 Page Vertical	1.71875"	4.6875"

- Publication Size: 8.375" × 10.875" (W x H)
- Live area: 1/2" from gutter and 3/8" from all other edges
- No partial page bleeds.
- Publication Style: Perfect bound
- Printing Method: Web offset press
- Software Used: PC InDesign CS6

- Supported formats:
  - TIFF
  - EPS
  - BMP
  - JPEG
  - PDF
  - PC InDesign, Illustrator, and Photoshop

Send ad materials to:
ASPRS/PE&RS Production
425 Barlow Place, Suite 210
Bethesda, Maryland 20814
505-819-3599
rkelley@asprs.org

Ship inserts to:
Alicia Coard
Walsworth
2180 Maiden Lane
St. Joseph, MI 49085
888-563-3220 (toll free)
269-428-1021 (direct)
269-428-1095 (fax)
alicia.coard@walsworth.com

ource: *PE&RS* Readership Survey, Summer 2017

For more information, contact Bill Spilman at bill@innovativemediasolutions.com | (877) 878-3260 toll-free | (309) 483-6467 direct | (309) 483-2371 fax

PE&RS Readership Highlights

ASPRS is in the Top 20!

From May 1 to 31, 2020, PE&RS ranked 15th out of over 11,000 journals for content downloads with Ingenta Connect.

"We are very proud of this accomplishment" says Jesse Winch, Acting Executive Director. "When ASPRS was organized in 1934 our primary mission was to advance the knowledge and improve the understanding of the mapping sciences. PE&RS is of tremendous value to the geospatial community. Not only does it provide an important avenue for researchers to publish their findings but it also provides an area where corporations can highlight areas in which their products are being used."

Circulation: 3,200
Total audience: 6,400*

Digital Edition Monthly Unique Views: 2,000+

Professional Demographics

Years in profession (mean): 16.7 years

	% Composition
Work Setting	
Corporate	38.5%
Academia	26.9%
Government	26.9%
Sole Proprietor LLC	3.8%
Education	
Post graduate+ Doctorate degree	26.9%
4-year college degree	30.8%

ASPRS Certifications	**Amount**
ASPRS Certified Photogrammetrists	330+
ASPRS Certified Mapping Scientists*	110+
Certified Metrologists	30+
ASPRS Certified Technologists	20+

*Includes our new and fast-growing Lidar certification

_PE&RS_ readers make the purchasing decisions for their organizations and have interest and budgets to buy what you sell!

_PE&RS_ is well-read, influential and of great value to its high-powered readership.

Readership Habits

	% Composition
Read regularly (at least 3 out of 4 issues)	69.2%

Took action as a result of reading	
Clipped or copied article(s) of interest	80.8%
Discussed an article with a colleague	80.8%
Saved the issue for future reference	73.1%
Visited an advertiser's website	69.2%
Pointed out a product to a colleage	61.5%
Contacted an author/key figure for information	46.2%
Adopted/modified a process or procedure	42.3%
Contacted an advertiser by email or phone	30.8%
Purchased an advertised product	19.2%

For more information, contact Bill Spilman at bill@innovativemediasolutions.com | (877) 878-3260 toll-free | (309) 483-6467 direct | (309) 483-2371 fax

PE&RS Media Kit 2021

Special Advertising Opportunities

FRONT COVER SPONSORSHIP

A *PE&RS* cover sponsorship is a unique opportunity to capture the undivided attention of your target market through three premium points of contact.

1— *PE&RS* FRONT COVER

(Only twelve available, first-come, first-served)
PE&RS is world-renowned for the outstanding imagery displayed monthly on its front cover—and readers have told us they eagerly anticipate every issue. This is a premium opportunity for any company, government agency, university or non-profit organization to provide a strong image that demonstrates their expertise in the geospatial information industry.

2— FREE ACCOMPANYING "HIGHLIGHT" ARTICLE

A detailed article to enhance your cover image is welcome but not a condition of placing an image. Many readers have asked for more information about the covers and your article is a highly visible way to tell your story in more depth for an audience keenly interested in your products and services. No article is guaranteed publication, as it must pass ASPRS editorial review. For more information, contact Rae Kelley at rkelley@asprs.org.

3— FREE TABLE OF CONTENTS COVER DESCRIPTION

Use this highly visible position to showcase your organization by featuring highlights of the technology used in capturing the front cover imagery. Limit 200-word description.

Terms: Fifty percent nonrefundable deposit with space reservation and payment of balance on or before materials closing deadline.

Cover Specifications:

Bleed size: 8 5/8" × 11 1/4" Trim: 8 3/8" × 10 7/8"

Offprints of the cover, Table of Contents page, and highlight article are available at the time of publication. These must be ordered and paid for in advance.

For front cover offprints or other quantities, contact
Rae Kelley, ASPRS Assistant Director – Publications
505-819-3599
e-mail rkelley@asprs.org.

PRICING

	Corporate Member Exhibiting at a 2021 ASPRS Conference	Corporate Member	Exhibitor	Non Member
Cover 1	$1,850	$2,000	$2,350	$2,500

Belly Bands, Inserts, Outserts & More!
Make your material the first impression readers have when they get their copy of *PE&RS*. Contact Bill Spilman at bill@innovativemediasolutions.com

VENDOR SEMINARS

ASPRS Sustaining Members now have the opportunity to hold a 1-hour informational session as a Virtual Vendor Seminar that will be free to all ASPRS Members wishing to attend. There will be one opportunity per month to reach out to all ASPRS Members with a demonstration of a new product, service, or other information. ASPRS will promote the Seminar through a blast email to all members, a notice on the ASPRS web site home page, and ads in the print and digital editions of *PE&RS*.

The Virtual Seminar will be hosted by ASPRS through its Zoom capability and has the capacity to accommodate 500 attendees.

Vendor Seminars	
Fee	$2,500 (no discounts)

EMPLOYMENT PROMOTION

When you need to fill a position right away, use this direct, right-to-the-desktop approach to announce your employment opportunity. The employment opportunity will be sent once to all ASPRS members in our regular Wednesday email newsletter to members, and will be posted on the ASPRS Web site for one month. This type of advertising gets results when you provide a web link with your text.

Employment Opportunity	Net Rate
30-Day Web + 1 email	$500/opportunity
Web-only (no email)	$300/opportunity

Do you have multiple vacancies that need to be filled? Contact us for pricing details for multiple listings.

NEWSLETTER DISPLAY ADVERTISING

Your vertical ad will show up in the right hand column of our weekly newsletter, which is sent to more than 3,000 people, including our membership and interested parties. **Open Rate: 32.9%**

Newsletter vertical banner ad	Net Rate
180 pixels x 240 pixels max	$500/opportunity

PE&RS Digital Edition

Digital Edition E-mail Blast: 5,800+
PE&RS is available online in both a public version that is available to anyone but does not include the peer-reviewed articles, and a full version that is available to ASPRS members only upon login.

The enhanced version of *PE&RS* contains hot links for all ASPRS Sustaining Member Companies, as well as hot links on advertisements, ASPRS Who's Who, and internet references.

Become a sponsor today!
The e-mail blast sponsorship opportunity includes a **180 x 240 pixel ad** in the email announcement that goes out to our membership announcing the availability of the electronic issue.

Digital Edition Opportunities	Net Rate
E-mail Blast Sponsorship*	$1,000

For more information, contact Bill Spilman at bill@innovativemediasolutions.com | (877) 878-3260 toll-free | (309) 483-6467 direct | (309) 483-2371 fax

2021 ASPRS ADVERTISING ORDER FORM

Company

Ad Type | Frequency

Rate

Purchase Order Number

Contract Authorized by (print)

Authorized Signature | Date

ADVERTISING CONTACT

Name

Company

Address

City/State/Zip

Phone | Fax

Email

BILL TO (if different from advertising contact)

Name

Company

Address

City/State/Zip

Phone | Fax

Email

PE&RS AD TYPE

- ❑ Cover 1
- ❑ Cover 2
- ❑ Cover 3
- ❑ Cover 4
- ❑ Advertorial
- ❑ Full Page
- ❑ 2 page spread
- ❑ 2/3 Page
- ❑ 1/2 Page
- ❑ 1/3 Page
- ❑ 1/4 Page
- ❑ 1/6 Page
- ❑ 1/8 Page
- ❑ Belly band
- ❑ Insert
- ❑ Outsert
- ❑ Digital Edition Email Blast

Ad Placement

- ❑ January
- ❑ February
- ❑ March
- ❑ April
- ❑ May
- ❑ June
- ❑ July
- ❑ August
- ❑ September
- ❑ October
- ❑ November
- ❑ December

Specialty Ad Opportunities

- ❑ Newsletter vertical banner ad
  Date _____
- ❑ Employment Opportunity
  Date _____
- ❑ Vendor Seminar
  Date _____

IMPORTANT

- Advertiser and advertising is subject to approval by ASPRS
- Individual ads cannot be canceled after space close deadline.
- Any files that do not follow the requirements are subject to an additional production charge.

ADVERTISING REPRESENTATIVE

Bill Spilman, President
Innovative Media Solutions
320 W. Chestnut St.
P.O. Box 399, Oneida, IL 61467
(877) 878-3260 toll-free
(309) 483-6467 direct
(309) 483-2371 fax
bill@innovativemediasolutions.com

ASPRS Code of Ethics

Honesty, justice, and courtesy form a moral philosophy which, associated with mutual interest among people, should be the principles on which ethics are founded.

Each person who is engaged in the use, development, and improvement of the mapping sciences (Photogrammetry, Remote Sensing, Geographic Information Systems, and related disciplines) should accept those principles as a set of dynamic guides for conduct and a way of life rather than merely for passive observance. It is an inherent obligation to apply oneself to one's profession with all diligence and in so doing to be guided by this Code of Ethics.

Accordingly, each person in the mapping sciences profession shall have full regard for achieving excellence in the practice of the profession and the essentiality of maintaining the highest standards of ethical conduct in responsibilities and work for an employer, all clients, colleagues and associates, and society at large, and shall . . .

1. Be guided in all professional activities by the highest standards and be a faithful trustee or agent in all matters for each client or employer.

2. At all times function in such a manner as will bring credit and dignity to the mapping sciences profession.

3. Not compete unfairly with anyone who is engaged in the mapping sciences profession by:

   a. Advertising in a self-laudatory manner;

   b. Monetarily exploiting one's own or another's employment position;

   c. Publicly criticizing other persons working in or having an interest in the mapping sciences;

   d. Exercising undue influence or pressure, or soliciting favors through offering monetary inducements.

4. Work to strengthen the profession of mapping sciences by:

   a. Personal effort directed toward improving personal skills and knowledge;

   b. Interchange of information and experience with other persons interested in and using a mapping science, with other professions, and with students and the public;

   c. Seeking to provide opportunities for professional development and advancement of persons working under his or her supervision;

   d. Promoting the principle of appropriate compensation for work done by person in their employ.

5. Undertake only such assignments in the use of mapping sciences for which one is qualified by education, training, and experience, and employ or advise the employment of experts and specialists when and whenever clients' or employers' interests will be best served thereby.

6. Give appropriate credit to other persons and/or firms for their professional contributions.

7. Recognize the proprietary, privacy, legal, and ethical interests and rights of others. This not only refers to the adoption of these principles in the general conduct of business and professional activities, but also as they relate specifically to the appropriate and honest application of photogramme try, remote sensing, geographic information systems, and related spatial technologies. Subscribers to this code shall not condone, promote, advocate, or tolerate any organization's or individual's use of these technologies in a manner that knowingly contributes to:

   a. deception through data alteration;

   b. circumvention of the law;

   c. transgression of reasonable and legitimate expectation of privacy.

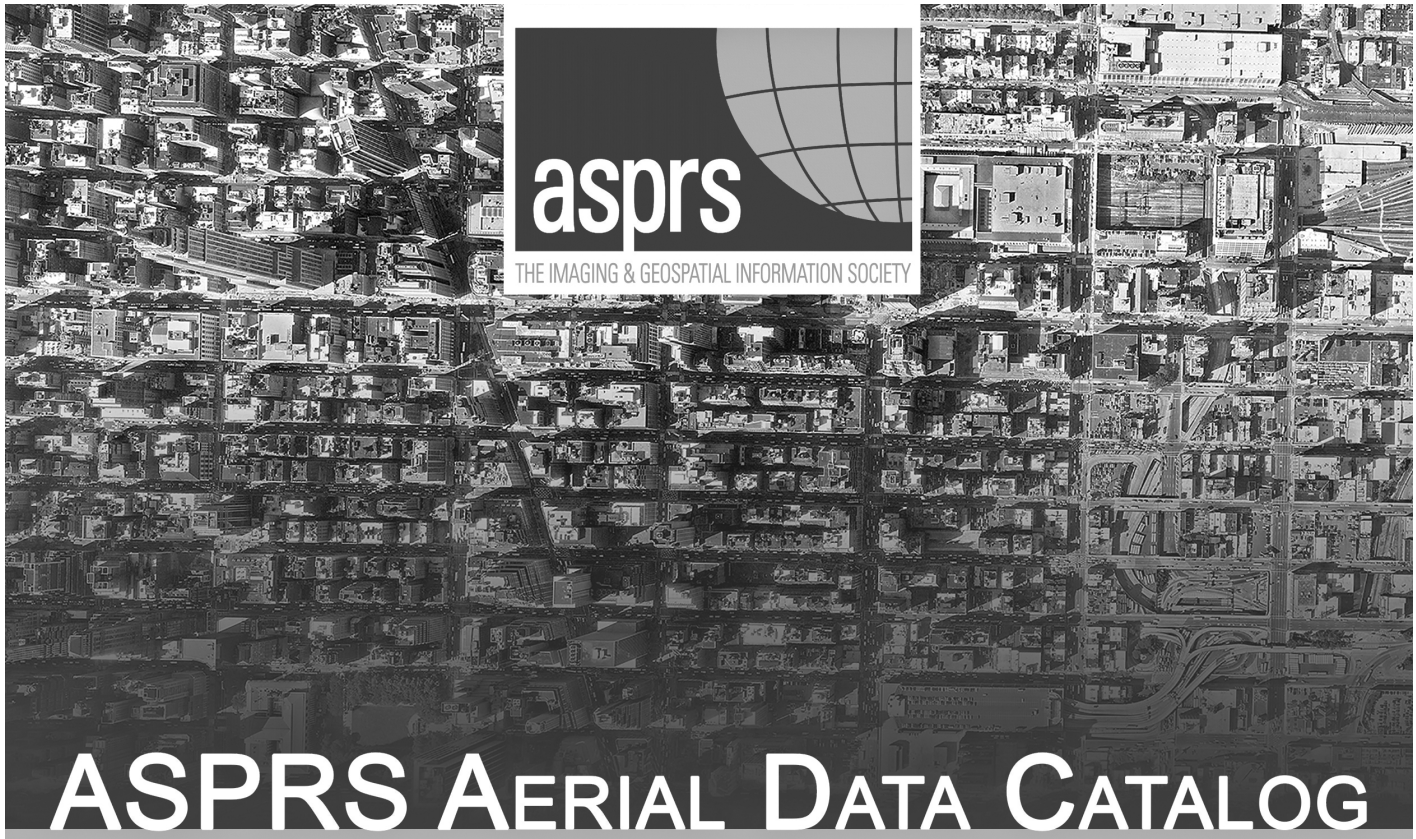

asprs

THE IMAGING & GEOSPATIAL INFORMATION SOCIETY

ASPRS Aerial Data Catalog

"The Source for Finding Aerial Collections"

http://dpac.asprs.org

The ASPRS Aerial Data Catalog is a tool allowing owners of aerial photography to list details and contact information about individual collections.

By providing this free and open metadata catalog with no commercial intrests, the Data Preservation and Archiving Committee (DPAC) aims to provide a definitive metadata resource for all users in the geospatial community to locate previously unkown imagery.

DPAC hopes this Catalog will contribute to the protection and preservation of aerial photography around the world!

ASPRS Members: We Need Your Help! There are three ways to get involved

1 USE — Use the catalog to browse over 5,000 entries from all 50 states and many countries. Millions of frames from as early as 1924!

2 SUPPLY — Caretakers of collections, with or without metadata, should contact DPAC to add their datasets to the catolog free of charge!

3 TELL — Spread the word about the catalog! New users and data collections are key to making this a useful tool for the community!

For More Details or To Get Involved Contact:

David Ruiz • druiz@quantumspatial.com • 510-834-2001 OR David Day • dday@kasurveys.com • 215-677-3119

Landsat's Enduring Legacy

Pioneering Global Land Observations from Space

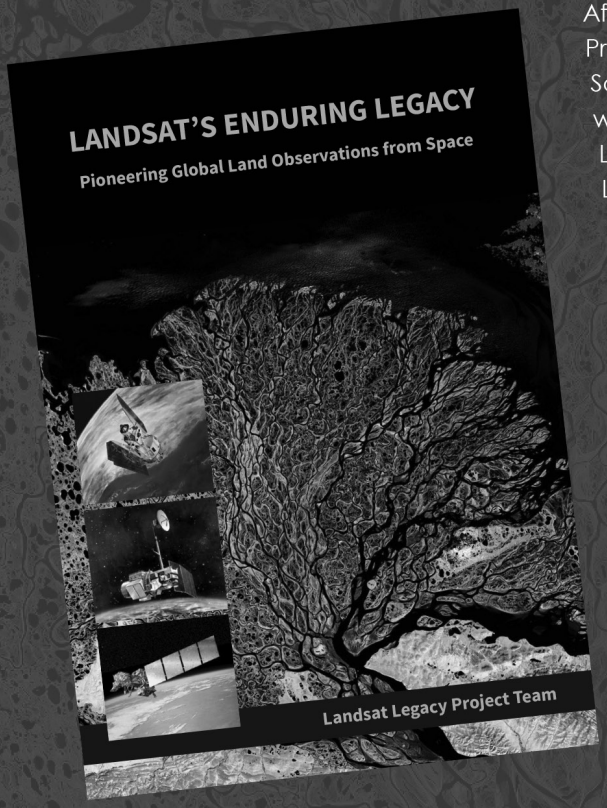

After more than 15 years of research and writing, the Landsat Legacy Project Team is about to publish, in collaboration with the American Society for Photogrammetry and Remote Sensing (ASPRS), a seminal work on the nearly half-century of monitoring the Earth's lands with Landsat. Born of technologies that evolved from the Second World War, Landsat not only pioneered global land monitoring but in the process drove innovation in digital imaging technologies and encouraged development of global imagery archives. Access to this imagery led to early breakthroughs in natural resources assessments, particularly for agriculture, forestry, and geology. The technical Landsat remote sensing revolution was not simple or straightforward. Early conflicts between civilian and defense satellite remote sensing users gave way to disagreements over whether the Landsat system should be a public service or a private enterprise. The failed attempts to privatize Landsat nearly led to its demise. Only the combined engagement of civilian and defense organizations ultimately saved this pioneer satellite land monitoring program. With the emergence of 21st century Earth system science research, the full value of the Landsat concept and its continuous 45-year global archive has been recognized and embraced. Discussion of Landsat's future continues but its heritage will not be forgotten.

The pioneering satellite system's vital history is captured in this notable volume on Landsat's Enduring Legacy.

Landsat Legacy Project Team

Samuel N. Goward
Darrel L. Williams
Terry Arvidson
Laura E. P. Rocchio
James R. Irons
Carol A. Russell
Shaida S. Johnston

Landsat's Enduring Legacy

Hardback. 2017, ISBN 1-57083-101-7

Student	$60*
Member	$80*
Non-member	$100*

* Plus shipping

Order online at

www.asprs.org/landsat

asprs THE IMAGING & GEOSPATIAL INFORMATION SOCIETY

Digital Elevation Model Technologies and Applications: The DEM Users Manual, 3rd Edition

Edited by David F. Maune, PhD, CP
and Amar Nayegandhi, CP, CMS

To order, visit https://www.asprs.org/dem

The 3rd edition of the DEM Users Manual includes 15 chapters and three appendices. References in the eBook version are hyperlinked. Chapter and appendix titles include:

1. Introduction to DEMs
   David F. Maune, Hans Karl Heidemann, Stephen M. Kopp, and Clayton A. Crawford
2. Vertical Datums
   Dru Smith
3. Standards, Guidelines & Specifications
   David F. Maune
4. The National Elevation Dataset (NED)
   Dean B. Gesch, Gayla A. Evans, Michael J. Oimoen, and Samantha T. Arundel
5. The 3D Elevation Program (3DEP)
   Jason M. Stoker, Vicki Lukas, Allyson L. Jason, Diane F. Eldridge, and Larry J. Sugarbaker
6. Photogrammetry
   J. Chris McGlone and Scott Arko
7. IfSAR
   Scott Hensley and Lorraine Tighe
8. Airborne Topographic Lidar
   Amar Nayegandhi and Joshua Nimetz
9. Lidar Data Processing
   Joshua M. Novac
10. Airborne Lidar Bathymetry
    Jennifer Wozencraft and Amar Nayegandhi
11. Sonar
    Guy T. Noll and Douglas Lockhart
12. Enabling Technologies
    Bruno M. Scherzinger, Joseph J. Hutton, and Mohamed M.R. Mostafa
13. DEM User Applications
    David F. Maune
14. DEM User Requirements & Benefits
    David F. Maune
15. Quality Assessment of Elevation Data
    Jennifer Novac

Appendix A. Acronyms

Appendix B. Definitions

Appendix C. Sample Datasets

This book is your guide to 3D elevation technologies, products and applications. It will guide you through the inception and implementation of the U.S. Geological Survey's (USGS) 3D Elevation Program (3DEP) to provide not just bare earth DEMs, but a full suite of 3D elevation products using Quality Levels (QLs) that are standardized and consistent across the U.S. and territories. The 3DEP is based on the National Enhanced Elevation Assessment (NEEA) which evaluated 602 different mission-critical requirements for and benefits from enhanced elevation data of various QLs for 34 Federal agencies, all 50 states (with local and Tribal input), and 13 non-governmental organizations.

The NEEA documented the highest Return on Investment from QL2 lidar for the conterminous states, Hawaii and U.S. territories, and QL5 IfSAR for Alaska.

Chapters 3, 5, 8, 9, 13, 14, and 15 are "must-read" chapters for users and providers of topographic lidar data. Chapter 8 addresses linear mode, single photon and Geiger mode lidar technologies, and Chapter 10 addresses the latest in topobathymetric lidar. The remaining chapters are either relevant to all DEM technologies or address alternative technologies including photogrammetry, IfSAR, and sonar.

As demonstrated by the figures selected for the front cover of this manual, readers will recognize the editors' vision for the future – a 3D Nation that seamlessly merges topographic and bathymetric data from the tops of the mountains, beneath rivers and lakes, to the depths of the sea.

Co-Editors

David F. Maune, PhD, CP and
Amar Nayegandhi, CP, CMS

PRICING

Student (must submit copy of Student ID)	$50 +S&H
ASPRS Member	$80 +S&H
Non-member	$100 +S&H
E-Book (only available in the Amazon Kindle store)	$85

LEARN
DO
GIVE
BELONG

ASPRS

AMERICAN SOCIETY FOR PHOTOGRAMMETRY & REMOTE SENSING

ASPRS Offers

- » Cutting-edge conference programs
- » Professional development workshops
- » Accredited professional certifications
- » Scholarships and awards
- » Career advancing mentoring programs
- » *PE&RS*, the scientific journal of ASPRS

asprs.org